

**Finite Element Computation of the DC Corona
Currents Injected into the AC Conductors of a
Hybrid AC/DC Transmission Line**

by

© Albert F. Penner

A thesis
presented to the University of Manitoba
in partial fulfillment of the
requirements for the degree of
Master of Science
in
Electrical Engineering

Winnipeg, Manitoba

(c) Albert F. Penner, 1989



National Library
of Canada

Bibliothèque nationale
du Canada

Canadian Theses Service Service des thèses canadiennes

Ottawa, Canada
K1A 0N4

The author has granted an irrevocable non-exclusive licence allowing the National Library of Canada to reproduce, loan, distribute or sell copies of his/her thesis by any means and in any form or format, making this thesis available to interested persons.

The author retains ownership of the copyright in his/her thesis. Neither the thesis nor substantial extracts from it may be printed or otherwise reproduced without his/her permission.

L'auteur a accordé une licence irrévocable et non exclusive permettant à la Bibliothèque nationale du Canada de reproduire, prêter, distribuer ou vendre des copies de sa thèse de quelque manière et sous quelque forme que ce soit pour mettre des exemplaires de cette thèse à la disposition des personnes intéressées.

L'auteur conserve la propriété du droit d'auteur qui protège sa thèse. Ni la thèse ni des extraits substantiels de celle-ci ne doivent être imprimés ou autrement reproduits sans son autorisation.

ISBN 0-315-51600-3

FINITE ELEMENT COMPUTATION OF THE DC CORONA CURRENTS INJECTED
INTO THE AC CONDUCTORS OF A HYBRID AC/DC TRANSMISSION LINE

BY

ALBERT F. PENNER

A thesis submitted to the Faculty of Graduate Studies of
the University of Manitoba in partial fulfillment of the requirements
of the degree of

MASTER OF SCIENCE

© 1989

Permission has been granted to the LIBRARY OF THE UNIVER-
SITY OF MANITOBA to lend or sell copies of this thesis, to
the NATIONAL LIBRARY OF CANADA to microfilm this
thesis and to lend or sell copies of the film, and UNIVERSITY
MICROFILMS to publish an abstract of this thesis.

The author reserves other publication rights, and neither the
thesis nor extensive extracts from it may be printed or other-
wise reproduced without the author's written permission.

I hereby declare that I am the sole author of this thesis.

I authorize the University of Manitoba to lend this thesis to other institutions or individuals for the purpose of scholarly research.

Albert F. Penner

I further authorize the University of Manitoba to reproduce this thesis by photocopying or by other means, in total or in part, at the request of other institutions or individuals for the purpose of scholarly research.

Albert F. Penner

The University of Manitoba requires the signatures of all persons using or photocopying this thesis. Please sign below, and give address and date.

ABSTRACT

The increasing use of dc transmission has raised the possibility of ac and dc transmission lines operating on the same tower. An important characteristic of such hybrid ac/dc lines is the field and ion interactions between conductors. This thesis presents a method for evaluating the ionic dc current injected from a dc line into an ac conductor during corona. The method is based on the solution for the time invariant ionized field by an iterative Finite Element procedure. The influence of the alternating potential is determined from its effect on the space charge free electric field on the surfaces of the dc conductors.

A comparison of the calculated and experimental results for a laboratory line is presented along with calculated data for a practical hybrid transmission line configuration. The calculated results for the dc current injected into ac conductors agrees well with the experimental results however inconsistencies in the results of the calculations for the space charge density distribution indicate that the boundary conditions used in the iterative Finite Element procedure should be improved.

ACKNOWLEDGEMENTS

The author would like to thank Dr. M. R. Raghuveer and Dr. I. M. R. Ciric for their guidance during the completion of this thesis.

The author would also like to acknowledge the financial support received from the Manitoba High Voltage Direct Current Research Centre and The National Science and Engineering Research Council.

TABLE OF CONTENTS

Chapter	Page
ABSTRACT	iv
ACKNOWLEDGEMENTS	v
LIST OF FIGURES	ix
LIST OF TABLES	xi
1. INTRODUCTION	1
1.1 Literature Review	2
1.1.1 Analysis of DC Corona	2
1.1.2 Analysis of Corona on Hybrid AC/DC Lines	7
1.2 Line Geometries	8
2. DC CORONA MODEL	11
3. ITERATIVE FINITE ELEMENT PROCEDURE	15
3.1 Outline of Iterative FE Procedure	15
3.2 The Space Charge Free Electric Field	17
3.2.1 Determination of the Space Charge Free Field	17
3.2.2 The Effect of the AC Potential on Ion Trajectories	19
3.2.3 Determination of the Region of Interest	21
3.3 Mesh Generation	22
3.3.1 Mesh Generation Procedure	22
3.3.2 Evaluation of Mesh Accuracy	24
3.4 Initial Approximation for the Space Charge	33
3.4.1 Deutsch Initial Approximation	33
3.4.1 Concentric Cylinders Initial Approximation	33

Chapter	Page
3.5 Iterative Procedure	34
3.5.1 Update Algorithm	34
3.5.2 Exit Criteria	35
3.5.3 Choice of Update Algorithm Parameters	37
3.5.4 Comments on Iterative Procedure	39
3.6 Calculation of the Injected Corona Current	43
3.6.1 Integration over DC Conductor Surface	43
3.6.2 Integration over the Region of Interest	44
3.6.3 Comparison of Methods for Determining the Injected Current	45
4. RESULTS OF ITERATIVE FINITE ELEMENT METHOD	47
4.1 Comparison with Experimental Results	47
4.2 Comparison of Deutsch and Finite Element Solutions	48
4.3 Comparison of the Initial Approximations	50
4.3.1 Speed of Convergence	50
4.3.2 DC Injected Current	54
4.3.3 Space Charge Distribution on the Coronating Conductor	56
4.4 Accuracy of the Iterative FE Results	58
4.4.1 Inaccuracy Inherent in the Iterative FE Method	59
4.4.2 Comparison with Experimental	59
4.4.3 Effect of the Initial Approximation	60
4.5 Comparison with Empirical Results	63
5. INCLUSION OF THE EFFECT OF THE AC POTENTIAL	66
5.1 Method of Inclusion	66
5.2 Results of the Inclusion of the AC Potential	67
6. CONCLUSIONS	70
REFERENCES	73

Chapter	Page
APPENDIX A, MISCELLANEOUS EQUATIONS	75
A.1 Runge-Kutta Determination of Ion Paths	75
A.2 Initial Approximations for the Space Charge	77
A.2.1 Deutsch Initial Approximation	77
A.2.2 Concentric Cylinders Initial Approximation	79
A.3 Empirical I-V Relationship for Hybrid ac/dc Lines	81
APPENDIX B, PROGRAM LISTING	84
B.1 Angle Determination Program	84
B.2 Mesh Generation Program	88
B.3 Initial Space Charge Distribution Approximations	100
B.3.1 Deutsch Initial Approximation Program	100
B.3.2 Concentric Cylinders Initial Approximation Program	108
B.4 Iterative Finite Element Program	110

LIST OF FIGURES

Figure	Page
1.1: Line 1, Laboratory Line.	8
1.2: Lines 2 and 3.	9
2.1: Electric Field Lines and Solution Region, Geometry 1.	12
3.1: Theta maximum versus Phase Angle (δ), Geometry 1, Vdc=38 kV.	20
3.2: Artificial Boundaries, Geometry 1.	21
3.3a: Finite Element Mesh 1M3ca, Geometry 1.	28
3.3b: Finite Element Mesh 2T3ca, Geometry 2.	30
3.3c: Finite Element Mesh 3A3ca, Geometry 3.	32
3.4a: Exit Parameter ΔV Versus Iteration, Geometry 1, m=1.0, Vdc=50 kV.	40
3.4b: Exit Parameter ΔE Versus Iteration, Geometry 1, m=1.0, Vdc=50 kV.	40
3.4c: Exit Parameter $\Delta \rho$ Versus Iteration, Geometry 1, m=1.0, Vdc=50 kV.	41
3.4d: Exit Parameter ΔE_{O1} Versus Iteration, Geometry 1, m=1.0, Vdc=50 kV.	41
3.4e: Exit Parameter ΔE_{O2} Versus Iteration, Geometry 1, m=1.0, Vdc=50 kV.	42
3.5: Injected Current Versus Iteration, Geometry 1, m=1.0, Vdc=50 kV.	46
4.1: dc Injected Current - Experimental and Calculated, Geometry 1, Vac=0.	47
4.2a: dc Injected Current - Deutsch and FE, Geometry 1, m=1.0, Vac=0.	48
4.2b: dc Injected Current - Deutsch and FE, Geometry 2, Vac=0.	49
4.2c: dc Injected Current - Deutsch and FE, Geometry 3, Vac=0.	49
4.3a: Exit Parameter ΔV versus Iteration, Geometry 3, Deutsch initial approximation.	52
4.3b: Exit Parameter ΔV versus Iteration, Geometry 3, Concentric Cylinders initial approximation.	52
4.4a: dc Injected Current - Comparison of the effect of the Initial Approximation, Geometry 1, m=1.0.	54
4.4b: dc Injected Current - Comparison of the effect of the Initial Approximation, Geometry 2.	55

Figure	Page
4.4c: dc Injected Current - Comparison of the effect of the Initial Approximation, Geometry 3.	55
4.5a: Variation of Space Charge around dc Conductor Surface, Geometry 1, m=1.0, Vdc=50 kV.	56
4.5b: Variation of Space Charge around dc Conductor Surface, Geometry 1, m=1.0, Vdc=60 kV.	57
4.5a: Variation of Space Charge around dc Conductor Surface, Geometry 2, Conductor 1, Vdc=300 kV.	58
4.6a: dc Injected Current - FE and Empirical, Geometry 1, m=1.0.	64
4.6b: dc Injected Current - FE and Empirical, Geometry 2.	65
4.6c: dc Injected Current - FE and Empirical, Geometry 3.	65
5.1: dc Injected Current - Zero and Nonzero ac Potential, Geometry 1, m=0.95.	67
5.2: dc Injected Current - Zero and Nonzero ac Potential, Geometry 2.	68
5.3: dc Injected Current - Zero and nonzero ac Potential, Geometry 3.	69

LIST OF TABLES

Table	Page
1.1: Dimensions of Line Geometries 2 and 3.	10
3.1: Average Value of θ_{\max} Versus AC Potential, Geometry 1, Vdc=38 kV.	20
3.2a: Error in Finite Element Meshes, Geometry 1.	26
3.2b: Error in Finite Element Meshes, Geometry 2.	29
3.2c: Error in Finite Element Meshes, Geometry 3.	31
3.3: Convergence of Different Constant α , β and γ 's, Geometry 1, m=0.95, Vdc=38 kV.	37
3.4: Variable α , β and γ Update Convergence, Geometry 1, m=0.95, Vdc=38 kV.	38
3.5: Potential Update Convergence, Geometry 1, Vdc=38 kV, m=0.95.	39
3.6a: Effect of Mesh on Convergence, Geometry 1, m=1.0, Vdc=50 kV.	42
3.6b: Effect of Mesh on Convergence, Geometry 2, Vdc=300 kV.	43
3.7: Limits on the Current in a Corridor, Geometry 1, Vdc=50 kV, m=1.0.	44
3.8: Comparison of Methods for Determining dc Injected Current, Geometry 1, m=0.95.	45
4.1a: Convergence for Deutsch and Concentric Cylinder Initial Approximations, Geometry 1, m=1.0, $\alpha=-1.0$, $\beta=-0.5$, $\gamma=-0.25$.	50
4.1b: Convergence for Deutsch and Concentric Cylinder Initial Approximations, Geometry 3, $\alpha=-2.0$, $\beta=-1.0$, $\gamma=-0.5$.	51
4.2a: Difference Between Final Solutions Obtained With Deutsch and Concentric Cylinders Initial Approximations, Geometry 1, m=1.0, Vdc=50 kV.	61
4.2b: Difference Between Final Solutions + 20 Iterations Obtained With Deutsch and Concentric Cylinders Initial Approximations, Geometry 1, m=1.0, Vdc=50 kV.	62
4.2c: Change in Solution Before and After Convergence, Deutsch Initial Approximation, Geometry 1, m=1.0, Vdc=50 kV.	62
4.2d: Change in Solution Before and After Convergence, Concentric Cylinders Initial Approximation, Geometry 1, m=1.0, Vdc=50 kV.	62
A.1: The Effect of the Maximum Error per step on Theta max., Geometry 1, Vdc=38 kV, Vac=0.	76

Chapter 1

INTRODUCTION

A hybrid ac/dc transmission line is a transmission line with both ac and dc conductors on the same or adjacent towers. Interest in hybrid transmission lines has been sparked by the increasing use of dc transmission which raises the possibility of dc lines being included in existing ac networks. Advantages due to the combination of dc with ac transmission include: improvements in the stability and controllability of ac networks [2] and improvements in the power transfer capacity of a right-of-way.

Corona is created by the ionization of the air near the surface of a high voltage conductor due to the high magnitude of the electric field near the conductor. These ions form a space charge around the conductor which in turn affects the electric field around the conductor. In general, around a positively charged dc conductor the electrons created by the ionization of the air are attracted by and neutralized on the conductor, while the positively charged ions will be driven away from the conductor. This results in a net positive charge in the vicinity of a positively charged conductor. Similarly, a negatively charged conductor will be surrounded by a negative space charge. The alternating nature of the field around an ac transmission line complicates the actions of the space charge generated by corona with the attraction and repulsion of ions and electrons alternating. One result of this attraction and repulsion of ions by ac lines is that the ions created remain near the conductors and a significant space charge is not created further from the conductor.

The amount of corona activity of a transmission line is affected by numerous variables. The electric field on the surface of a conductor will be affected by the line geometry and line voltage. The maximum electric field on the conductor surface will also be affected by the smoothness of the conductor. The environmental conditions: humidity, rain, fog, wind and the temperature will affect the creation of ions.

Corona affects many aspects of high voltage transmission. The creation and movement of ions causes a power loss. The flow of ions away from a conductor will also deposit a charge

on insulated objects located near a dc transmission line. Corona also causes audible noise (AN) and radio (RI) and television (TVI) interference. The amount of corona activity also affects the response of the transmission line to transient voltages and currents. In a hybrid ac/dc transmission line some of the ions flowing away from dc conductors will be attracted to ac conductors resulting in a dc current in the ac conductors. This dc current in ac conductors can cause the saturation of transformers located at the ends of the ac line. Due to the above effects the generation of corona is an important consideration in the design of high voltage transmission lines.

This thesis will present a method for the computation of the dc current injected in the ac conductors of a hybrid ac/dc transmission line. The method is based on a numerical solution for the ionized field created by corona on dc transmission lines by an iterative Finite Element (FE) method. The method differs from previous FE solutions for dc corona [16]-[19] in that it uses a novel boundary on the solution area. The solution for the dc current injected into ac conductors of a hybrid ac/dc transmission line improves on previous analysis [3] by including the effect of the ac potential on this dc current.

1.1 Literature Review

The analysis of a time varying ionized field requires a prohibitively large computational effort. As a result, all solutions for corona on ac/dc lines are based on solutions for dc corona.

1.1.1 Analysis of DC Corona

Equations and Assumptions

The equations and assumptions common to all previous analysis of dc corona are presented in this Section. The time invariant electric and potential fields in the presence of space charge are governed by the following equations:

$$\nabla \cdot \mathbf{E} = \rho / \epsilon_0 \quad (1.1)$$

$$\mathbf{J} = k\rho\mathbf{E} \quad (1.2)$$

$$\nabla \cdot \mathbf{J} = 0 \quad (1.3)$$

$$\mathbf{E} = -\nabla\Phi \quad (1.4)$$

where \mathbf{E} is the electric field, \mathbf{J} the current density, Φ the scalar potential and ρ the space charge density distribution. k is the ionic mobility and ϵ_0 is the permittivity of free space. The use of equations (1.1)-(1.4) implies five main assumptions and simplifications. The first is that there is an equivalent steady state, that dc corona does not vary with time. In general dc corona exhibits a pulsating nature [10], however due to the difficulty of solving for time varying ionized fields, this variable nature of dc corona is not considered. The second simplification is that there is no wind. The presence of wind will cause an increase in the corona loss of a conductor [20, pg. 31]. The third assumption is that the diffusion of ions due to temperature differences is insignificant compared with the movement of ions due to the electric field, as has been shown in reference [5]. The fourth simplification is that the mobility of ions is constant and does not depend on time or the strength of the electric field. Experimental results indicate that the mobility of ions decreases with time since generation [5]. However, different studies show considerably different mobility versus time profiles for ions [13] and also that the mobilities of individual ions can vary considerably. The use of constant ionic mobilities is a necessary simplification. The final assumption is that the ionization layer around the dc conductor is negligibly thin. Previous researchers have determined that the extent of this ionization layer is "negligible" [6] and approximately 3 orders of magnitude less than the conductor spacing [9]. The above assumptions have been accepted by all researchers with several minor exceptions as noted.

Equations (1.1)-(1.4) can be combined to yield a single third order partial differential equation:

$$\nabla \cdot [(\nabla^2\Phi)\nabla\Phi] = 0 \quad (1.5)$$

In order to solve this equation three boundary conditions are necessary. The potentials on the conductors provide two of these boundary conditions. The choice of the third boundary condition varies in the different solution methods.

Non-Finite Element Analysis of DC Corona

The first analytic solution of dc corona was made by Townsend [4]. Townsend solved for the voltage-current relation of the concentric cylinders geometry. The voltage-current relation is the relation between the potential difference between two conductors and the ionic current driven from one conductor to the other during corona. Due to the symmetry of the concentric cylinders geometry, the region in which equation (1.5) must be solved can be reduced to a single dimension which greatly simplifies it's solution. The third boundary condition used by Townsend was the electric field on the surface of the coronating conductor. Townsend assumed that this electric field remained constant at it's onset value during corona.

$$|-\frac{d\Phi}{dn}|=E_0 \text{ on the surface of coronating conductors} \quad (1.6)$$

where E_0 is the value of the electric field on the surface of the conductor at the onset of corona.

This assumption provides the most common choice for the third boundary condition and is known as the Kaptzov assumption. Experimental results show that the electric field on the surface of positively charged dc conductors decreases from it's onset value during corona while on negatively charged conductors the electric field increases from it's onset value [7]. These results also show that electric field on a coronating conductor is not the same at all points on the surface. However, these deviations are negligible for practical levels of corona activity [7].

An extension of the solution for dc corona to practical geometries was made by Deutsch. (Deutsch's work is in German and this overview of it is taken from references [5],

[6] and [8].) Deutsch solved the single conductor over a conducting ground plane (monopolar line) geometry. In order to solve this two dimensional problem Deutsch introduced several additional assumptions, the most important of which was the assumption that the presence of space charge affects only the magnitude and not the direction of the electric field. E.g. the direction of the ionized electric field is in the same as the direction of the space charge free electric field. As the direction of the space charge free electric field can be easily determined, this assumption allows the solution for the ionized field to be made separately along each electric field line which amounts to the reduction of the solution region to a single dimension. This assumption that the presence of space charge does not affect the direction of the electric field has become known as the Deutsch assumption.

Popkov [5] analyzed the monopolar line geometry using the Deutsch and Kaptzov assumptions and additional assumptions about the distribution of the space charge on the ground plane. Popkov also presented semi-empirical expressions for the voltage-current relationship for the monopolar line geometry based on Townsend's expression for the concentric cylinder geometry and experimental results for the monopolar line geometry.

The availability of high speed computers allowed improvements in the analysis of dc corona. Sarma and Janischewskyj introduced an iterative numerical method, making use of the Deutsch and Kaptzov assumptions, to determine the ionized field solution of monopolar [6] and bipolar line [7] geometries.

Abdel-Salam et al. [8] removed the Deutsch assumption in the monopolar line geometry by assuming the space charge density distribution was known. This is the only non-Finite-Element method which solves for the ionized field without using the Deutsch assumption. As the space charge distribution cannot be known accurately beforehand this method has limited practical use.

Khalifa et al. [9] replaced the Kaptzov boundary condition on the electric field on the surface of the coronating conductor by using the space charge distribution on the surface of the

coronating conductor as the third boundary condition. This space charge distribution was determined based on an avalanche model for corona.

Sunaga et al. [10] also used the space charge density on the surface of the coronating conductor as the third boundary condition. They determined this space charge density by assuming a distribution for the space charge around the conductor and using experimental results for the total current discharged to determine the magnitude of the space charge. This solution was for the monopolar line geometry and retained the Deutsch assumption.

Recently, several researchers have presented simplified methods for the calculations of fields in the presence of space charge [11]+[14]. These methods use the Deutsch and Kaptzov assumptions but simplify the calculations.

Abdel-Salam et al. [13] improved the analysis of dc corona by including the effect of the variation of ion mobility with time. They also made use of the Deutsch and Kaptzov assumptions.

Finite Element Analysis of DC Corona

The attempts to solve for corona in the single conductor over a ground plane geometry listed above are limited by the use of the Deutsch assumption. The Deutsch assumption can be assumed to be valid if the magnitude of the space charge density is small and thus has only a small effect on the electric field, but for larger values of space charge the Deutsch assumption may not be valid. The Finite Element (FE) method can be used to eliminate the necessity of the Deutsch assumption. The FE method allows for the solution of second order partial differential equations in two (or three) dimensional regions. In FE solutions for the ionized field, equations (1.1)-(1.4) are combined into a pair of second order partial differential equations which are solved iteratively.

Janischewskyj et al. [16] were the first to use an iterative FE procedure to solve for dc corona. They made use of the Kaptzov assumption for the third boundary condition and solved the concentric cylinders geometry.

Takuma et al. [17] analyzed the monopolar line geometry using the FE method. They used the space charge on the surface of the coronating conductor as the third boundary condition and included analysis of the effects of wind. Due to the fact that the FE method can only be used within a finite region and for the line above ground geometry the region is unbounded, Takuma et al. placed an artificial boundary on the finite element mesh at a distance from the conductor approximately equal to the height of the conductor over ground. On this artificial boundary the potential is set equal to the space charge free potential as the boundary is assumed to be far enough away from the conductor so that the voltage is not affected by the space charge.

Abdel-Salam et al. [19] analyzed the monopolar line geometry using the FE method and replacing the Kaptzov assumption by using the space charge distribution along the axis of symmetry, determined using the Deutsch assumption, as the third boundary condition. They used an artificial boundary similar to the one used by Takuma et al. [17].

A comparison by Janischewskyj et al. [18] of solutions to dc corona problems by a FE method and a method using the Deutsch assumption concluded that the method using the Deutsch assumption gives "adequate" results.

1.1.2 Analysis of Corona on Hybrid AC/DC Lines

Chartier et al. [1] presented the first analysis of corona on hybrid ac/dc lines. Their analysis was based on the solution for the electric field without considering the effect of space charge. They also derived empirical expressions for the radio interference (RI) and audible noise (AN) of hybrid ac/dc lines based on similar expressions for ac and dc lines.

Maruvada et al. [3] included the effects of the space charge created by corona on the calculation of the electric and potential fields around a hybrid ac/dc line. They used a numerical method using both the Deutsch and Kaptzov assumptions. They also used the simplification that the ac conductors could be assumed to be at ground potential, justifying this assumption by showing that the ac voltage has a negligible effect on the trajectories of ions.

1.2 Line Geometries

Three line geometries are analyzed. The first is a laboratory line consisting of a conductor energized with a positive dc voltage directly above a conductor energized with an ac voltage.

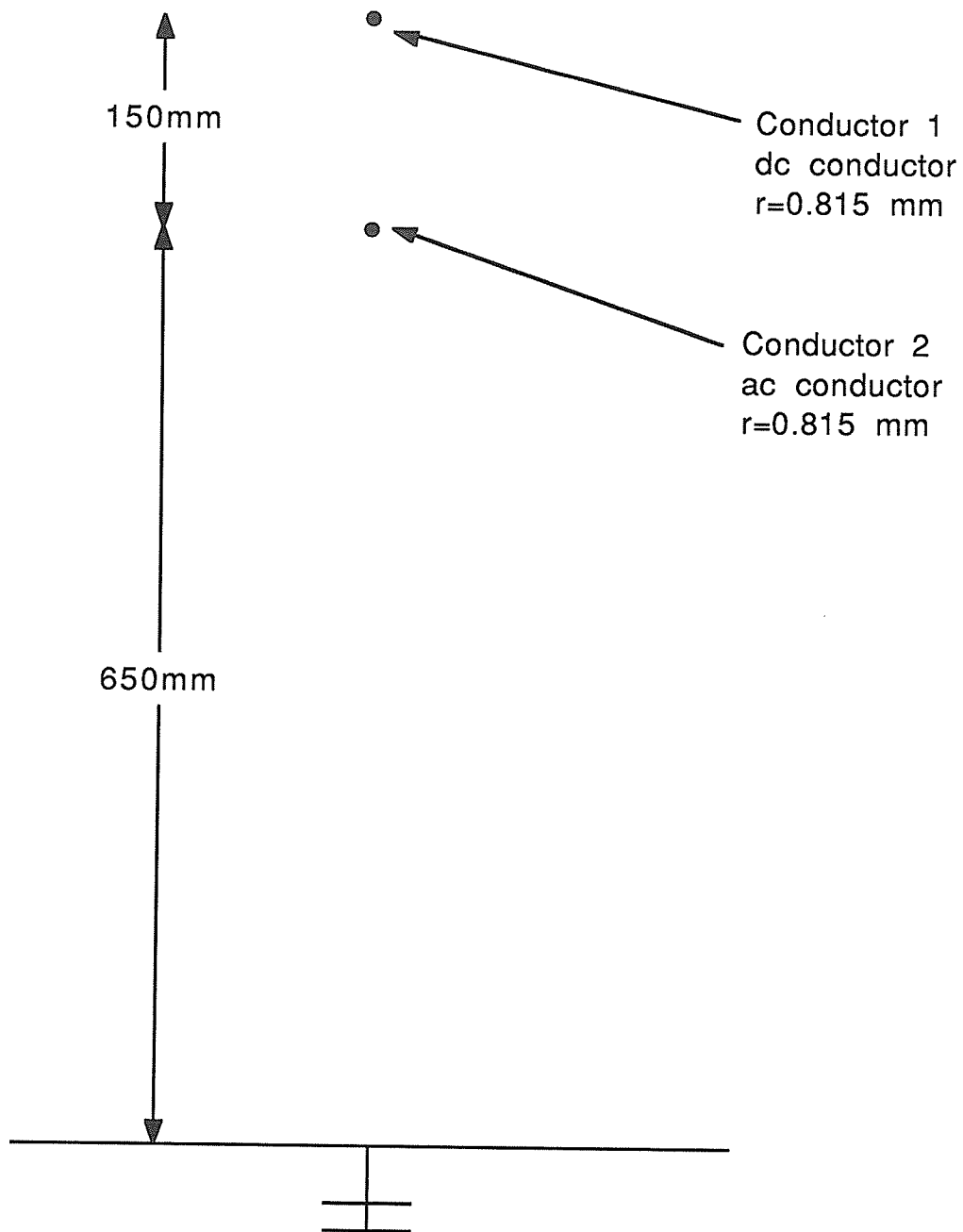


Figure 1.1: Line 1, Laboratory Line.

The second geometry is based on a modified Manitoba Hydro Gulfport line tower, with a bipolar dc transmission line replacing the ground wires of a three phase ac line. The third geometry is the same as the second with the dc line situated at a greater height.

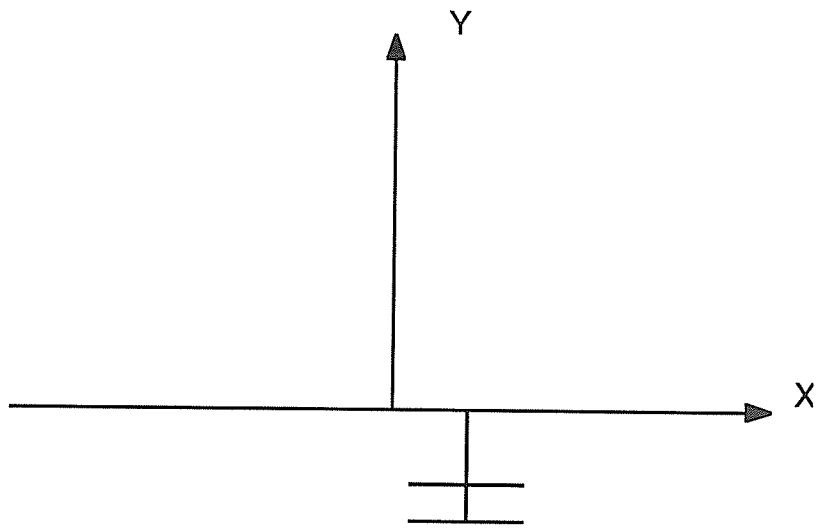
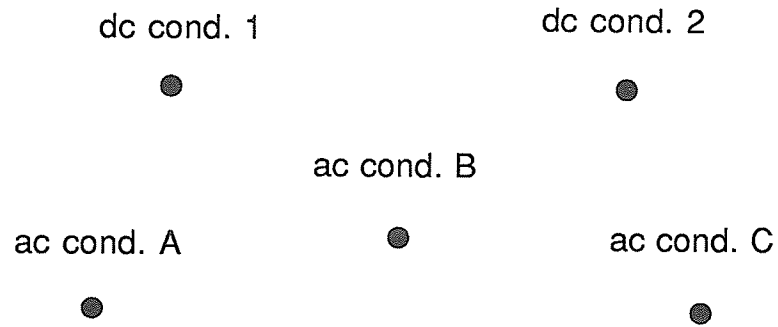


Figure 1.2: Lines 2 and 3.

Conductor	Geometry 1		Geometry 2	
	X (m)	Y (m)	X (m)	Y (m)
dc 1	-4.57	16.34	-4.57	17.34
dc 2	4.57	16.34	4.57	17.34
ac A	-5.49	12.38	-5.49	12.38
ac B	0.0	14.20	0.0	14.20
ac C	5.49	12.38	5.49	12.38

Table 1.1: Dimensions of Line Geometries 2 and 3.

The radii of the conductors in Geometries 2 and 3 are: dc conductors 1.755 cm, ac conductors 1.599 cm. The height of the conductors in geometries 2 and 3 is taken as the average height, i.e. the maximum height minus 2/3 of the sag.

The h/r (height/radius) ratios for the three lines are: Line 1: 982 dc, 798 ac; Line 2: 931 dc, 815 and 935; Line 3: 988 dc, 815 and 935 ac. The similarity of the h/r ratios for the experimental with those of the actual line should ensure that the results for the experimental line will follow the same pattern as those for the actual line [18].

Chapter 2

DC CORONA MODEL

The assumption used by Maruvada et al. [3] that the ac voltage does not significantly affect the the trajectories of ions in a hybrid ac/dc is used to reduce the problem to that of a dc corona problem. This chapter gives the model adopted for dc corona including all assumptions and simplifications.

The equation governing the dc field in the presence of space charge is as before:

$$\nabla \cdot [(\nabla^2 \Phi) \nabla \Phi] = 0 \quad (2.1)$$

The above equation implies the use of the five assumptions given in Subsection 1.1.1.

An iterative Finite Element method is used to solve the above equation in the inter-electrode region in order to partially eliminate the Deutsch assumption. (The assumption that the direction of the electric field is unaffected by the presence of space charge.) To minimize the area in which the ionized field must be determined the artificial boundary is placed so that the region of interest (the region in which the FE method is used to solve for the ionized field) includes only the area of the electric flux between two conductors. As shown in Figure 2.1 the region of interest includes only the electric field lines between the two conductors. The bounding electric field line is determined from the space charge free field and a natural Neuman, $d\Phi/dn=0$, boundary condition is imposed on this boundary. This results in the Deutsch assumption being imposed on the boundaries of the region of interest.

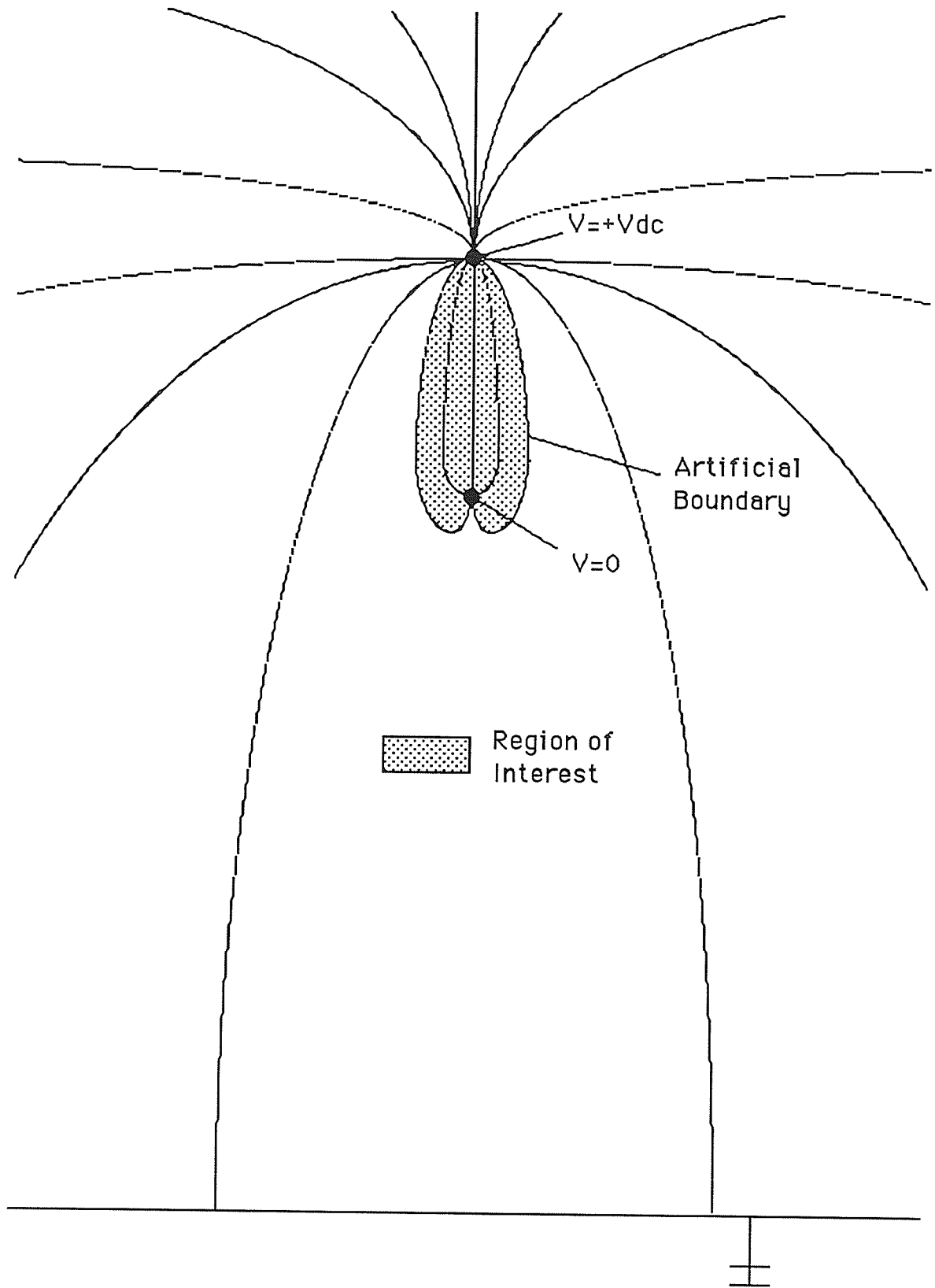


Figure 2.1: Electric Field Lines and Solution Region, Geometry 1.

This artificial boundary is a departure from previous FE solutions for dc corona [17], [18] and [19]. These solutions all use an artificial boundary remote from any conductors, assuming that far from the conductors there will be limited space charge and ionized field can be approximated by the space charge free field. The advantage of the artificial boundary used in this thesis is that it limits the area of the region of interest, decreasing the time necessary for the solution and/or making it possible to increase the accuracy of the solution. The disadvantage is that the Deutsch assumption must be used on the artificial boundary where it may not be valid possibly resulting in inaccurate results.

Another advantage of the present choice for the artificial boundary is that the solution region will only contain two conductors. As a result, in multiconductor lines (Geometries 2 and 3) the entire problem area can be subdivided into smaller regions each containing two conductors and all the electric flux lines originating on one of the conductors and ending on the other. This results in the subdivision of the problem into several smaller problems, reducing the time needed for a solution.

The boundary conditions used in the method are:

$$\Phi = V_{eq} \text{ on the surface of dc conductors.} \quad (2.2)$$

$$\Phi = 0 \text{ on the surface of ac conductors.} \quad (2.3)$$

$$|-d\Phi/dn| = E_0 \text{ on the surface of dc conductors.} \quad (2.4)$$

Maruvada et al. [3] used the fact that the ac voltage did not effect the trajectories of ions in a hybrid ac/dc system to assume that the ac voltage had no effect on the dc corona. However, although it may not affect the trajectories of ions significantly, the ac potential may affect the corona on dc conductors through changes in the magnitude of the electric field and/or the number of ions formed. As the experimental results presented later in this thesis will show, the ac voltage does have a significant effect on the magnitude of the corona current discharged from the dc line. The effect of the ac voltage is included in this analysis through the

use of an "equivalent" dc voltage, V_{eq} , on the dc conductor. This equivalent voltage is determined by an analysis of the effect of the ac voltage on the electric field on the surface of the dc conductor. Only the effect of the ac voltage on the dc current injected into the ac conductor is examined, the effect of the ac conductor on the electric and potential fields in the region of interest is not examined.

The third boundary condition used, $|-d\Phi/dn|=E_0$ on the surface of dc conductors, is based on the Kaptzov assumption. The value of E_0 is determined using Peek's equation [20, pg. 23]:

$$E_0=30m(1+0.301/\sqrt{r}) \text{ [kV/cm]} \quad (2.5)$$

where r is the radius of the conductor in question (in [cm]) and m is the surface factor. The surface factor is used to account for non-smooth conductors. For a small radius conductors, such as those in the laboratory line, surface irregularities have little effect [20, pg 18]. The surface factor can also be used to account for environmental factors such as poor weather with $m=0.5$ typical for good weather and $m=0.3$ for poor weather [20, pg. 19] on full scale transmission lines. For Geometry 1 surface factors of $m=0.95$ and 1.0 are examined and for Geometries 2 and 3 the surface factor is taken as $m=0.5$.

Chapter 3

ITERATIVE FINITE ELEMENT PROCEDURE

This chapter details the solution for the ionized field between two dc conductors by the iterative Finite Element (FE) method. The results obtained are presented in the next chapter.

3.1 Outline of the Iterative FE Procedure

Equations (1.1)-(1.4) can be combined to form a pair of second order partial differential equations:

$$\nabla^2\Phi = -\rho/\epsilon_0 \quad (3.01)$$

$$\nabla \cdot (\rho \nabla \Phi) = 0 \quad (3.02)$$

The boundary conditions for these equations are the potentials on the ac and dc conductors.

$$\Phi = V_{eq} \text{ on the surface of dc conductors.} \quad (3.03)$$

$$\Phi = 0 \text{ on the surface of ac conductors.} \quad (3.04)$$

where V_{eq} is the dc voltage plus an additional voltage to account for the ac potential. In the remainder of this chapter the effect of the ac potential is ignored and thus voltage on the ac conductor is taken at zero and V_{eq} is equal to V_{dc} .

The space charge distribution (ρ) in equations (3.01) and (3.02) is initially unknown and must be approximated. Using this approximation equations (3.01) and (3.02) are each solved separately with the boundary conditions given by equations (3.03) and (3.04) and a natural Neuman ($d\Phi/dn=0$) boundary condition on the artificial boundary. As the approximation for the space charge distribution is inaccurate, the solutions for the electric and potential fields determined by equations (3.01) and (3.02) will be different. A new approximation for the space charge distribution is then made based on the old approximation and the difference

between the solutions to equations (3.01) and (3.02). The solutions for the electric field on the dc conductor surface obtained from equations (3.01) and (3.02) will also be different from the third boundary condition ($|-d\Phi/dn|=E_0$ on the surface of the coronating dc conductor.) This difference also provides information for the updated approximation for the space charge distribution. The third boundary condition should ensure that the fields determined by equations (3.01) and (3.02) converge to a unique solution. This iterative procedure is continued until the solutions for the electric and potential fields given by equations (3.01) and (3.02) are substantially the same and the third boundary condition is met by the two solutions. As there will always be some difference between the two solutions for the ionized field, the final solution for the electric and/or potential field at any point is taken as the average of the fields given by the solutions to equations (3.01) and (3.02) at that point. The dc current injected into the ac conductor is determined from the final approximation for the space charge distribution. The iterative FE procedure is used for various dc voltages resulting in Current-Voltage characteristics for each geometry.

The steps in the method are:

1. The limits of the region of interest are determined: Subsection 3.2.3.
2. The region is divided into triangular elements for the FE solution: Section 3.3.
3. An initial approximation for the space charge distribution is made: Section 3.4.
4. Equations (3.01) and (3.02) are solved in the region by the FE method.
5. Based on the difference between the solutions to equations (3.01) and (3.02) and the third boundary condition, the approximation for the space charge distribution is updated: Subsection 3.5.3.
6. The difference the solutions to equations (3.01) and (3.02) is evaluated. If the difference is greater than the exit criteria steps 4-6 are repeated, if the solution does meet the exit criteria the iterative solution is complete: Subsection 3.5.2.
7. The total corona current injected into the ac conductors is determined from the final solution for the ionized field and the final space charge distribution: Section 3.6.

3.2 The Space Charge Free Electric Field

The space charge free field is the electric or potential field determined without considering the presence of space charge. The solution for the space charge free field has two uses. The first is to show the effect of the alternating ac voltage on the direction of the electric field and thus the trajectories of ions and the second is to determine the artificial boundary for the FE mesh.

3.2.1 Determination of the Space Charge Free Electric Field

The space charge free electric field is determined by approximating each conductor by an infinite line of charge located at the center of the conductor. The effect of the ground plane is included by imaging each conductor through the ground plane. E.g. an image of each conductor, bearing the opposite charge, is placed at the same distance below the ground plane as the actual conductor is above the ground plane. The magnitude of the line of charge replacing each conductor is determined from:

$$\Phi_i = \frac{1}{2\pi\epsilon_0} \sum_{i \in N} q_i \ln \frac{|r_{gj}|}{|r_i|} \quad (3.05)$$

where Φ_i is the voltage on conductor i , r_i is the radius of conductor i , r_{gj} is the distance from the center of the conductor to the ground plane, N is the set of all conductors (including imaged conductors) and q_i is the magnitude of the line of charge replacing conductor i . Using equation (3.05) for all conductors a system of equations is formed:

$$\Phi = PQ \quad (3.06)$$

where Φ is the column vector of the conductor voltages, Q is the column vector of the magnitudes of the lines of charge replacing the conductors, and P is the square coefficient matrix. The magnitude of charge replacing each conductor is determined by inverting the coefficient matrix:

$$Q = P^{-1}\Phi \quad (3.07)$$

Knowing the charges on each conductor, the space charge free electric and potential fields at any point can be determined from:

$$\mathbf{E}(p) = \frac{1}{2\pi\epsilon_0} \sum_{i \in N} \frac{q_i}{|r_{ip}|^2} \mathbf{r}_{ip} \quad (3.08)$$

and

$$\Phi(p) = \frac{1}{2\pi\epsilon_0} \sum_{i \in N} q_i \ln \frac{|r_{gi}|}{|r_{ip}|} \quad (3.09)$$

where p is the point in question and r_{ip} is the vector from line of charge i to the point p . This method is suitable for determining the space charge free field when the h/r ratios for conductors are greater than ten [21] as is the case in all the geometries used.

3.2.2 The Effect of the AC Potential on Ion Trajectories

This subsection shows that the "average" effect of the ac potential on the trajectories of ions is negligible in order to justify the use of the same artificial boundaries for both zero and non-zero ac voltages. This is a verification of the results presented by Maruvada et al. [3].

The time varying space charge free electric field for the first geometry is determined by the method presented in the previous section with the following voltages on conductors.

$$V=V_{dc} \text{ on dc conductor.} \quad (3.10)$$

$$V=\sqrt{2} V_{ac} \cos(\omega t-\delta) \text{ on ac conductor.} \quad (3.11)$$

The effect of the ac potential on ion trajectories is determined by tracing the paths of ions emitted by the dc conductor in Geometry 1. The velocity of an ion is given by:

$$\frac{dr}{dt}=kE(r,t) \quad (3.12)$$

Where r is the position vector, k is the ionic mobility (taken as $0.00015 \text{ [m}^2/\text{V}\cdot\text{s]}$ for positive ions [6]) and the space charge free electric field is determined as previously. The path of an ion is determined by integrating equation (3.12) with respect to time as shown in Appendix A.1. The path of an ion emitted from the dc conductor can be completely determined knowing: the point on the surface of the dc conductor from which it is emitted, the magnitudes of the dc and ac potentials and the phase angle of the ac potential at the time at which the ion is emitted. The net effect of the ac voltage on ion trajectories is found by determining whether an ion emitted from the dc conductor lands on the ac conductor or the ground plane. As shown in Figure 3.2, the angles θ_{max} and θ_{min} are the maximum and minimum angles on the dc conductor from within which an ion emitted will reach the ac conductor. E.g. Ions emitted at an angle $\theta_{min} < \theta <$

θ_{max} will reach the ac conductors while ions outside that range will land on the ground plane. If the dc and ac potentials are constant, θ_{max} and θ_{min} will only be influenced by the phase angle of the ac potential.

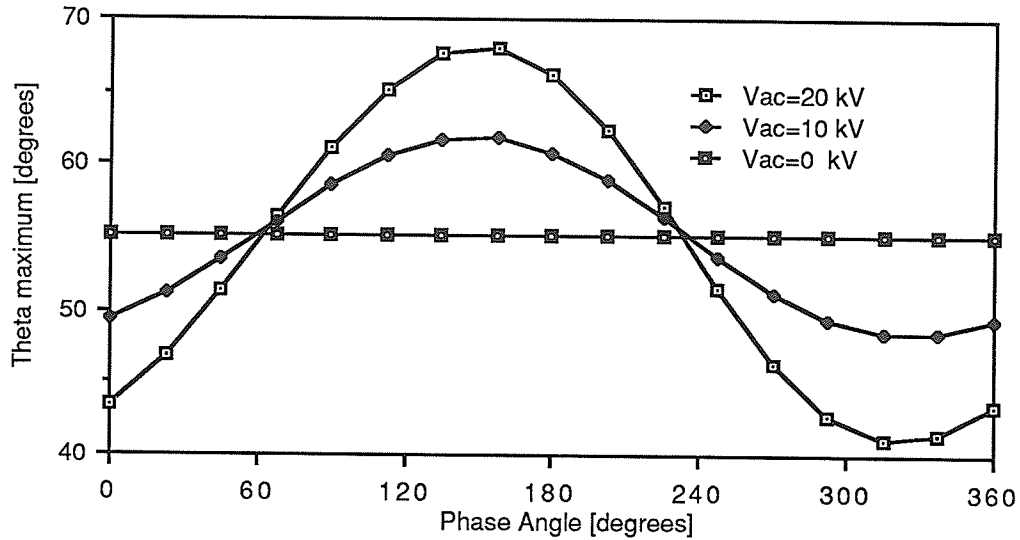


Figure 3.1: Theta maximum Versus Phase Angle (δ), Geometry 1, $V_{dc}=38$ kV.

Figure 3.1 shows the maximum angle on the surface of the dc conductor at which an ion emitted will land on the ac conductor and not the ground plane. The phase angle (δ) is the phase angle of the ac potential measured at the point in time when the ion is emitted from the dc conductor. As shown in Figure 3.2, theta is measured from the vertical in Geometry 1 and due to symmetry, $\theta_{min}=-\theta_{max}$. The results presented in Figure 3.1 demonstrate that the greater the ac voltage the greater effect it has on θ_{max} and thus the ion trajectory. However, for every ac voltage the average over the phase angle of the maximum theta is only minimally affected by the ac voltage.

AC Voltage [kV]	Average value of θ_{max} [degrees]
0	55.20
10	55.02
20	54.38

Table 3.1: Average Value of θ_{max} Versus AC Potential, Geometry 1, $V_{dc}=38$ kV.

As a result the average number of electric field lines originating on the dc conductor and terminating on the ac conductor is unaffected by the ac voltage. The above results are assumed to be valid for Geometries 2 and 3.

3.2.3 Determination of the Region of Interest

The region of interest is the region in which the solution is determined. The artificial boundaries of the region of interest are the space charge free electric field lines which leave the dc conductor at angles of θ_{\max} and θ_{\min} with the ac voltage equal to zero. As stated previously, the use of this artificial boundary assumes that the Deutsch assumption is valid along these lines. In the iterative FE solution a natural Neuman boundary condition is applied on the artificial boundary.

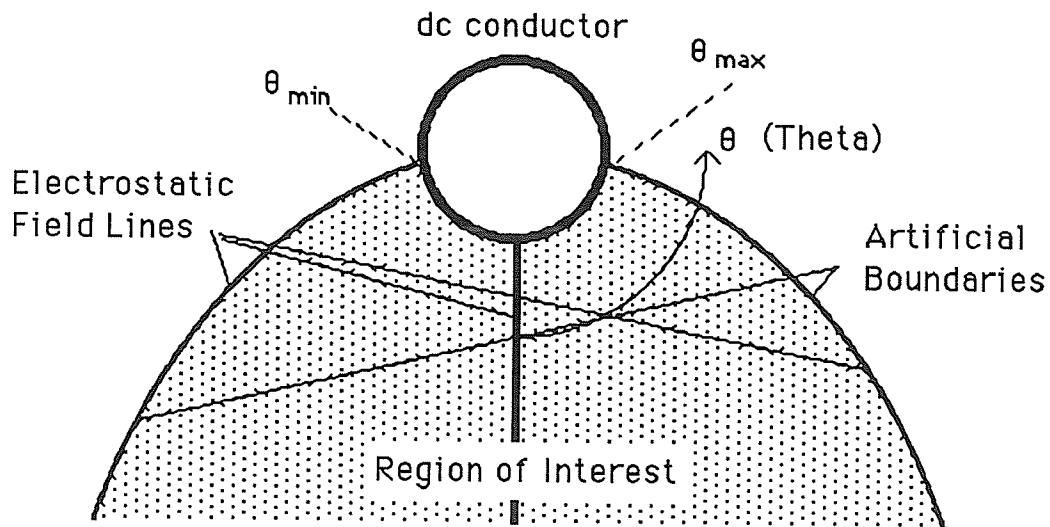


Figure 3.2: Artificial Boundaries, Geometry 1.

Figure 3.2 shows that the artificial boundaries are determined by the average θ_{\max} and θ_{\min} . Figure 2.1 shows the entire region of interest for Geometry 1.

In Geometries 2 and 3 there are four solution regions: between conductors 1 and A, 1 and B, 2 and B, and 2 and C. Each of these regions is analyzed separately with the artificial boundaries for each of these regions determined as above. The main analysis is presented for

the region between conductors 1 and A. The region between conductors 2 and C is a mirror image of that between 1 and A and the solutions in these two regions will only differ due to factors such as the difference between positive and negative ionic mobilities and/or a different inception point for corona on negatively charged conductors. The region between conductors 1 and B (and conductors 2 and B) is very small for Geometries 2 and 3, consisting of less than two degrees on the dc conductor. As a result the dc corona current injected into conductor B from conductor 1 will be relatively small. In addition the dc currents injected into conductor B from conductors 1 and 2 will be of opposite polarity and thus partially cancel further reducing the dc current in conductor B. As the current injected into conductor B will be insignificant compared with that injected into conductors A and C it is not determined.

3.3 Mesh Generation

The formation of a mesh is one of the most time consuming parts of a finite element solution. An automatic mesh generation program is necessary to reduce this time.

The finite element program used, MANFEP [22], uses triangular elements. The aspect ratios of the triangular elements has a significant effect on the accuracy of the FE solution as will be shown.

3.3.1 Mesh Generation Procedure

The automatic mesh generation procedure is based on tracing the electric field lines between the two conductors. The steps in the mesh generation program are explained below.

First the number of nodes (triangle vertices) on the surface of the dc conductor is chosen. The number of triangular elements bordering on the dc conductor will be one less than the number of nodes on the conductor surface. These nodes are evenly distributed over the portion of the dc conductor surface bordering the region of interest. The electric field lines which originate at these dc conductor nodes are determined and these field lines divide the region of interest into a series of corridors, each corridor extending from the dc to the ac

conductor and the total number of corridors being one less than the number of nodes on the dc conductor. The electric field lines forming the boundaries of these corridors are in turn divided into shorter segments. Starting at the dc conductor, the length of the first segment is given by the parameter L_{dc} . Each segment, moving away from the dc conductor, increases in length by a growth factor g .

$$\text{Length of segment } i = g^i L_{dc} \quad (3.13)$$

In the application of (3.13), $i=1$ on the dc conductor and is increased by 1 for each segment. This process is continued until half the distance (measured along the field line) to the ac conductor is reached. Then the same procedure is followed beginning on the ac conductor. This procedure is repeated for each field line. The end points of each segment form nodes which are joined with other nodes from adjacent field lines to form triangles. By increasing the length of the segments further from the conductors the shape of triangles is kept nearly equilateral and more elements are formed where the electric and potential fields vary most rapidly, e.g. near the conductors. The meshes used for the three geometries are shown in Figures 3.3a-3.3c.

In the second and third geometries the total angle on the ac conductor in the region of interest is much greater than the angle on the dc conductor. As a result it is impractical to have the same number of elements on the ac as the dc conductor and the number of elements on the ac conductor is doubled in these geometries by subdividing the original triangles on the ac conductor into smaller triangles. This is shown in Figures 3.3b and 3.3c.

The parameters which must be specified for the mesh generation program are;

- the number of nodes on the dc conductor,
- the initial segment length on the dc and ac conductors,
- and the growth factor.

The triangular elements in MANFEP may be either of the first, second or third order. The order of elements refers to the maximum order of the variation of the potential within an

element. MANFEP also allows element sides to be curved to better conform with the physical boundaries. A curved boundary is formed by adding nodes on the sides of elements which make up the boundary, two nodes for third order elements and one node for second order triangles. The element border is then formed by the third or second order curve through the nodes of the element. (The elements are referred to as triangles and the centroids of elements are determined by the average of the element vertices regardless of any curved boundaries.) The electric field at a node is computed in MANFEP by assigning the node to one of the adjacent elements.

3.3.2 Evaluation of Mesh Accuracy

The meshes generated are evaluated by comparing the solutions for the space charge free electric field determined using the numerical (FE) and analytical methods (Section 3.2). Tables 3.2a-3.2c present the differences between the two solutions for the various meshes evaluated. The following is a Key to the parameters used in Tables 3.2a-3.2c

Mesh - identifying label.

Ndc - number of nodes on the dc conductor.

Ldc - initial segment length on dc conductor.
(r - radius of dc conductor.)

Lac - initial segment length on ac conductor.
(r - radius of ac conductor.)

g - growth factor.

Order - the order of triangular elements.

Curv. - refers to which element borders are curved to conform with the physical boundaries.

(all - elements on the conductor and artificial boundaries have their sides curved.

cond. - only elements on the conductor boundaries have their sides curved.

none - no curved boundaries are used.)

Ntri - total number of triangular elements in a mesh.

Nodal error, Centroid error, DC cond. error - the difference between the numerical (FE) and analytical (Section 5.2) solutions for the electric field. The root mean square (RMS) and maximum differences are determined.

$$(\text{error})_{\text{RMS}} = \sqrt{\frac{\sum_{i=1}^N \frac{(E_{mi} - E_{ei})^2}{0.5(E_{mi} + E_{ei})}}{N}} \quad (3.14)$$

where E_{mi} and E_{ei} are the solutions for the magnitude of the electric field at point i from the FE method and the Section 5.2 method respectively. The difference is determined separately for: all the nodes, all the triangle centroids and all the dc conductor nodes. The accuracy of a mesh at the dc conductor is important for the imposition of the Kaptsov ($|\frac{d\Phi}{dn}| = E_0$ on the coronating conductor) boundary condition. In Tables 3.2a-3.2c the RMS error is found in the upper left corner of a box and the maximum difference is in the lower right corner.

CPU Time - the time to evaluate the mesh accuracy.

Mesh	Ndc	Ldc	Lac	g	Order	Curv.	Ntri	Nodal error RMS/ Maximum [%]	Centroid error RMS/ Maximum [%]	DC cond. error RMS/ Maximum [%]	CPU time [sec.]
1A2na	4	r	r	1.5	2	none	116	19.14 >100	2.94 11.2	9.36 12.5	6.72
1A3a	4	r	r	1.5	3	all	116	24.55 >100	2.79 22.4	8.85 17.1	18.85
1A3ca	4	r	r	1.5	3	cond.	116	20.06 >100	2.52 14.1	3.99 5.8	13.44
1A3na	4	r	r	1.5	3	none	116	20.9 >100	3.0 13.6	3.5 6.1	9.61
1B3a	5	r	r	1.6	3	all	124	19.8 >100	2.6 13.0	7.9 17.0	18.70
1B3ca	5	r	r	1.6	3	cond.	124	13.1 >100	3.9 20.8	4.2 6.1	15.30
1D3a	4	r	r	1.7	3	all	92	23.3 >100	3.3 22.0	8.8 17.1	12.90
1D3ca	4	r	r	1.7	3	cond.	92	15.5 >100	4.1 18.6	4.3 6.2	9.60
1G3a	4	2r	2r	1.4	3	all	110	19.6 >100	2.7 20.7	12.5 20.0	17.83
1G3ca	4	2r	2r	1.4	3	cond.	110	8.3 53.1	1.9 8.9	8.5 9.4	12.41
1G3na	4	2r	2r	1.4	3	none	110	8.7 52.8	2.2 8.5	7.9 11.1	8.80
1H3ca	4	r/2	r/2	1.5	3	cond.	132	13.7 94.9	3.6 5.9	5.7 58.7	15.60
1I3ca	4	r/2	r	1.4	3	cond.	147	7.9 45.5	1.4 8.0	1.5 2.0	18.22
1J3ca	5	r/3	r	1.5	3	cond.	182	21.4 >100	7.3 40.7	58.9 128.2	25.75
1K3ca	4	r/2	r	1.6	3	cond.	118	9.7 72.0	1.8 8.5	1.7 2.2	14.01
1L3ca	5	0.4r	r	1.5	3	cond.	176	9.4 72.6	1.2 8.0	1.1 1.7	25.07
1M3ca	6	0.3r	r	1.5	3	cond.	238	7.8 67.8	1.1 8.1	0.88 1.3	41.51

Table 3.2a: Error in Finite Element Meshes, Geometry 1.

Table 3.2a allows us to make some comments and draw some conclusions about the FE method and the mesh generation program. The Table shows that the FE method is clearly more accurate at centroids rather than at nodes. The maximum errors occur at nodes on the artificial boundary and at the centroids of triangles adjacent to the artificial boundary. The FE method generally gives less accurate results nearer boundaries. The choices for L_{dc} and L_{ac}

and the growth factor (g) have a significant effect on the shapes of triangles and the numbers of triangles. An increase in the number of elements improves the accuracy of a mesh but also increases the solution time. The use of curved boundaries significantly increases the time of solution. Curving the conductor boundaries improves the accuracy of the solution near the conductors but curving the borders of elements on the artificial boundary does not seem to improve the solution accuracy. Second order elements seem to have almost as good accuracy as third order elements while significantly decreasing the computation time. However, for an unknown reason, MANFEP would not allow curved boundaries to be used with second order elements and therefore meshes using second order elements could not give very accurate results on the dc conductor surface.

Mesh 1M3ca is used for the iterative solution for Geometry 1 unless stated otherwise.

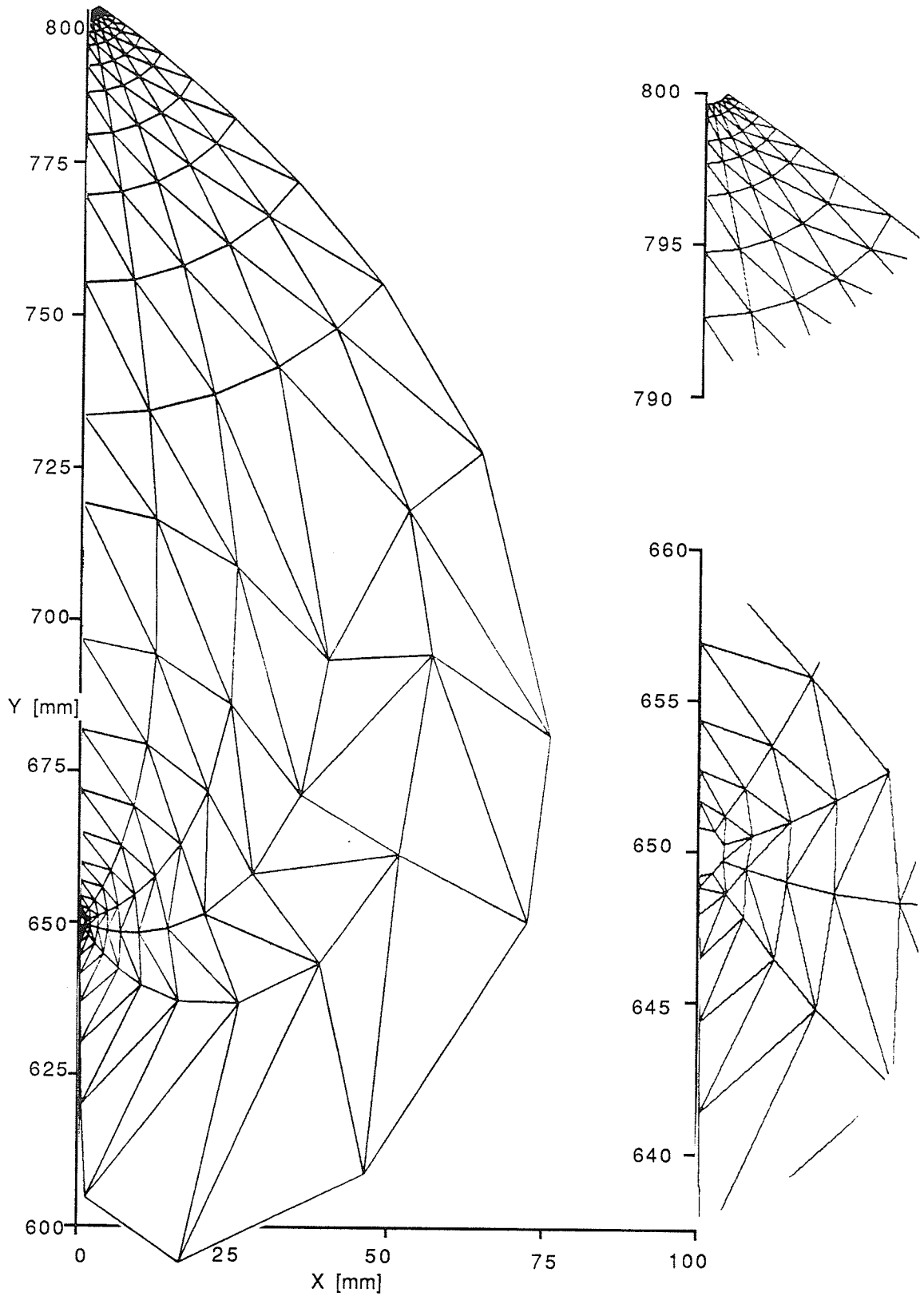


Figure 3.3a: Finite Element Mesh 1M3ca, Geometry 1.

Figure 3.3a shows the mesh for Geometry 1. A magnified view of the mesh in the vicinity of the conductors is on the left.

Mesh	Ndc	Nac	Ldc	Lac	g	Curv.	Ntri	Nodal error RMS/ Maximum [%]	Centroid error RMS/ Maximum [%]	DC cond. error RMS/ Maximum [%]	CPU time [sec.]
2N3ca	5	9	r	r	1.6	cond.	189	17.8 >100	2.6 13.9	3.5 3.8	22.80
2N3na	5	9	r	r	1.6	none	189	19.3 >100	3.2 11.6	2.7 5.0	14.75
2O3ca	5	5	r	r	1.6	cond.	153	26.2 >100	18.6 >100	3.3 3.6	16.07
2P3ca	6	6	r	2r	1.6	cond.	174	17.0 >100	5.7 62.9	3.7 3.9	20.35
2P3na	6	6	r	2r	1.6	none	174	16.0 89.6	3.1 15.5	3.2 4.9	13.13
2Q3ca	5	9	r	r	1.7	cond.	175	17.3 >100	2.9 14.6	3.7 4.0	21.27
2Q3na	5	9	r	r	1.7	none	175	19.0 87.2	3.5 14.7	2.9 5.2	13.43
2R3ca	6	11	r	r	1.7	cond.	218	18.1 >100	2.1 12.5	3.8 4.1	29.55
2R3na	6	11	r	r	1.7	none	218	18.5 >100	2.4 12.4	3.1 4.8	18.73
2S3ca	7	13	0.8r	r	1.4	cond.	351	7.0 61.4	1.3 10.3	1.4 1.6	62.11
2T3ca	6	11	0.8r	r	1.6	cond.	239	11.9 89.5	2.0 10.0	1.6 1.8	34.71

Table 3.2b: Error in Finite Element Meshes, Geometry 2.

The same comments apply to this table as the previous. All parameters are the same as before with the exception that: all the meshes use third order elements and Nac is the number of nodes on the ac conductor. Mesh 2T3ca is used for the iterative solutions.

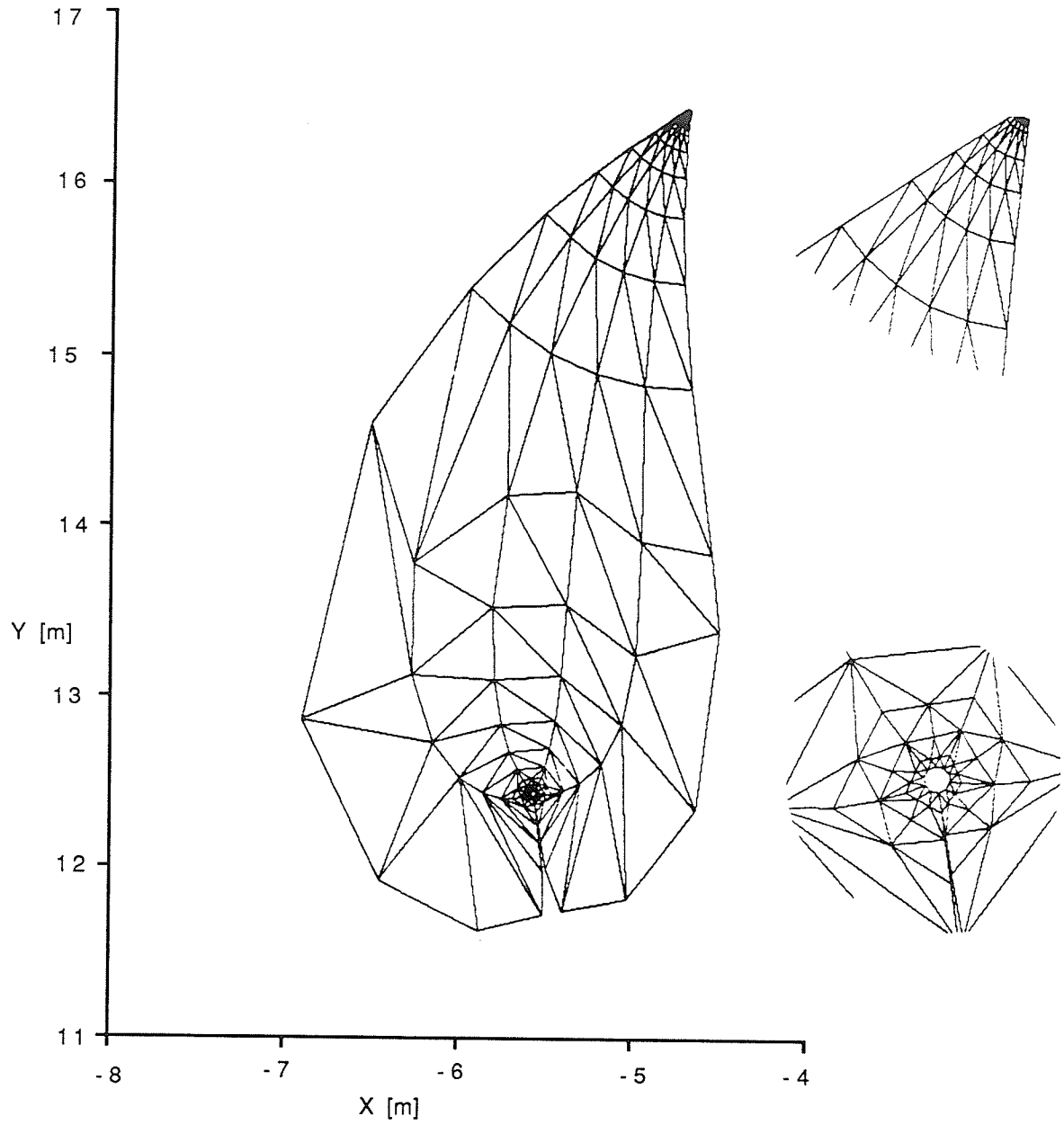


Figure 3.3b: Finite Element Mesh 2T3ca, Geometry 2.

Figure 3.3b shows the mesh used for Geometry 2. The mesh in the vicinity of the conductors, shown to the left, is enlarged 5X the given scale.

Mesh	Ndc	Nac	Ldc	Lac	g	Curv.	Ntri	Nodal error RMS/ Maximum [%]	Centroid error RMS/ Maximum [%]	DC cond. error RMS/ Maximum [%]	CPU time [sec.]
3A3ca	6	11	0.8r	r	1.6	cond.	197	16.0 99.5	2.56 10.8	1.8 2.0	24.82
3B3ca	6	11	0.8r	r	1.58	cond.	201	18.3 75.6	3.23 12.5	2.0 2.2	25.96
3C3ca	6	11	0.8r	r	1.57	cond.	206	19.9 69.4	2.87 17.5	1.7 2.0	26.77

Table 3.2c: Error in Finite Element Meshes, Geometry 3.

All the meshes in Table 3.2c use third order elements. Mesh 3A3ca is used for the iterative solutions.

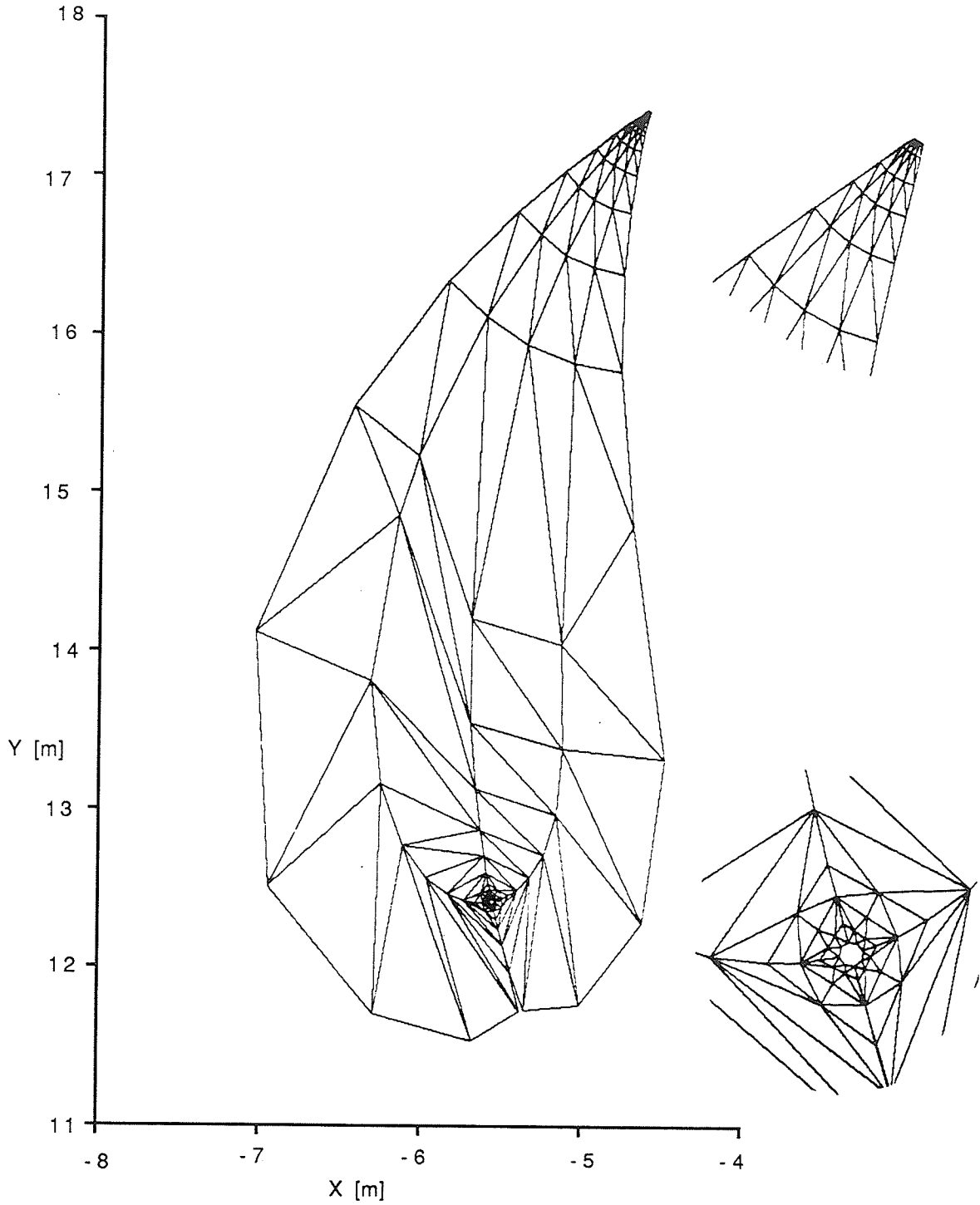


Figure 3.3c: Finite Element Mesh 3A3ca, Geometry 3.

Figure 3.3c shows the mesh used for Geometry 3. The mesh near the conductors, shown to the left, is enlarged 5X the given scale.

3.4 Initial Approximation for the Space Charge

In the Finite Element program used the space charge density is constant within each element. Before the iterative procedure can be begun an initial approximation is needed for the space charge density distribution. This initial approximation for the charge distribution will affect the convergence of the iterative procedure. Two initial approximations are examined, the first uses the Deutsch assumption and the second is a simplified approximation based on a concentric cylinder geometry. The effects of the different initial approximations are compared, in Section 4.3, on the basis of the number of iterations needed to obtain a final solution and a comparison of the accuracy of the final solutions obtained.

3.4.1 Deutsch Initial Approximation

The solution for the space charge distribution using the Deutsch assumption is made using the method of Ciric et al. [14]. The steps in this method are summarized in Appendix A.2.1. All iterative FE results presented use this Deutsch initial approximation unless otherwise noted. Previous researchers have generally used a method using the Deutsch assumption to determine an initial approximation for iterative FE methods [18,19].

3.4.2 Concentric Cylinders Initial Approximation

The concentric cylinders approximation for the space charge is derived from the solution for the space charge distribution in an concentric cylinders geometry derived from the actual geometry. The method summarized in Appendix A.2.2. This initial approximation is simpler and can be calculated more quickly than the initial approximation using the Deutsch assumption.

3.5 Iterative Procedure

In the iterative procedure equations (3.01) and (3.02) are each solved separately, using the FE method, with the boundary conditions given by equations (3.03) and (3.04). The difference between the two solutions for the electric and/or potential fields provides information for an update of the charge distribution approximation. The difference between the electric field at the dc conductor determined by equations (3.01) and (3.02) and the Kaptzov boundary condition ($|-d\Phi/dn|=E_0$ on the coronating conductor) also provides information for the update of the charge distribution. After the update, equations (3.01) and (3.02) are again solved with the new approximation for the space charge distribution. This process is repeated until the difference between the solutions for the electric and potential fields determined from equations (3.01) and (3.02) meets some exit criteria. The difference between electric field on the dc conductor determined from equations (3.01) and (3.02) and E_0 provides a further exit criteria. The update algorithm must be carefully chosen to ensure convergence.

3.5.1 Update Algorithm

The following equation is used for the update algorithm:

$$\rho_{\text{new } i} = \rho_{\text{old } i} \left[1 + \alpha \frac{E_{1i} - E_{2i}}{E_{1i} + E_{2i}} \right] \left\{ \left[1 + \beta \frac{E_0 - E_{1j}}{E_0} \right] \left[1 + \gamma \frac{E_0 - E_{2j}}{E_0} \right] \right\}^{\left[\frac{K-k}{K} \right]} \quad (3.15)$$

where $\rho_{\text{new } i}$ and $\rho_{\text{old } i}$ are the new and old approximations for the space charge density of element i . E_{1i} and E_{2i} are the absolute values of the electric fields at the centroid of element i determined from equations (3.01) and (3.02) respectively. This initial (non-exponentiated) part of this equation is designed to bring convergence between the solutions of equations (3.01) and (3.02). The second (exponentiated) part of the equation enforces the Kaptzov boundary condition. E_0 is the onset electric field determined using Peek's equation (2.5). E_{1j} and E_{2j} are the

absolute values of the solutions for the electric field at dc conductor node j from equations (3.01) and (3.02) respectively. Each dc conductor node is assigned to a corresponding corridor of elements. The parameter K is the total number of elements in a corridor. The value of the integer k is determined by the relative position of an element in a corridor with respect to the dc conductor, beginning at 1 for elements adjacent to the dc conductor and increasing linearly to K for elements adjacent to the ac conductor. This $[(K-k)/K]$ exponent ensures that the correction to enforce the Kaptzov boundary condition has a greater effect near the dc conductor. In equation (3.15) α , β and γ are parameters chosen to ensure convergence.

The applicability and efficiency of different updates is evaluated based on the speed with which they meet the exit criteria. It was found that the CPU time for the iterative procedure for a mesh could be approximated by the following relation:

$$\text{CPU time} \approx 0.7 \times (\text{Number of Iterations}) \times (\text{CPU time to evaluate the accuracy of the mesh}) \text{ [sec.]} \quad (3.16)$$

3.5.2 Exit Criteria

The iterative procedure is terminated when the solutions for the electric and potential fields from equations (3.01) and (3.02) meet the exit criteria. The accuracy of the space charge free field solution of a given FE mesh (determined in Subsection 3.3.2) gives a lower limit on the accuracy of the ionized field solution and the final exit criteria were chosen with this in mind. An evaluation of the suitability of the exit criteria used is given in Subsection 4.4.3.

The exit criteria used are:

$$\Delta V = \left[\frac{\Phi_{1i} - \Phi_{2i}}{0.5(\Phi_{1i} + \Phi_{2i})} \right]_{\text{RMS}} < 0.2 \% \quad (3.17)$$

$$\Delta E = \left[\frac{E_{1i} - E_{2i}}{E_o} \right]_{\text{RMS}} < 0.1 \% \quad (3.18)$$

$$\Delta \rho = \left[\frac{\rho_{\text{new } i} - \rho_{\text{old } i}}{\rho_{\text{old } i}} \right]_{\text{RMS}} < 0.5 \% \quad (3.19)$$

where the RMS (root mean square) difference is determined over all triangle centroids. Also, to ensure that the Kaptzov boundary condition is met:

$$\Delta E_{o1} = \left[\frac{E_o - E_{1j}}{E_o} \right]_{\text{RMS}} < 1.0 \% \quad (3.20)$$

$$\Delta E_{o2} = \left[\frac{E_o - E_{2j}}{E_o} \right]_{\text{RMS}} < 1.0 \% \quad (3.21)$$

where the RMS difference is computed over the dc conductor nodes.

The iterative procedure is stopped when all of the above exit criteria are met simultaneously.

3.5.3 Choice of Update Algorithm Parameters

Three variations on equation (3.15) were evaluated.

Constant α , β and γ

In this procedure α , β and γ are kept constant. The choice for the optimum α , β and γ is determined by the number of iterations needed for convergence.

α	β	γ	Number of iterations to meet exit criteria defined in equation:					meets all exit criteria
			(3.17) ΔV	(3.18) ΔE	(3.19) $\Delta \rho$	(3.20) ΔE_{01}	(3.21) ΔE_{02}	
-1.0	-1.0	-1.0	4	8	48+	7	3	48+
-1.0	-0.5	-0.5	4	2	5	9	4	9
-1.0	-0.2	-0.2	4	2	4	11	4	11
-1.0	-0.2	-0.4	4	2	4	14	3	14
-1.0	-0.4	-0.2	4	2	5	6	4	6
-1.0	-0.6	-0.2	4	2	6	4	5	6
-1.0	-0.5	-0.25	4	2	5	5	4	5
-2.0	-1.0	-0.5	2	1	11	3	2	11
-4.0	-2.0	-1.0	Does not converge					
-0.5	-0.25	-.125	4	8	2	9	8	9

Table 3.3: Convergence of Different Constant α , β and γ 's, Geometry 1, $m=0.95$, $V_{dc}=38$ kV.

Table 3.3 shows the rates of convergence for different values of α , β and γ . The relative values of α , β and γ are adjusted to so that all the exit criteria are met at approximately the same iteration. The best relative values of α , β and γ for convergence were with $\beta=0.5\alpha$, and $\gamma=0.25\alpha$. The speed of convergence generally increases with increasing magnitudes of α , β and γ , but if the magnitudes are too large the procedure becomes unstable and diverges. The 48+ number of iterations indicates that the solutions were converging slowly, but had not met the exit criteria, when the procedure was stopped at 48 iterations. The iterative procedure diverged if any of α , β or γ were positive.

Variable α , β and γ

The parameters α , β and γ need not remain constant throughout the update. They can be changed as the number of iterations increases and/or varied for different elements/nodes based on the position of the element/node within the mesh.

In the Variable α , β and γ update used the α for each element (and the β and γ for each dc conductor node) is changed after each iteration based on whether the outcome of the previous iteration was successful. A successful iteration is one where the difference between E_1 and E_2 at that centroid/node decreases relative to the previous iteration. After a successful step α , β or γ is multiplied by the success factor. If the step is unsuccessful, α , β or γ is multiplied by the failure factor. In this update α , β and γ are initially set equal to 1.0 everywhere.

Success factor	Failure factor	Number of iterations to meet exit criteria defined in equation:					meets all exit criteria
		(3.17) ΔV	(3.18) ΔE	(3.19) $\Delta \rho$	(3.20) ΔE_{o1}	(3.21) ΔE_{o2}	
1.10	-0.90	Does not converge					
1.05	-0.95	36	4	48+	7	19	48+
1.02	-0.98	21	4	18	7	21	21

Table 3.4: Variable α , β and γ Update Convergence, Geometry 1, $m=0.95$, $V_{dc}=38$ kV.

As Table 3.4 shows, this method can converge but it is slower than using well chosen, constant α , β and γ parameters.

Update based on the Potential

Very little information is given in the literature about an update algorithm. References [16] and [19] give updates based on the potential, of the form:

$$\rho_{new} = \rho_{old} \left[1 + f \frac{(\Phi_1 - \Phi_2)}{0.5(\Phi_1 + \Phi_2)} \right] \tag{3.22}$$

Where Φ_1 and Φ_2 are the solutions to equations (3.01) and (3.02) for the potential and f is an acceleration constant. No information is given on the enforcement of the third boundary condition. In the present work, an update based on the solution for the potential was tested.

$$\rho_{\text{new } i} = \rho_{\text{old } i} \left[1 + \alpha \frac{\Phi_{1i} - \Phi_{2i}}{\Phi_{1i} + \Phi_{2i}} \right] \left\{ \left[1 + \beta \frac{E_o - E_{1j}}{E_o} \right] \left[1 + \gamma \frac{E_o - E_{2j}}{E_o} \right] \right\}^{\left[\frac{K-k}{K} \right]} \quad (3.23)$$

Φ_{1i} and Φ_{2i} are the potentials at the centroid of triangle i , from equations (3.01) and (3.02) respectively. The only difference between this equation and equation (3.15) is that the potential is used in the initial (non-exponentiated) part of the equation instead of the magnitude of the electric field.

α	β	γ	Number of iterations to meet exit criteria defined in equation:					meets all exit criteria
			(3.17) ΔV	(3.18) ΔE	(3.19) $\Delta \rho$	(3.20) ΔE_{o1}	(3.21) ΔE_{o2}	
-1.0	-0.2	-0.4	12	48+	0	48+	48+	48+
-10.0	-0.5	-0.25	Does not Converge					
-5.0	-0.5	-0.25	6	48+	6	31	48+	48+
-1.0	-0.5	-0.25	10	48+	0	48+	48+	48+

Table 3.5: Potential Update Convergence, Geometry 1, $m=0.95$, $V_{dc}=38$ kV.

Table 3.5 demonstrates that this potential based update takes longer to converge than the electric field based update (Table 3.3). Furthermore, in this case α is negative while in the references, [16] and [19], the corresponding parameter, f , (equation (3.22)) is implied to be positive. All potential based updates using positive α 's diverged.

3.5.4 Comments on Iterative Procedure

The update with α , β and γ maintained constant is more efficient than the other updates examined and is used throughout the remainder of this work. Values of: α between -4 and -1, β between -2 and -0.5, and γ between -1 and -0.25 are used for the update with the optimum

values depending on the geometry and/or the mesh. In general, for a more accurate FE mesh larger magnitudes of α , β and γ can be used and convergence is faster.

Figures 3.4a-3.4e show the changes in the exit criteria parameters with respect to the number of iterations for three different sets of α , β and γ values.

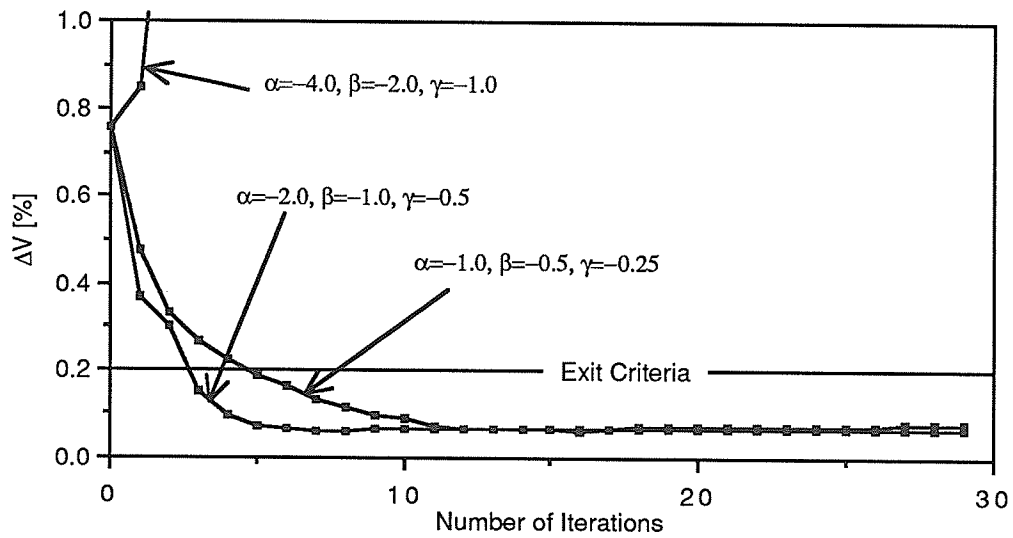


Figure 3.4a: Exit Parameter ΔV Versus Iteration, Geometry 1, $m=1.0$, $V_{dc}=50$ kV.

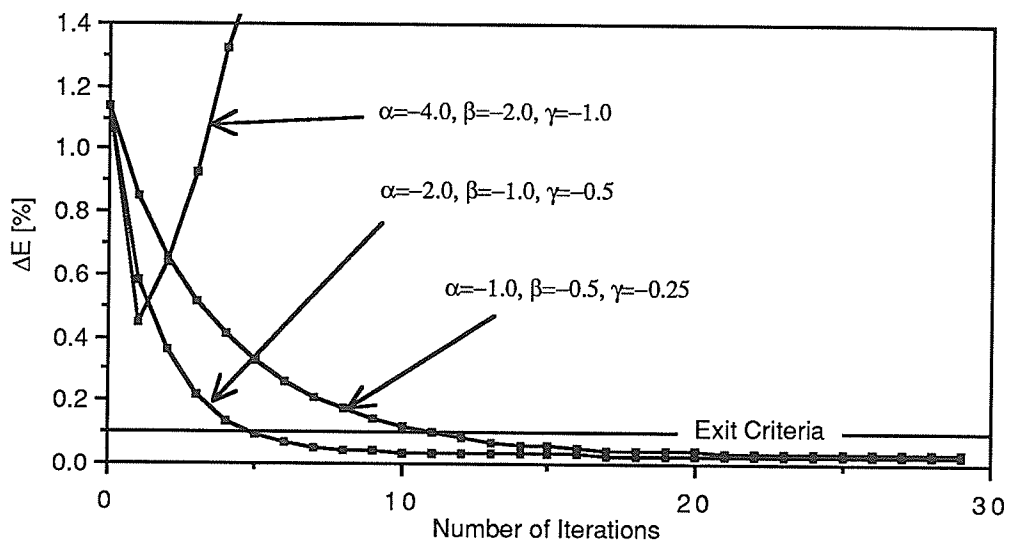


Figure 3.4b: Exit Parameter ΔE Versus Iteration, Geometry 1, $m=1.0$, $V_{dc}=50$ kV.

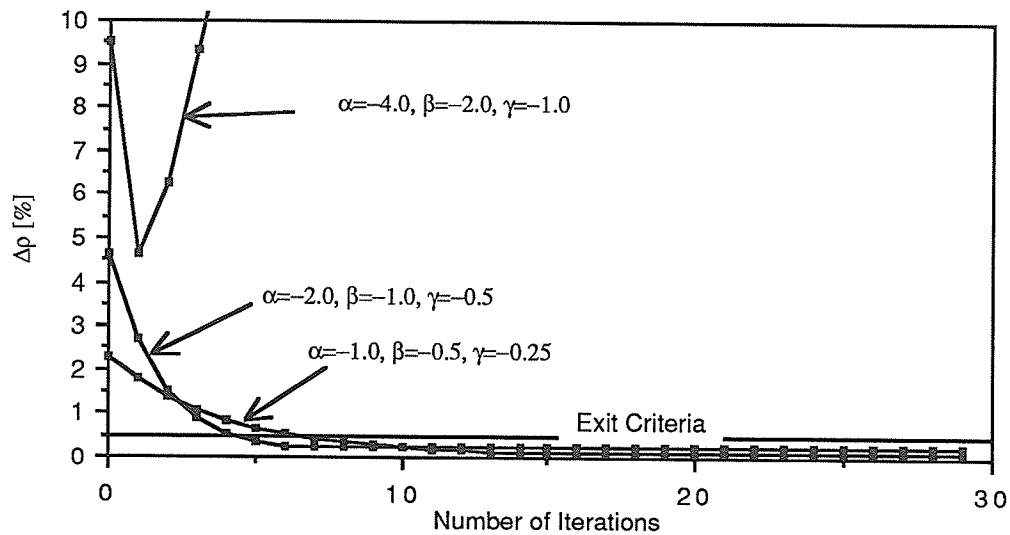


Figure 3.4c: Exit Parameter $\Delta\rho$ Versus Iteration, Geometry 1, $m=1.0$, $V_{dc}=50$ kV.

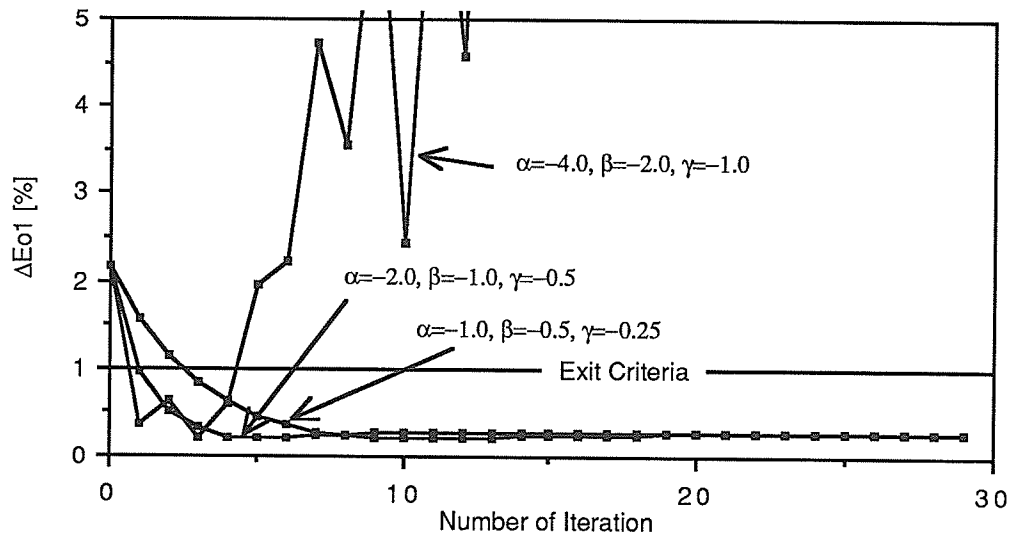


Figure 3.4d: Exit Parameter ΔE_{o1} Versus Iteration, Geometry 1, $m=1.0$, $V_{dc}=50$ kV.

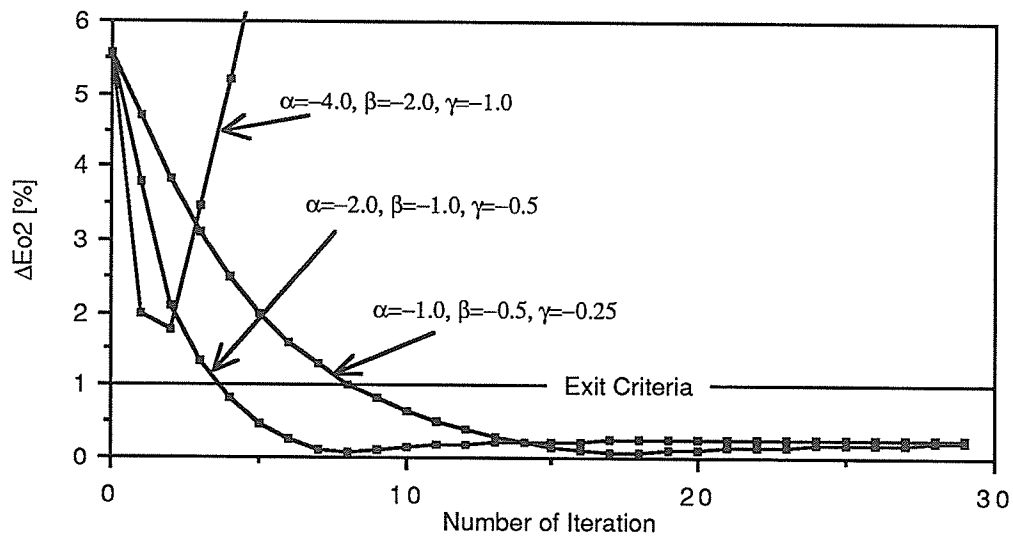


Figure 3.4e: Exit Parameter ΔE_{O2} Versus Iteration, Geometry 1, $m=1.0$, $V_{DC}=50$ kV.

The preceding figures give a more complete picture of the effects of α , β and γ on the convergence of the various exit criteria. The $\alpha=-4.0$, $\beta=-2.0$, $\gamma=-1.0$ update diverges in this case. When α , β and γ have a relatively large magnitude, the exit criteria parameters do not converge monotonically and as a result, for large magnitudes of α , β and γ , (e.g. $|\alpha|>2$) the iterative procedure is not stopped until the all the exit criteria are met for two consecutive iterations.

The Effect of the Mesh Accuracy on Convergence

As stated the accuracy of a mesh affects the number of iterations needed for convergence.

Mesh	Centroid error RMS [%]	DC Cond. error RMS [%]	Number of lters. for convergence	CPU time [sec.]
1I3ca	1.4	1.5	12	129.52
1M3ca	1.1	0.88	11	283.45

Table 3.6a: Effect of Mesh on Convergence, Geometry 1, $m=1.0$, $V_{DC}=50$ kV.

Mesh	Centroid error RMS [%]	DC Cond. error RMS [%]	Number of lters. for convergence	CPU time [sec.]
2N3ca	2.6	3.5	18	333.94
2T3ca	2.0	1.6	13	378.77

Table 3.6b: Effect of Mesh on Convergence, Geometry 2, $V_{dc}=300$ kV.

In the above tables the errors are the differences between the numerical and analytic solutions for the space charge free fields as determined in Subsection 3.3.2. The α , β and γ parameters used in the update are the same for the different meshes. Tables 3.6a and 3.6b show that a mesh with a more accurate field solution reduces the number of iterations needed for convergence. This result also tends to confirm the assumption that a mesh giving a more accurate space charge free field solution will also give a more accurate ionized field solution. These results also show that but that the overall solution time increases for the more accurate mesh due to the greater time needed for each iterations.

Information on the effect of the initial approximation for the space charge distribution on convergence and the effect of the dc voltage on convergence is given in Subsection 4.3.1.

3.6 Calculation of the Injected Corona Current

The injected corona current is the dc current injected into the ac conductor by corona. This current was determined by two methods.

3.6.1 Integration over DC Conductor Surface

The first method of determining the dc current injected into the (grounded) ac conductor during corona is to determine the current leaving the dc conductor within the limits of the artificial boundaries is determined. All this current must reach the ac conductor.

$$I_{inj} = k E_0 r \int_{\theta_{min}}^{\theta_{max}} \rho d\theta \quad (3.24)$$

This equation is integrated using the trapezoidal rule.

3.6.2 Integration over the Region of Interest

The preceding method for determining the dc injected current has the disadvantage that it uses results from only one section of the region of interest to determine the injected current. There may be errors in the calculation of the space charge distribution on the surface of the dc conductor which are not present elsewhere. In order to eliminate this possibility a second method of determining the dc injected current is tested which uses the solution for the ionized field throughout the region of interest and should average any errors which occur in the solution for the ionized field. In this method the corona current passing through each element in the same direction as the space charge free electric field is determined. The average current for each corridor is determined by averaging the current through all the elements of that corridor. The total current is then the sum of the averages for all corridors.

Corridor Number	Current in Corridor [$\mu\text{A}/\text{m}$]		
	Average	Minimum	Maximum
1	2.68	2.54	2.81
2	2.52	2.36	2.63
3	2.08	1.92	2.13
4	1.44	1.20	1.59
5	0.665	0.482	0.803

Table 3.7: Limits on the Current in a Corridor, Geometry 1, $m=1.0$, $V_{dc}=50$ kV.

Table 3.7 shows the limits on the current through each element of a corridor in Geometry 1. The corridors are numbered consecutively from the axis of symmetry (Figure 3.3a). Each corridor is one element wide and consists of approximately 50 elements. The variation of the current within a corridor gives some idea of the accuracy of the calculation of the current. The most significant variation is in the fifth tube. This tube is adjacent to the

artificial boundary and as noted in Section 3.3 the FE method gives less accurate results near boundaries and this must be responsible for some of this variation. However the variation may also be caused because the Deutsch assumption is not a good approximation in this region, suggesting that the artificial boundary is poorly chosen. In the case of the total current the averaging and the fact that the fifth corridor provides only a small portion of the total current should eliminate most of the effects of any inaccuracies.

3.6.3 Comparison of Methods for Determining the Injected Current

The results from the two methods for determining the dc injected current are compared below.

Vdc [kV]	Injected Current [uA/m]	
	dc conductor integration	overall integration
38.0	4.63	4.61
40.0	6.75	6.73
45.0	13.1	13.0
50.0	20.7	20.7
55.0	29.7	29.6
60.0	39.9	39.8

Table 3.8: Comparison of Methods for Determining dc Injected Current, Geometry 1, $m=0.95$.

There is almost no difference between the results for the total current determined by the two methods. Therefore the method of integrating around the dc conductor is used as it is simpler.

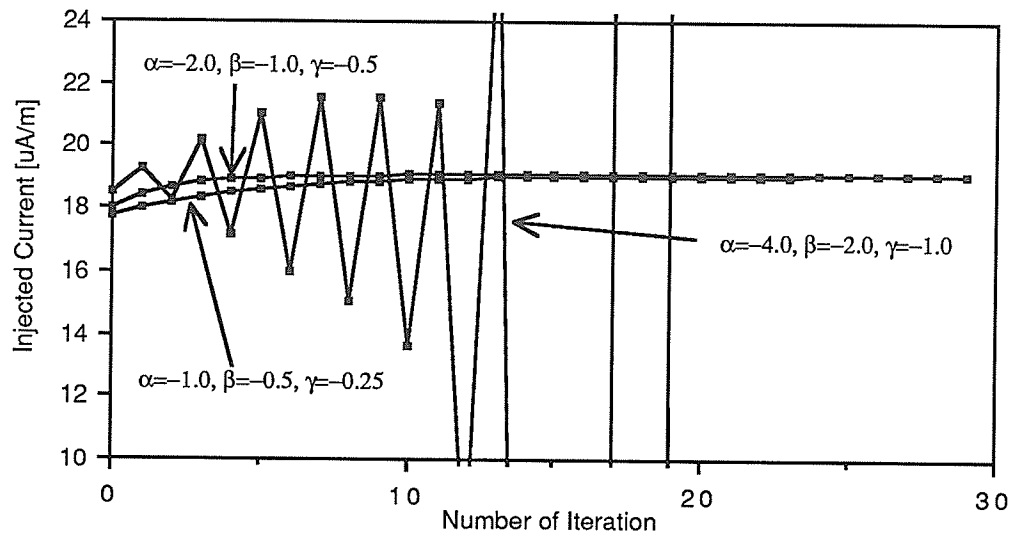


Figure 3.5: Injected Current Versus Iteration, Geometry 1, $m=1.0$, $V_{DC}=50$ kV.

Figure 3.5 is a companion to Figures 3.4a-3.4e, showing the dc current injected into the ac conductor in Geometry 1 as a function of the number of iterations for three sets of α , β and γ values.

Chapter 4

RESULTS OF ITERATIVE FINITE ELEMENT METHOD

This chapter presents the results for the dc injected current determined by the iterative Finite Element method presented in the previous chapter. The effect of a non-zero ac potential is considered in the next chapter.

4.1 Comparison with Experimental Results

Experimental results giving the dc current injected into the ac line are available for the laboratory line [23]. The laboratory line has the dimensions of Geometry 1 and is three meters long. The accuracy of the experimental results is poor, particularly for low levels of corona.

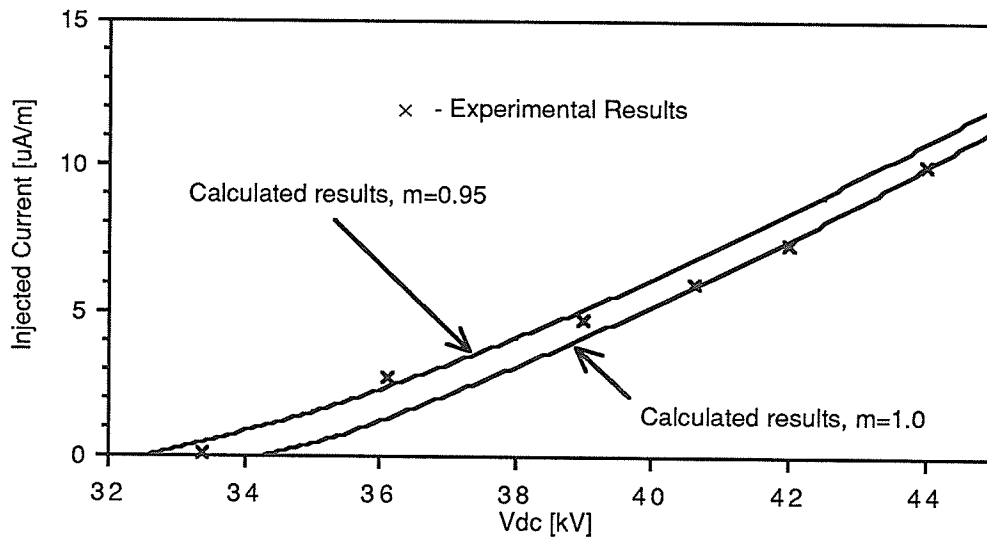


Figure 4.1: dc Injected Current - Experimental and Calculated, Geometry 1, $V_{ac}=0$.

Figure 4.1 shows the dc current injected into the ac line from the dc line in Geometry 1. The calculated results are determined by the iterative Finite Element method with the Deutsch assumption used to determine the initial space charge approximation. The calculated results are in broad agreement with the experimental for a surface factor of between 0.95 and 1.0.

4.2 Comparison of Deutsch and Finite Element Solutions

As mentioned, the Deutsch assumption states that the direction of the electric field is unaffected by the presence of the space charge. In this section the injected current determined by the method using the Deutsch assumption [14] (Subsection 3.4.1) is compared with the injected current determined using the iterative Finite Element method. As noted previously, the iterative FE method does not eliminate the Deutsch assumption completely but imposes it on the artificial boundary. Also, the iterative FE method uses the space charge determined by the Deutsch assumption method as an initial approximation. The method employing the Deutsch assumption should give accurate results for low levels of corona - where the magnitude of the space charge is small and thus has limited effect on the direction of the electric field.

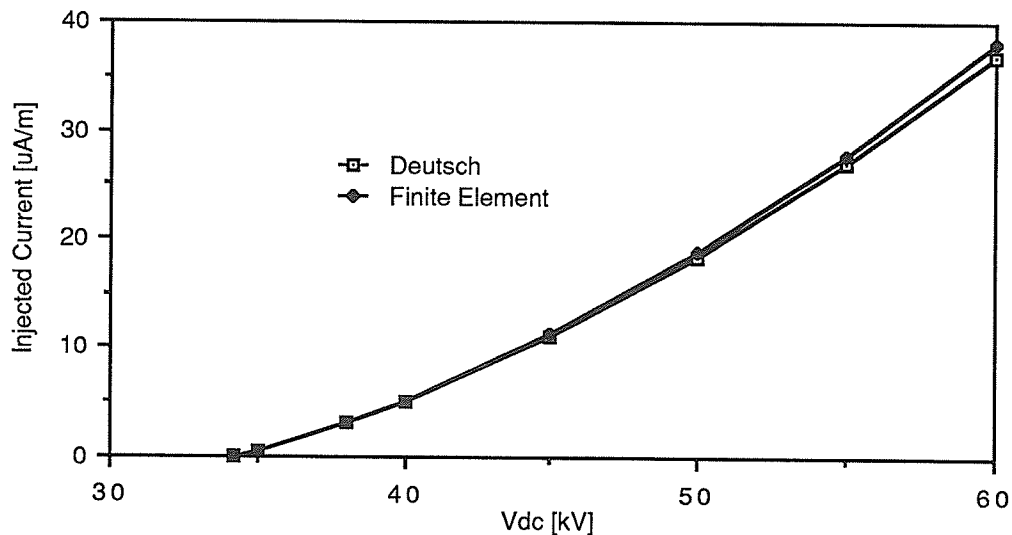


Figure 4.2a: dc Injected Current - Deutsch and Finite Element, Geometry 1, $m=1.0$, $V_{ac}=0$.

Figure 4.2a shows that the Deutsch and Iterative Finite Element methods give almost the same current-voltage characteristics for Geometry 1. For higher voltages the Finite Element method gives slightly greater values for the injected current than the Deutsch method but the difference is not significant. The experimental results are for dc voltages less than 45 kV; in this range of voltages the Deutsch and Finite Element solutions are practically identical.

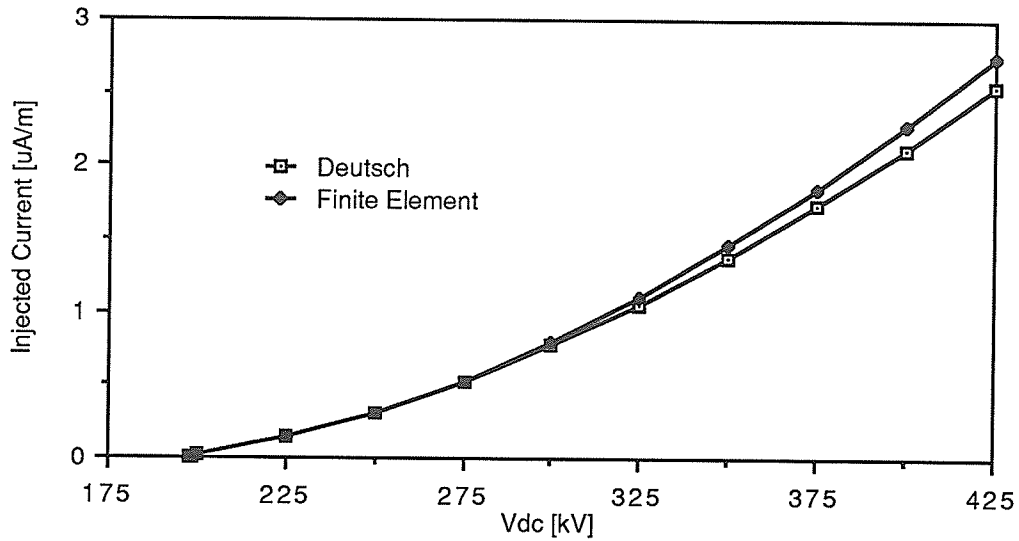


Figure 4.2b: dc Injected Current - Deutsch and Finite Element, Geometry 2, Vac=0.

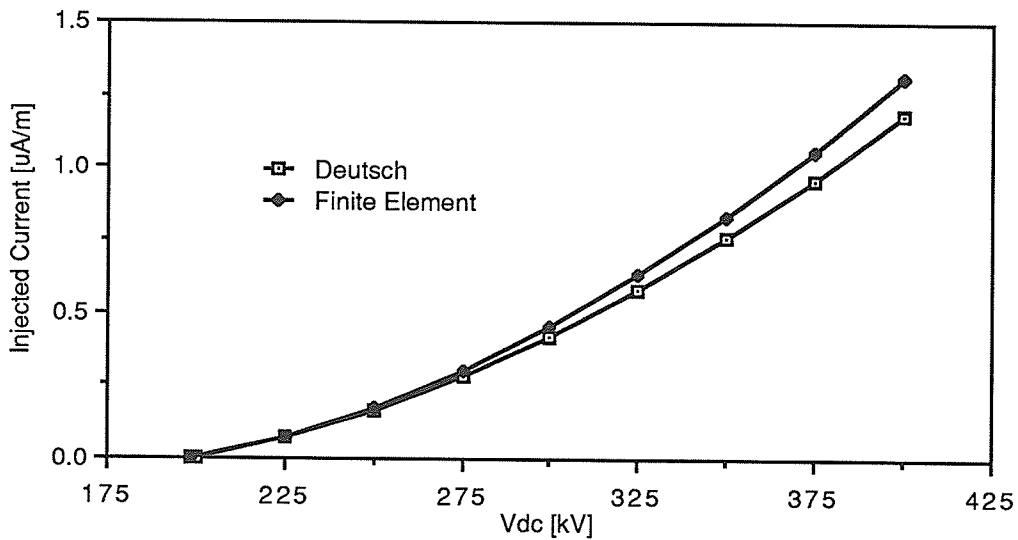


Figure 4.2c: dc Injected Current - Deutsch and Finite Element, Geometry 3, Vac=0.

Figures 4.2b and 4.2c show similar results as Figure 4.2a. The Deutsch and Finite Element methods give very similar results for low levels of corona, while for higher levels of corona the Finite Element method gives slightly higher values for the injected corona current.

The Deutsch approximation method is considerably simpler to implement and faster than the FE method. The CPU time to determine the Deutsch solution at the nodes of a given mesh is

approximately equal to the time for 1.5 iterations of the FE method using the same mesh. The above results indicate that the Deutsch assumptions does not have a significant effect on the injected current confirming the conclusion of Janischewskyj et al. [18] that methods using the Deutsch assumption give adequate results.

4.3 Comparison of the Initial Approximations

The two initial approximations for the space charge distribution are the one using the Deutsch assumption and a simplified approximation based on an "equivalent" concentric cylinders geometry (Section 3.4).

4.3.1 Speed of Convergence

The relative speeds of convergence of the two methods gives some idea of the advantages of the simplified initial approximation. The longer CPU time needed to evaluate the Deutsch initial approximation can be included by adding 1.5 iterations to the number of iterations needed for convergence. The time needed to evaluate the Concentric Cylinders initial approximation is negligible by comparison.

Vdc [kV]	Number of Iterations for convergence:	
	Deutsch	Concentric Cylinders
34.2	Corona Onset	Corona Onset
35	13	30+
38	12	37
40	12	39
45	11	26
50	11	23
55	12	22
60	12	22

Table 4.1a: Convergence for Deutsch and Concentric Cylinders Initial Approximations, Geometry 1, $m=1.0$, $\alpha=-1.0$, $\beta=-0.5$, $\gamma=-0.25$.

Table 4.1a shows that the Deutsch initial approximation provides substantially faster convergence than the concentric cylinders initial approximation.

Vdc [kV]	Number of Iterations for convergence:	
	Deutsch	Concentric Cylinders
198.5	Corona Onset	Corona Onset
200	30+	-
225	21	23
250	21	17
275	21	15
300	21	14
325	21	12
350	21	11
375	21	11
400	21	11

Table 4.1b: Convergence for Deutsch and Concentric Cylinders Initial Approximations, Geometry 3, $\alpha=-2.0$, $\beta=-1.0$, $\gamma=-0.5$.

Table 4.1b shows that the Concentric Cylinders initial approximation converges faster for Geometry 3. (Different values of α , β and γ were used in the updates for the two different initial approximations for Geometry 2 and the results for the number of iterations for convergence cannot be compared.)

As tables 4.1a and 4.1b give contradictory results, convergence must be dependant on additional factors. To get a better understanding of the effects of the initial approximation on convergence the following two figures show the changes in the ΔV parameter as a function of the number of iterations for the two different initial approximations. The exit criteria on the ΔV parameter was always the last of the five exit criteria (equations (3.17)-(3.21)) to be met for Geometry 3 and therefore these figures should give a good measure of the accuracy of the solution after each iteration.

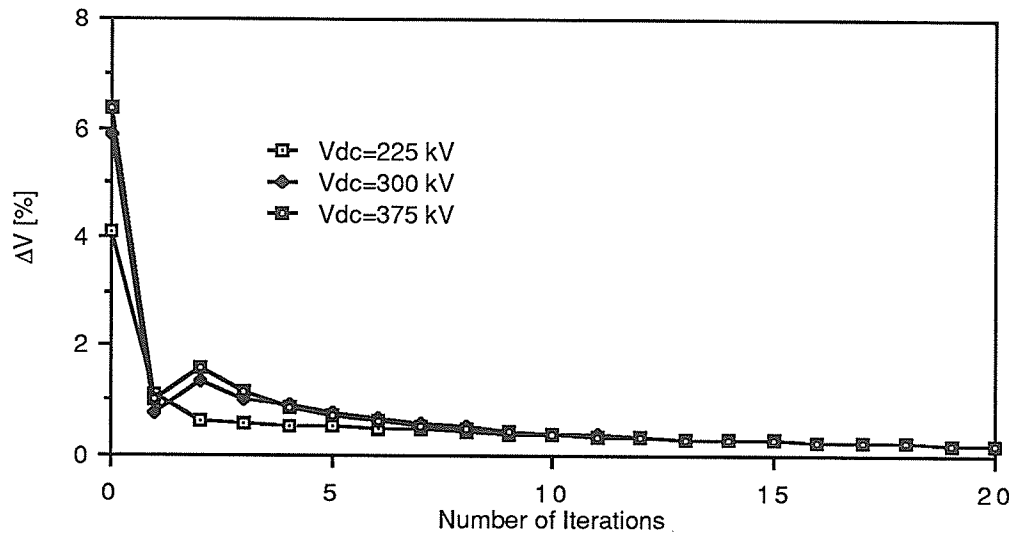


Figure 4.3a: Exit Parameter ΔV versus Iteration, Geometry 3, Deutsch initial approximation.

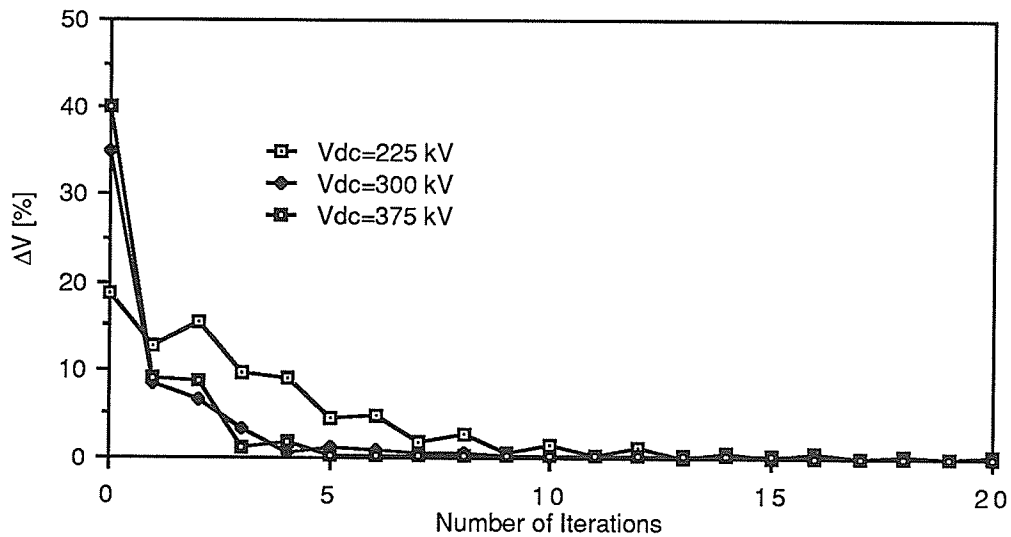


Figure 4.3b: Exit Parameter ΔV versus Iteration, Geometry 3, Concentric Cylinders initial approximation.

Figures 4.3a and 4.3b show two effects of the initial approximation on the convergence of the iterative FE procedure. The first is that at the start of the procedure using the Concentric Cylinders initial approximation ΔV is much larger (approximately 10X larger) than ΔV for the procedure using the Deutsch initial approximation. This agrees with our expectations that the Deutsch initial approximation is more accurate than the Concentric

Cylinders initial approximation. The greater initial accuracy of the Deutsch initial approximation was observed for every geometry. The second effect of the initial approximation shown in Figures 4.3a and 4.3b is that the procedure using the Concentric Cylinders initial approximation meets the exit criteria ($\Delta V < 0.2\%$) before the procedure using the Deutsch initial approximation. This indicates that while the Concentric Cylinder initial approximation is less accurate than the Deutsch, the relative decrease in ΔV for each iteration of procedures using the Concentric Cylinder initial approximation is greater than that for procedures using the Deutsch initial approximation. However this effect was not observed for every geometry. Specifically, for Geometries 2 and 3 for procedures using the Concentric Cylinder initial approximation the relative decrease in the exit parameters for each iteration was greater than for procedure using the Deutsch initial approximation, while for Geometry 1 the initial approximation did not affect the relative decrease in the exit parameters. This coupled with the evidence of Tables 4.1a and 4.1b leads to the conclusion that the effect of the initial approximation on the number of iterations needed for convergence depends greatly on the line geometry. There is no obvious reason why this should be so.

Figures 4.3a and 4.3b allow some observations on the effect of the dc potential on the convergence of the iterative procedure. These figures show that the initial ΔV is greater for greater potentials while Tables 4.1a and 4.1b show that the number of iterations needed for convergence decreases as the dc potential increases. This leads to the conclusion that the relative reduction in the exit criteria parameters, per iteration, increases as the dc potential increases. This can be explained by the greater effect the space charge distribution has on the ionized field when the dc potential increases. For a dc potential near corona onset there is only a small amount of space charge and as a result the accuracy of the space charge distribution does not have a significant effect on the ionized field. In this case the ionized field is similar to the space charge free field. For a greater dc potential more space charge will be created and the space charge distribution will have a significant effect on the ionized field. The net result

of the above is that the accuracy of the space charge distribution and the accuracy of the ionized field solution will be more closely linked for higher dc potentials.

4.3.2 DC Injected Current

In this section the solutions for the dc current injected in the ac line obtained with different initial approximations are examined.

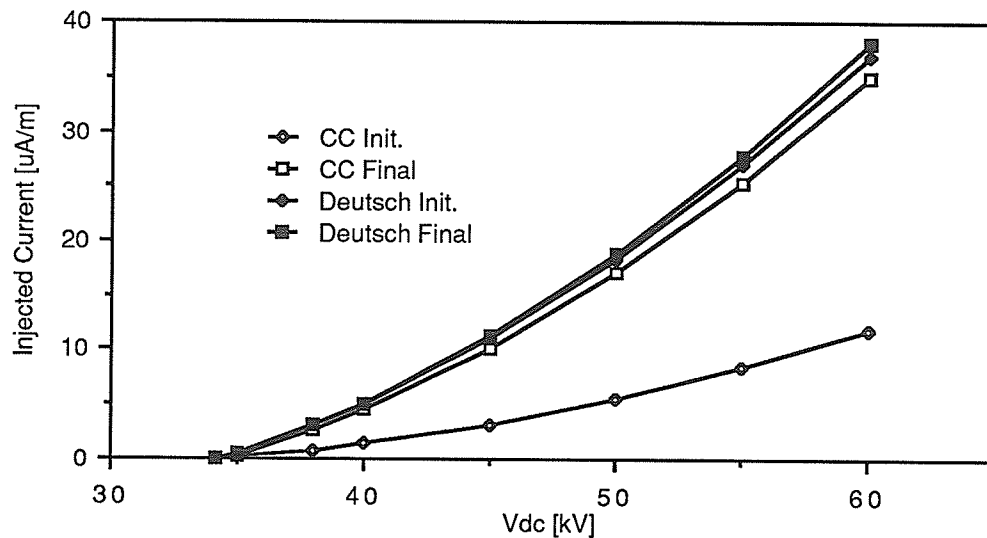


Figure 4.4a: dc Injected Current - Comparison of the effect of the Initial Approximation, Geometry 1, $m=1.0$.

In the legend for the above figure, Deutsch and CC refer to the Deutsch and Concentric Cylinders initial approximations, while Init. refers to the injected current determined from the initial approximation for the space charge and Final refers to injected current determined from the solution for the space charge distribution after the iterative procedure meets the exit criteria. E.g. Deutsch Init. is the injected current determined using the Deutsch assumption solution (Subsection 3.4.1), while Deutsch Final is the iterative FE solution which uses the Deutsch assumption solution for the initial space charge approximation. Figure 4.4a shows that final results obtained for the injected current with the different initial approximations in Geometry 1 are close. The accuracy of the dc injected current obtained from Concentric Cylinders initial approximation is very poor.

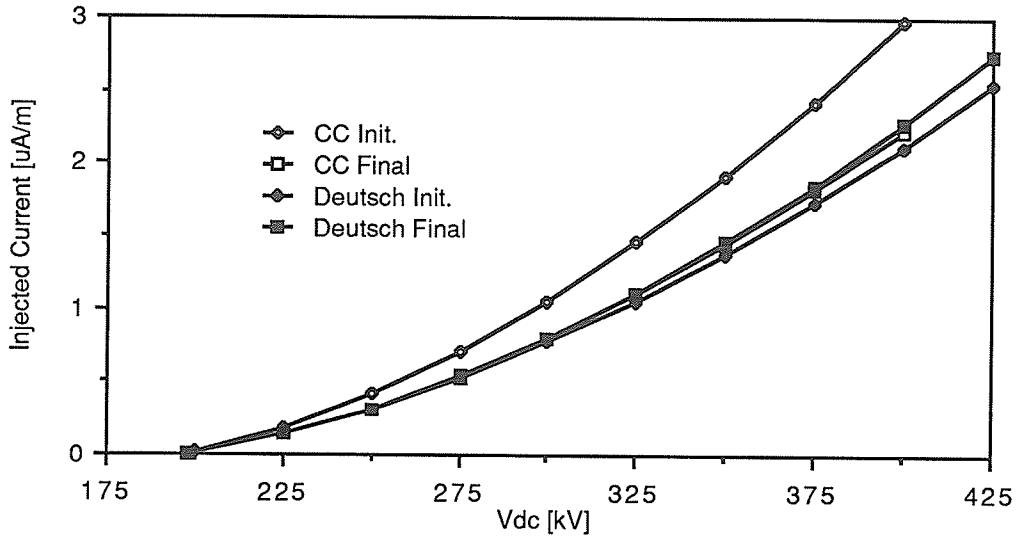


Figure 4.4b: dc Injected Current - Comparison of the effect of the Initial Approximation, Geometry 2.

The final solution for the injected current in Geometry 2 do not appear to be affected by the initial approximation. For this geometry the Concentric Cylinders initial approximation is greater than the final result while for Geometry 1 it was significantly lower than the final results.

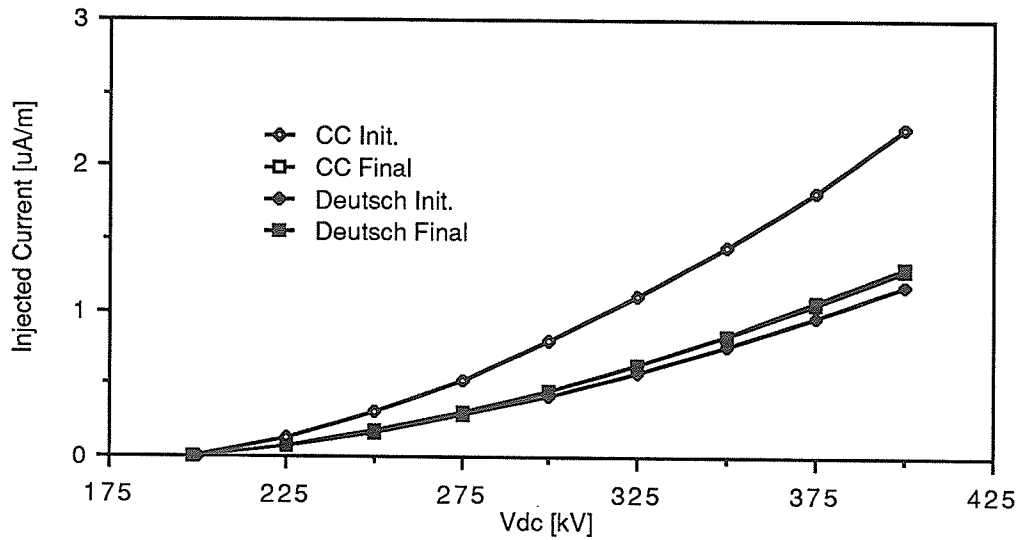


Figure 4.4c: dc Injected Current - Comparison of the effect of the Initial Approximation, Geometry 3.

In Figure 4.4c the final solutions for the dc injected current obtained with the different initial approximations are indistinguishable. Figures 4.4a-4.4c demonstrate that the final solution for the dc current injected into ac conductors is not affected by the initial approximation for the space charge distribution.

4.3.3 Space Charge Distribution on the Coronating Conductor

The variation of the space charge density around the conductor surface can also be determined from the various solutions.

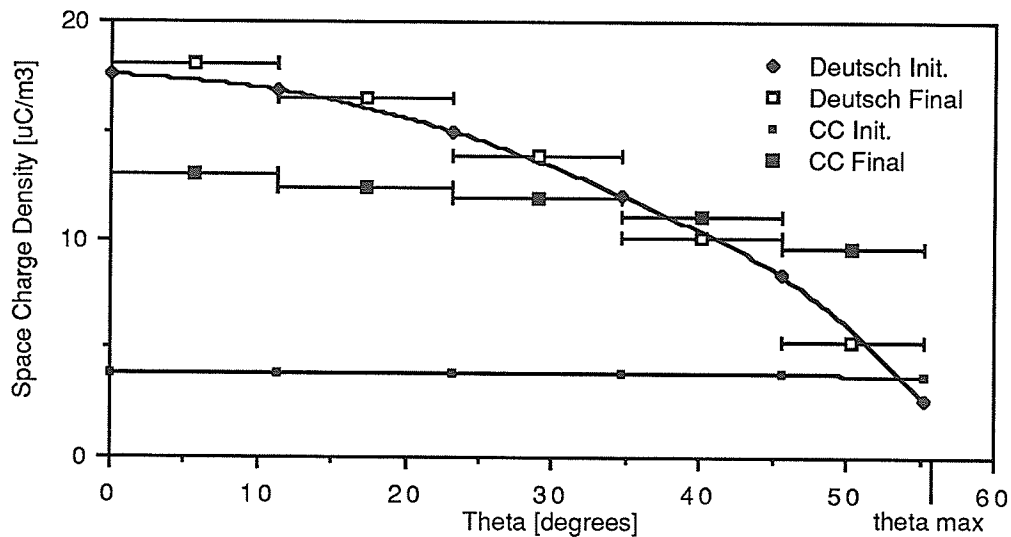


Figure 4.5a: Variation of Space Charge around dc Conductor Surface, Geometry 1, $m=1.0$, $V_{DC}=50$ kV.

The above figure shows the distribution of the space charge on the part of the coronating conductor within the region of interest. The space charge within each triangle in the FE method is constant and is shown as such in this figure to emphasize the non-smooth nature of modelling the space charge in the FE method.

Figure 4.5a shows a substantial difference between the final solutions obtained for the space charge distribution on the surface of the dc conductor using the different initial approximations. The low magnitude of the Concentric Cylinders initial approximation is to be expected given the low magnitude of the current-voltage characteristics determined from this

approximation (Figure 4.4a). The fact that the initial approximation for the space charge distribution affects the final result indicates that the final solution may be non-unique. The dc injected current is proportional to the area under the space charge density curves which explains why the results for the dc injected current obtained using the two different initial approximations were very similar while the results for the space charge density differ.

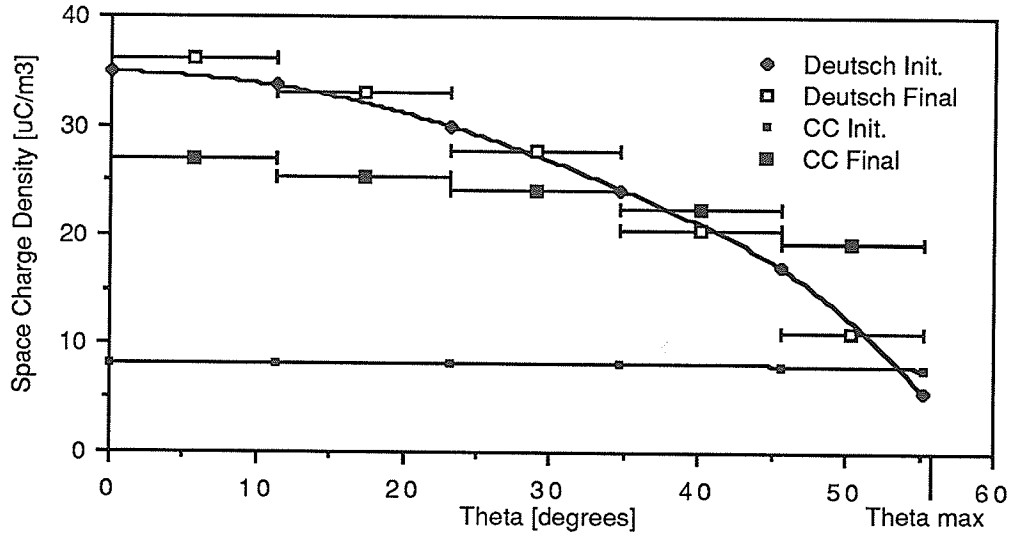


Figure 4.5b: Variation of Space Charge around dc Conductor Surface, Geometry 1, $m=1.0$, $V_{dc}=60$ kV

Figure 4.5b demonstrates that the trends observed in Figure 4.4a are also valid for higher levels of corona activity.

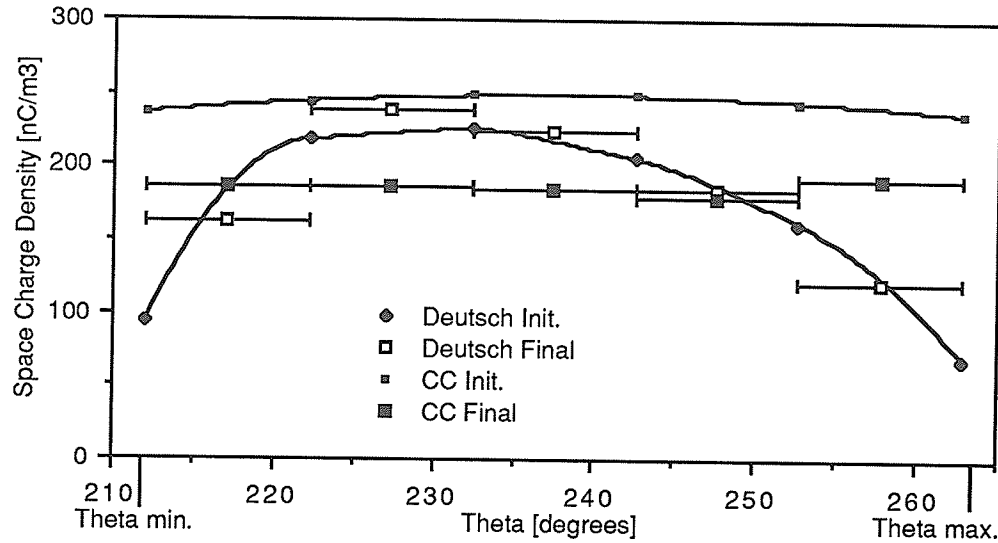


Figure 4.5c: Variation of Space Charge around dc Conductor Surface, Geometry 2, Conductor 1, $V_{dc}=300$ kV.

Again Figure 4.5c shows the final results for the space charge distribution on the dc conductor obtained using the two initial approximations are also significantly different for the second geometry.

In all the results for the space charge distribution on the dc conductor surface, the Deutsch assumption solution is close to the Finite Element solution using the Deutsch initial approximation while the Finite Element solution using the concentric cylinder initial approximation is close to neither.

4.4 Accuracy of the Iterative FE Results

The difference between the Finite Element solutions obtained with different initial approximations suggests that an evaluation of the accuracy of the Finite Element results is needed. There is no exact solution known for the problem considered and as a result the accuracy of the solution obtained using the iterative Finite Element method is difficult to determine.

Three methods are used to evaluate the accuracy of the finite element solution. The first method is to examine the error introduced in each step of the FE procedure and estimate

the effect of this error on the final solution. The second is to compare the final results obtained with experimental results. The third method is to compare the final solutions obtained using different update versions. E.g. change part of the procedure and examine the effect this has on the final solution. Each method has its own advantages and limitations.

4.4.1 Inaccuracy Inherent in the Iterative FE Method

The accuracy of the space charge free solution determined using each mesh was examined in Subsection 3.3.2. The solutions to each of equations (3.01) and (3.02) using the same meshes can be assumed to have similar errors. In addition, error is introduced by the difference between the final solutions for the electric and potential fields from (3.01) and (3.02) as set by the exit criteria. The error in the final solutions for the ionized field should be a combination of these two errors. This should result in an error roughly on the order of <2% rms and <5% maximum in the final solutions for the ionized field given that all assumptions are valid.

The accuracy of the solution obtained for the space charge distribution can be estimated from the accuracy for the solutions to the electric and potential fields. However as noted in Subsection 4.3.1, the solution for the ionized field is not closely linked with that for the space charge, particularly near onset. As a result the accuracy of the solution for the space charge distribution is unknown but it is assumed to be less accurate than the solutions for the ionized field.

The solution for the injected current is determined from the space charge density at the dc conductor and should be as accurate as the solution for the space charge density.

4.4.2 Comparison with Experimental

The accuracy of the solution method can only be determined by comparing it with experimental results. The comparison is limited because there are only experimental results for the total injected current and these experimental results include the effects of inaccuracies

in the experiment. Both the Deutsch and the iterative Finite Element results agree well with the experimental results (Figure 4.1) but this is not conclusive proof of the accuracy of the method as errors in the method may well cancel giving a deceptively accurate result for the total current.

4.4.3 Effect of the Initial Approximation

The accuracy of the solution can also be examined by varying the solution method and determining the effects of these variations in the method on the final result. As shown in the previous section the initial approximation for the space charge distribution has a significant effect on the final space charge distribution and as a result this will be examined more thoroughly. The difference between the final solutions obtained using different values of the α , β and γ update parameters could also be examined, however the effect of the values of the update parameters on the final solution is smaller than the effect of the initial approximation for the space charge distribution and therefore this aspect is not examined.

In order to examine the difference between two final solutions more thoroughly some new parameters must be introduced.

$$\delta V = \left| \frac{\Phi_{1i} - \Phi_{21}}{0.5(\Phi_{1i} + \Phi_{21})} \right| \quad (4.1)$$

$$\delta E = \left| \frac{E_{1i} - E_{21}}{0.5(E_{1i} + E_{21})} \right| \quad (4.2)$$

$$\delta \rho = \left| \frac{\rho_{1i} - \rho_{21}}{0.5(\rho_{1i} + \rho_{21})} \right| \quad (4.3)$$

Where the subscripts 1 and 2 refer to different final solutions for the ionized field and space charge density rather than the solutions to equations (3.01) and (3.02). (For each solution the electric and potential fields at a centroid are determined as the average of the solutions to equations (3.01) and (3.02).)

Comparison Between Initial Approx. (Iteration Number)	δV [%]		δE [%]		$\delta \rho$ [%]	
	RMS	max.	RMS	max.	RMS	max.
Deutsch (5) and CC (23)	1.22	2.93	1.56	6.34	33.61	72.39

Table 4.2a: Difference Between Final Solutions Obtained With Deutsch and Concentric Cylinders Initial Approximations, Geometry 1, $m=1.0$, $V_{dc}=50$ kV.

Table 4.2a presents a quantitative measure of the difference in the final solutions for the ionized field and the space charge distribution obtained with different initial approximations. Deutsch and CC refer to the initial approximation used by the iterative procedure (Deutsch and Concentric Cylinder respectively). The iteration number is for use in later tables and in the above case is the iteration where all exit criteria are met. The Root Mean Square difference is calculated over all element centroids. The maximum (max.) differences were recorded for elements near the ac conductor and/or the artificial boundary in the case of δV and δE and near the dc conductor and/or artificial boundary in the case of $\delta \rho$ for this and succeeding tables. (Note: the number of iterations differ from Table 4.1a as $\alpha=-2.0$, $\beta=-1.0$ and $\gamma=-0.5$ were used in the update for this table.) Table 4.2a shows that while the solutions for the electric and potential fields determined using different initial approximations are close, the solutions for the space charge density distribution are significantly different. This again emphasizes that the potential and electric fields are not strongly dependant on the space charge distribution even for voltages relatively far into corona. (The above results are for $V_{dc}=50$ kV and corona onset is at 34.2 kV.) It should be noted that the change in the space charge density between adjacent elements is smooth.

The above results suggest that either there is a non-unique solutions for the equations used or that the exit criteria are not stringent enough.

To ensure the exit criteria are adequate, the iterative Finite Element procedure was continued for 20 iterations beyond convergence using the same update with the results below.

Comparison Between Initial Approx. (Iteration Number)	δV [%]		δE [%]		$\delta \rho$ [%]	
	RMS	max.	RMS	max.	RMS	max.
Deutsch (25) and CC (43)	0.98	2.43	1.29	5.37	33.22	74.86

Table 4.2b: Difference Between Final Solutions + 20 iterations Obtained With Deutsch and Concentric Cylinders Initial Approximations, Geometry 1, $m=1.0$, $V_{dc}=50$ kV.

Comparison of the data in Table 4.2b with that in Table 4.2a shows that while δV and δE have decreased slightly, meaning that the solutions for the ionized field are slightly closer, the difference between the solutions for the space charge distribution ($\delta \rho$) has not diminished.

To further show that the exit criteria are adequate, the change in each solutions in the 20 iterations after convergence is presented.

Comparison Between Initial Approx. (Iteration Number)	δV [%]		δE [%]		$\delta \rho$ [%]	
	RMS	max.	RMS	max.	RMS	max.
Deutsch (0) and Deutsch (5)	1.60	4.10	2.40	7.64	9.18	28.38
Deutsch (5) and Deutsch (25)	0.12	0.38	0.31	0.91	4.16	12.27

Table 4.2c: Change in Solution Before and After Convergence, Deutsch Initial Approximation, Geometry 1, $m=1.0$, $V_{dc}=50$ kV.

The first line in the above table shows the difference between the Deutsch assumption solution and the iterative solution which meets the exit criteria and uses the Deutsch initial approximation. The second line shows the change in the solution when the iterative procedure is continued for 20 iterations beyond convergence. Except in the case of the space charge distribution, the changes in the solution in the 20 iterations after convergence are insignificant.

Comparison Between Initial Approx. (Iteration Number)	δV [%]		δE [%]		$\delta \rho$ [%]	
	RMS	max.	RMS	max.	RMS	max.
CC (0) and CC (23)	19.6	27.3	22.4	32.3	82.1	106.5
CC (23) and CC (43)	0.16	0.37	0.23	0.93	3.92	7.93

Table 4.2d: Change in Solution Before and After Convergence, Concentric Cylinders Initial Approximation, Geometry 1, $m=1.0$, $V_{dc}=50$ kV.

Table 4.2d is the same as Table 4.2c except using the Concentric Cylinders initial approximation. Table 4.2d shows that almost no change occurs in the ionized field in the 20 iterations after convergence while only small changes occur in the space charge distribution.

The above tables show that the exit criteria are adequate as there is no significant change in the solution for the ionized field in the 20 iterations after convergence. These results also emphasize that the electric and potential fields are not sensitive to changes in the space charge distribution as the small changes in the space charge distribution in the 20 iterations after convergence are not reflected by changes in the ionized field. All the above are for $V_{dc}=50$ kV but Figure 4.5b shows a similar pattern further into corona and near corona onset results show only a small variation in the fields with respect to the space charge density.

Summary of Error in Iterative Finite Element Method

The difference between the final space charge distributions determined with different initial approximations indicates that the final solution is non-unique. However the final results for the ionized field agree regardless of the initial approximation. Results for the injected current are not affected by the initial approximation and they also agree with the experimental results.

4.5 Comparison with Empirical Results

Previous researchers have derived some simple, semi-empirical expressions for the current-voltage (I-V) characteristics of a unipolar dc conductor over a ground plane. One of the earliest and most detailed of these is given by Popkov [5]. This expression has been modified to to give the dc current injected into ac conductors of hybrid ac/dc lines, as detailed in Appendix A.3, with the final I_{inj} -V characteristics as below:

$$0.41 P \frac{V - V_o}{V_o} \ln\left(\frac{2H_{eq}}{r_o}\right) = \sqrt{1+Y} - 1 + \ln\left(\frac{2}{1+\sqrt{1+Y}}\right) \quad (4.4)$$

$$Y = \frac{P I_{inj}/c}{2\pi\epsilon_0 k} \left(\frac{H_{eq}}{E_0 r_0} \right)^2 \quad (4.5)$$

where V_0 and E_0 are the onset potential and electric fields on the dc conductor. r_0 is the radius of the dc conductor and H_{eq} is the equivalent height over ground as determined in Appendix A.3. P is a parameter which accounts for the nonuniform distribution of the current on the ground plane and the constant c accounts for the fact that only a fraction of the current discharged from the dc conductor reaches the ac conductor.

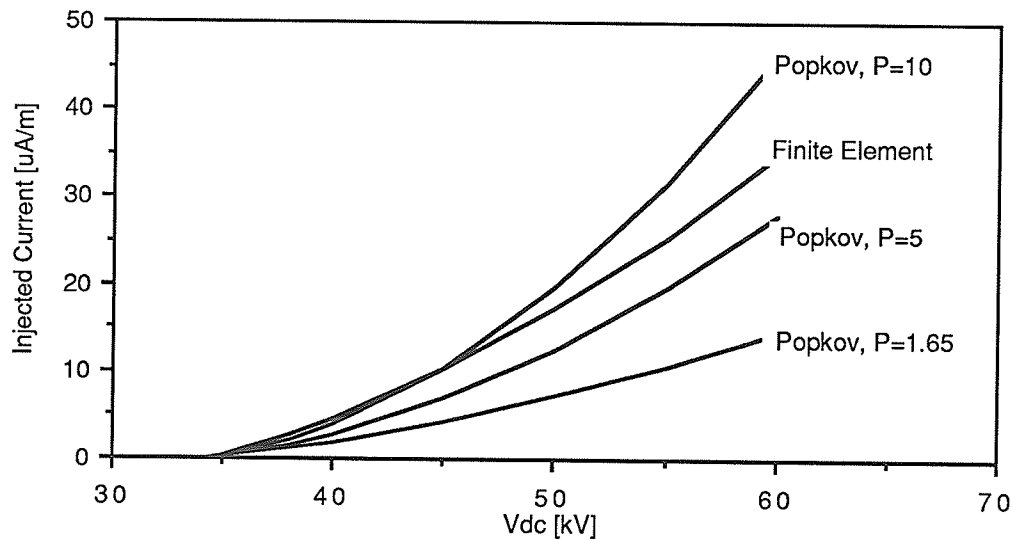


Figure 4.6a: dc Injected Current - FE and Empirical, Geometry 1, $m=1.0$

Figure 4.6a compares the iterative FE results for Geometry 1 with various empirical results based on the modified Popkov expression. Popkov determined a value of 1.65 for P , but later researchers suggested a value of about 5.0 [6]. These results indicate a P of between 5 and 10 would be accurate for hybrid lines.

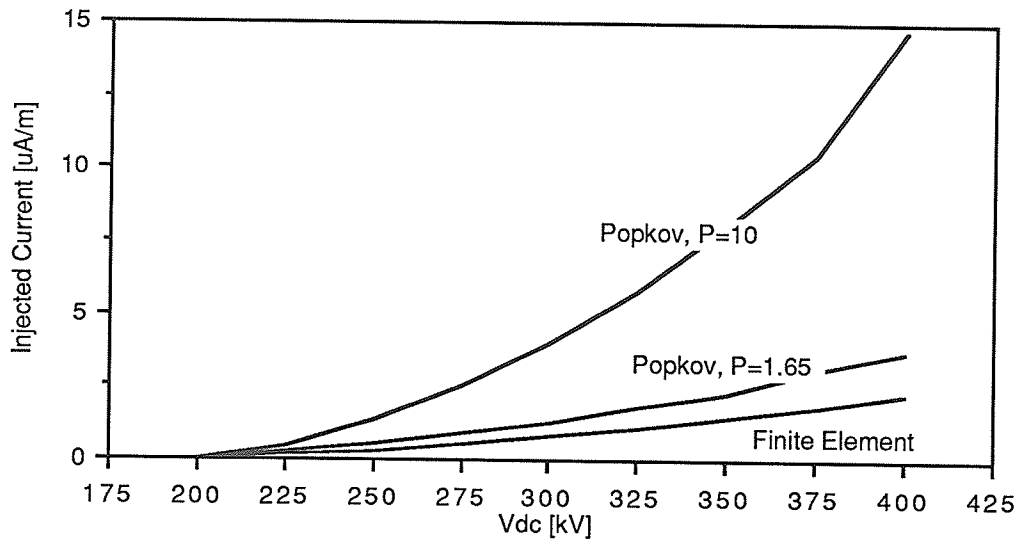


Figure 4.6b: dc Injected Current - FE and Empirical, Geometry 2.

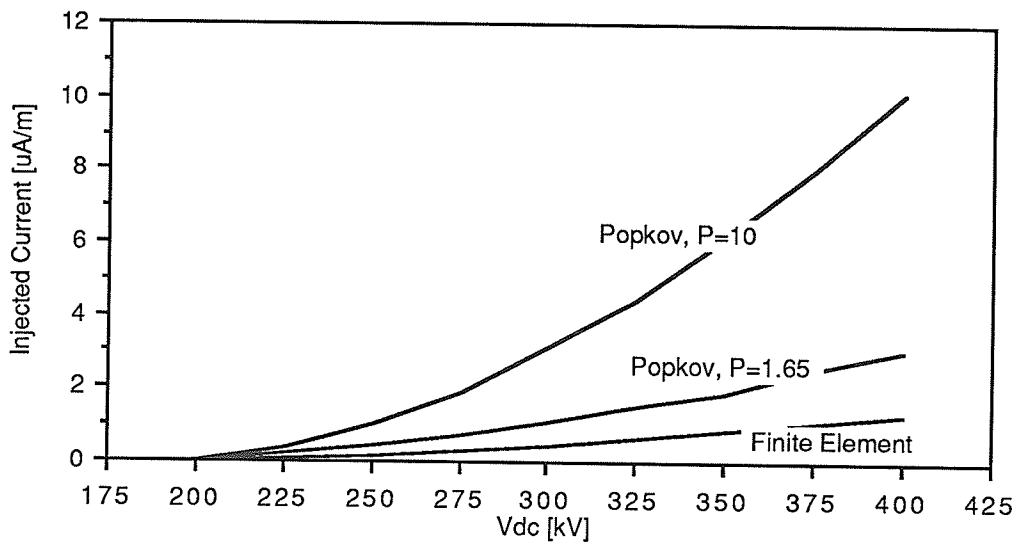


Figure 4.6c: dc Injected Current - FE and Empirical, Geometry 3.

The results for Geometries 2 and 3 do not agree very well with the results for Geometry 1. The empirical results can be made to agree with the Finite Element results by changing P, but as P seems to be heavily dependant on the geometry, there is not much practical use for this semi-empirical expression.

Chapter 5

INCLUSION OF THE EFFECT OF THE AC POTENTIAL

The ac potential has a considerable effect on the amount of dc current injected into ac conductors during corona. The experimental results show a significant increase in dc current injected into an ac conductor as the ac potential is increased [23]. This effect has not been considered by previous researchers.

5.1 Method of Inclusion

Calculation of the time varying ionized field is beyond the computational facilities available. Therefore ac potential is considered only in its effect on the corona current injected in ac conductors, not in its effect on the fields and space charge distribution.

The effect of the ac voltage is simulated by replacing the dc voltage with an equivalent voltage which is the dc voltage plus the effect of the ac potential on the space charge free electric field on the dc conductor surface. The steps in the method of including the effect of the ac potential are as follows:

- 1) The maximum space charge free electric field on the dc conductor due to the combined effects of the ac and dc voltages is determined using the method in Subsection 3.2.1. In Geometry 1 this occurs when the ac voltage is at its maximum negative value.
- 2) With the ac conductors at zero voltage, the dc voltage which gives the same maximum space charge free field on the surface of the dc conductor as step 1) is determined. This dc voltage is V_{eq} .
- 3) The injected current is determined from the dc I-V curve for the geometry determined by the iterative FE method by replacing V_{dc} with V_{eq} .

This effectively means that the dc axis of the current-voltage curve is shifted to the right.

5.2 Results of the Inclusion of the AC Potential

The dc injected current results shown in this chapter were determined using the Concentric Cylinders initial approximation for the space charge distribution. As noted in Subsection 4.3.2, the initial approximation for the space charge distribution has no significant effect on the dc injected current.

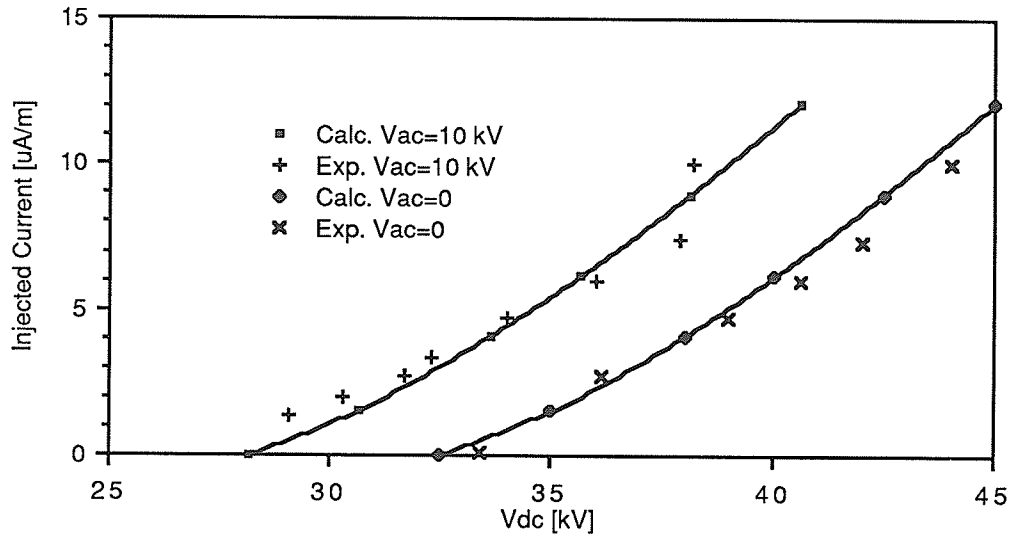


Figure 5.1: dc Injected Current - Zero and Nonzero ac Potential, Geometry 1, $m=0.95$.

Figure 5.1 shows that there is good agreement with the experimental results for $V_{ac}=10$ kV. When the effect of the ac potential is included the onset potential of dc corona is significantly decreased.

In the practical geometries the ac line is energized at 230 kV. The results for Geometries 2 and 3 are again for the dc current injected into Conductor A from Conductor 1. In Conductor C the dc current injected should be approximately the same magnitude as that injected into Conductor A but with an opposite polarity. In Conductor B the dc current injected should be insignificant (Subsection 3.2.3).

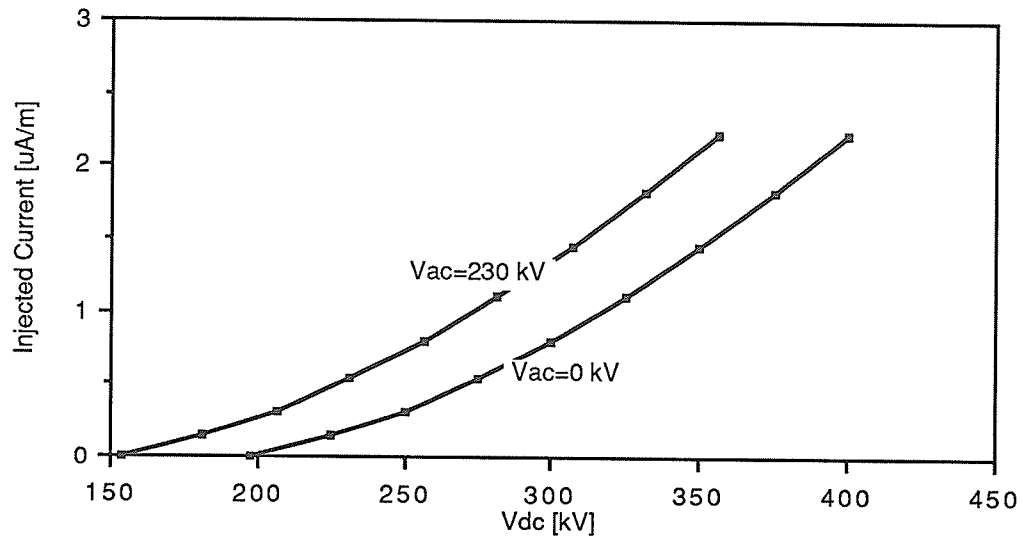


Figure 5.2: dc Injected Current - Zero and Nonzero ac Potential, Geometry 2.

With the dc line in Geometry 2 operating at a voltage of ± 250 kV the total current injected into the ac conductor increases from 0.3 to 0.7 $\mu\text{A}/\text{m}$ when the effect of the ac voltage is included. For a 100 km transmission line this would mean a dc current of $0.7 \mu\text{A}/\text{m} \times 100 \text{ km} / 2 = 35 \text{ mA}$ in the ac conductor at each end of the line.

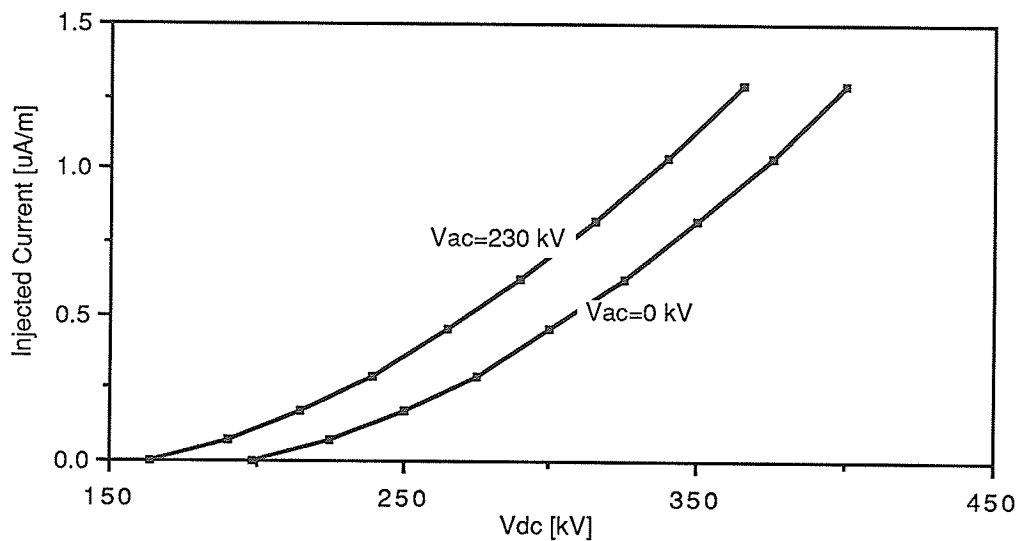


Figure 5.3: dc Injected Current - Zero and Nonzero ac Potential, Geometry 3.

A comparison with Figure 5.2 shows a decrease from 0.7 to 0.4 $\mu\text{A}/\text{m}$ in the injected current, at $V_{dc}=250$ kV, when the dc conductors are raised one meter relative to their position in Geometry 2.

Chapter 6

CONCLUSIONS

Convergence of Iterative Finite Element Method

The iterative FE method works very well in converging to a solution for the differential equations. The best updates converged for all geometries with several different values for the update parameters and with significantly inaccurate initial approximations for the space charge distribution.

Results of Iterative Finite Element Method

Ionized Field

The iterative FE procedure gives good results for the ionized field. The results agree quite well with the results of previous (Deutsch) methods and no matter what the final space charge distribution is the results for the electric and potential fields remain substantially the same.

Space Charge Distribution and DC Injected Current

The final results for the space charge distribution differ significantly depending on the initial approximation. As a result the correct final distribution cannot be known with any degree of certainty.

The results for the dc current injected into the ac conductor are derived directly from the results for the space charge distribution. However unlike the results for the space charge distribution, the results determined for the injected current agree regardless of the initial approximation for the space charge distribution. This appears to be because the initial approximation affects the final distribution of the space charge but not its magnitude. The results for the dc injected current also agree well with the results of previous methods

(Deutsch assumption) and with experimental results and can therefore be assumed to be reasonably accurate.

Deutsch Assumption

Again, the results for the fields and injected current determined using the iterative FE method do not differ significantly from those determined using a method which employs the Deutsch assumption. As the Deutsch assumption is used on the artificial boundary, the assumption has not been completely eliminated and therefore the effect of the Deutsch assumption on iterative FE method results cannot be completely determined. In general, methods using the Deutsch assumption give good results for the ionized field practical geometries. However the space charge distribution obtained using the Deutsch assumption may vary significantly from the actual distribution.

Artificial Boundaries

The artificial boundary was chosen to limit the solution area as much as possible in order to reduce the solution time and this objective was certainly achieved. The greatest variation in the final solutions for the space charge density obtained with different initial approximations also occurs adjacent to the artificial boundary. However, in the ionized field, the greatest differences between the solutions of the iterated equations, (3.01) and (3.02), occurs adjacent to the artificial boundary. This may be partially explained by the fact that the FE mesh gives the least accurate results at boundary elements, but it also may be due to the fact that the Deutsch assumption is less valid near the artificial boundary than elsewhere. However due to the non-uniqueness of the final solution the effect of the choice for the artificial boundary cannot be completely determined.

Inclusion of the AC Potential

Experimental data shows that the ac potential has a significant effect on the dc current injected into ac conductors of a hybrid ac/dc transmission line. The method of including the effect of the ac potential on the injected current is easy to implement and based on the agreement with experimental results, accurate for practical transmission lines.

REFERENCES

Corona on Hybrid AC/DC Lines

- [1] V. L. Chartier, S. H. Sarkinen, R. D. Stearns, A. L. Burns, "Investigation of Corona and Field Effects of AC/DC hybrid Transmission Lines", IEEE Transactions on Power Apparatus and Systems, Vol. PAS-100, No. 1, Jan. 1981, pp. 72-80.
- [2] H. L. Nakra, L. X. Bui, I. Iyoda, "System Considerations in Converting One Circuit of a Double Circuit AC Line to DC", IEEE Transactions on Power Apparatus and Systems, Vol. PAS-103, No. 10, Oct. 1984, pp. 3096-3103.
- [3] P. Sarma Maruvada, S. Drogi, "Field and Ion Interaction of Hybrid AC/DC Transmission Lines", IEEE Transactions on Power Delivery, Vol. 3, No. 3, July 1988, pp. 1165-1172.

Non-Finite Element DC Corona Analysis

- [4] J. S. Townsend, "The Potentials Required to Maintain Currents between Coaxial Cylinders", Philosophical Magazine and Journal of Science, Series 6, Vol. 28, 1914, pp. 83-90.
- [5] V. I. Popkov, "On the Theory of Unipolar DC Corona", Elektrichestvo, (1):33-48, 1949, NRC Technical Translation - 1093.
- [6] Maruvada P. Sarma, W. Janischewskyj, "Analysis of Corona Losses on DC Transmission Lines: 1-Unipolar Lines", IEEE Transactions on Power Apparatus and Systems, Vol. PAS-88, No. 5, May 1969, pp. 718-731.
- [7] Maruvada P. Sarma, W. Janischewskyj, "Analysis of Corona Losses on DC Transmission Lines: 2-Bipolar Lines", IEEE Transactions on Power Apparatus and Systems, Vol. PAS-88, No. 10, Oct. 1969, pp. 1476-1491
- [8] M. Abdel-Salam, M. Khalifa, "Considering Space Charge in Calculations of Monopolar DC Corona Loss", Acta Physica, Vol. 36(3), 1974, pp. 201-214.
- [9] M. Khalifa, M. Abdel-Salam, "Improved Method for Calculating DC Corona Losses", IEEE Transactions on Power Apparatus and Systems, Vol. PAS-93, 1974, pp. 720-726.
- [10] Y. Sunaga, Y. Sawada, "Method of Calculating Ionized Field of HVDC Transmission Lines and Analysis of Space Charge Effects on RI", IEEE Transactions on Power Apparatus and Systems, Vol. PAS-99, No. 2, M/A 1980, pp. 605-615.
- [11] H. Parekh, Y. L. Chow, K. D. Srivastava, "A Simple Method of Calculating Corona Loss On Unipolar DC Transmission Lines", IEEE Transactions on Electrical Insulation, Vol. EI-15, No. 6, Dec. 1980, pp. 455-460.
- [12] I. R. Ciric, E. Kuffel, "New Analytic Expressions for Calculating Unipolar DC Corona Losses", IEEE Transactions on Power Apparatus and Systems, Vol. PAS-101, No. 8, Aug. 1982, pp. 2988-2994.

- [13] M. Abdel-Salam, M. Farghally, S. Abdel-Sattar, "Monopolar Corona on Bundle Conductors", IEEE Transactions on Power Apparatus and Systems, Vol. PAS-101, No. 10, Oct. 1982, pp. 4079-4088.
- [14] I. R. Ciric, E. Kuffel, "Boundary Conditions Impact on Unipolar DC Corona Field Calculations", Fourth International Symposium on HV Engineering, Athens, Greece, 5-9 Sept 1983, Paper 13.07.
- [15] M. D'Amore, V. Daniele, G. Ghione, "New Analytical Approach for Computing DC Unipolar Corona Losses", IEE Proceedings, Vol. 131, Pt. A, No. 5, July 1984, pp. 318-324.

Finite Element Analysis of DC Corona

- [16] W. Janischewskyj, G. Gela, "Finite Element Solution for Electric Fields of Coronating DC Transmission Lines", IEEE Transactions on Power Apparatus and Systems, Vol. PAS-98, No. 3, May/June 1979, pp. 1000-1012.
- [17] T. Takuma, T. Ikeda, T. Kawamoto, "Calculation of Ion Flow Fields of HVDC Transmission Lines by the Finite Element Method", IEEE Transactions of Power Apparatus and Systems, Vol. PAS-100, No. 12, Dec. 1981, pp. 4802-4810.
- [18] W. Janischewskyj, P. Sarma Maruvada, G. Gela, "Corona Losses and Ionized Fields of HVDC Transmission Lines", CIGRE Paper 36-09, 1982.
- [19] M. Abdel-Salem, M. Farghally, S. Abdel-Sattar, "Finite Element Solution of Monopolar Corona Equation", IEEE Transactions on Electrical Insulation, Vol. EI-18, No. 2, April 1983, pp. 110-119.

Other References

- [20] Bonneville Power Administration, Transmission Line Reference Book - HVDC to ± 600 kV, Electrical Power Research Institute, Palo Alto, CA., 1977.
- [21] Maruvada. P. Sarma and W. Janischewskyj, "Electrostatic Field of a System of Parallel Cylindrical Conductors", IEEE Transactions on Power Apparatus and Systems, Vol. PAS-88, No. 7, July 1969, pp. 1069-1076.
- [22] M. Friedman, D. J. Richards, W. N. R. Stevens, A. Wexler, "MANFEP, User's Manual", Dept. of Elect. Eng., Univ. of Manitoba, Winnipeg, Can., 1979.
- [23] G. Allard "Hybrid Line Corona Currents and Components", B.Sc.(E.E.) Thesis, Univ. of Manitoba, 1987.
- [24] Lambert, Computational Methods in Ordinary Differential Equations, John Wiley and Sons Ltd., London, 1973.

Appendix A

MISCELLANEOUS EQUATIONS

A.1 Runge-Kutta Determination of Ion Paths

The path of an ion emitted by a dc conductor is determined from equation (3.12) which can be separated into two single dimensional equations:

$$\frac{dx}{dt} = kE_x(x, y, t) \quad (A.01)$$

$$\frac{dy}{dt} = kE_y(x, y, t) \quad (A.02)$$

where E_x and E_y are the space charge free electric fields in the x and y directions respectively and k is the ionic mobility. The path of an ion is determined by integrating the above equations with respect to time by the Runge-Kutta numerical method given in reference [24, pg. 133]. In the method the ion path is calculated in a series of steps, each step determining another point on the path. Each point is determined from:

$$x_{n+1} = x_n + \frac{\Delta t k}{6} (E_{x1} + 4E_{x2} + E_{x4}) \quad (A.03)$$

where:

$$E_{x1} = E_x(x_n, y_n, t)$$

$$E_{x2} = E_x\left(x_n + \frac{\Delta t k}{2} E_{x1}, y_n + \frac{\Delta t k}{2} E_{y1}, t + \frac{\Delta t}{2}\right)$$

$$E_{x3} = E_x\left(x_n + \frac{\Delta t k}{4} E_{x1} + \frac{\Delta t k}{4} E_{x2}, y_n + \frac{\Delta t k}{4} E_{y1} + \frac{\Delta t k}{4} E_{y2}, t + \frac{\Delta t}{2}\right) \quad (A.04)$$

$$E_{x4} = E_x \left(x_{n+1} \Delta t k E_{x2} + 2 \Delta t k E_{x3}, y_{n+1} \Delta t k E_{y2} + 2 \Delta t k E_{y3}, t + \Delta t \right)$$

$$E_{x5} = E_x \left[x_{n+1} \frac{\Delta t k}{27} (7E_{x1} + 10E_{x2} + E_{x4}), y_{n+1} \frac{\Delta t k}{27} (7E_{y1} + 10E_{y2} + E_{y4}), t + \frac{2\Delta t}{3} \right]$$

$$E_{x6} = E_x \left[\begin{array}{l} x_{n+1} \frac{\Delta t k}{625} (28E_{x1} - 125E_{x2} + 546E_{x3} + 54E_{x4} - 378E_{x5}), \\ y_{n+1} \frac{\Delta t k}{625} (28E_{y1} - 125E_{y2} + 546E_{y3} + 54E_{y4} - 378E_{y5}), t + \frac{\Delta t}{5} \end{array} \right]$$

With similar equations for y_{n+1} and E_{y1}, \dots, E_{y6} . An estimate of the error in the x direction for each step is:

$$T_{X_{n+1}} = \frac{\Delta t k}{336} (-42E_{x1} - 224E_{x3} - 21E_{x4} + 162E_{x5} + 125E_{x6}) \quad (A.05)$$

and an estimate of the total error in each step is:

$$T_{n+1} = \sqrt{T_{X_{n+1}}^2 + T_{Y_{n+1}}^2} \quad (A.06)$$

In the calculations, Δt is chosen so that the error in each step, T_{n+1} , is less than a given maximum, T_{max} . The total number of steps to reach the ac conductor from the dc is about 50.

T_{max} [m]	Theta max. [degrees]	CPU Time [sec.]
10^{-4}	55.11	1.59
10^{-6}	55.20	2.90

Table A.1: The Effect of the Maximum Error per step on Theta max., Geometry 1, $V_{dc}=38$ kV, $V_{ac}=0$.

Theta max. is the maximum angle at which an ion emitted from the dc conductor will land on the ac conductor. (A maximum T_{n+1} of 10^{-6} [m] is used for every geometry.) Table A.1 shows that the time step used determines the ion path accurately as Theta max. does not change significantly when a coarser time step is used.

A.2 Initial Approximations for the Space Charge

A.2.1 Deutsch Initial Approximation

The Deutsch solution used for the initial approximation is derived by Ciric et al. [14]. In this method the region between two conductors is divided into elementary flux tubes which correspond to the electric field lines. The I-V (current-voltage) relationship is then determined for these elementary flux tubes. Within each tube:

$$\rho = \frac{j}{kE} \quad (\text{A.07})$$

where ρ is the space charge density, j is the current density, k is the ionic mobility and E is the electric field. The current through any cross section of a flux tube will be constant.

$$j = \frac{\Delta I}{\Delta S} = E' \frac{\Delta I}{\Delta \Psi} \quad (\text{A.08})$$

where ΔI is the current in a tube, ΔS is the cross section area of a tube and E' is the space charge free electric field. $\Delta \Psi$ is the flux in a tube and is constant throughout the length of the tube. $\Delta \Psi$ for each tube is determined at the coronating conductor using:

$$\Delta \Psi = E'_o r_o \pi/360 \quad (\text{A.09})$$

E'_0 is the space charge free electric field on the surface of the dc conductor and r_0 is the radius of the conductor. The cross section area of each elementary flux tube is set at one degree on the coronating conductor. The ionized electric field along the flux tube can be determined from:

$$E = E' \left(A + \frac{2}{\epsilon_0 k} \frac{\Delta I}{\Delta \Psi} F(\Phi') \right)^2 \quad (\text{A.10})$$

Where the third boundary condition is imposed through the constant A.

$$A = \left(\frac{E_0}{E'_0} \right)^2 \quad (\text{A.11})$$

In the above equation E_0 is the onset value of the electric field on the coronating conductor and E'_0 the space charge free value of the electric field on the coronating conductor. The function $F(\Phi')$ is defined as:

$$F(\Phi') = \int_{\Phi'}^{V_{dc}} \frac{d\Phi'}{E'^2} \quad (\text{A.12})$$

Where Φ' is the space charge free potential and V_{dc} the dc voltage. The current-voltage characteristics of a tube are determined from:

$$V = \int_0^{V_{dc}} \left[A + \frac{2}{\epsilon_0 k} \frac{\Delta I}{\Delta \Psi} F(\Phi') \right]^2 d\Phi' \quad (\text{A.13})$$

This equation is solved iteratively by approximating ΔI and then updating the approximation until $V=V_{dc}$, at which point ΔI is known and the space charge at any point can be determined from (A.07). The integration in equations (A.12) and (A.13) is performed numerically along electric field lines using the same nodes as the FE mesh and the trapezoidal rule.

A.2.2 Concentric Cylinders Initial Approximation

This initial approximation for the charge distribution is derived from the solution for the charge distribution of a concentric cylinders geometry with parameters similar to the actual geometry by the following steps:

1) With the outer cylinder grounded the radius of the outer cylinder in the concentric geometry, R , is determined from:

$$R = r_o \exp\left(\frac{V_{dc}}{E_{peak} r_o}\right) \quad (\text{A.14})$$

where E_{peak} is the maximum space charge free electric field on the surface of the dc conductor in the actual geometry, r_o is the radius of the dc conductor and V_{dc} is the potential of the dc conductor in the actual geometry.

2) Knowing: the potential on both cylinders, the radius of each cylinder and the electric field on the surface of the inner cylinder, the equations given in reference [17] are solved for the space charge distribution.

$$\Phi = c - a \left[\sqrt{r^2 + b^2} - b \ln \left(\frac{\sqrt{r^2 + b^2} + b}{r} \right) \right] \quad (\text{A.15})$$

$$\rho = \frac{\epsilon_0 a}{\sqrt{r^2 + b^2}} \quad (\text{A.16})$$

$$E = \frac{a \sqrt{r^2 + b^2}}{r} \quad (\text{A.17})$$

where r is the radial distance and a , b and c are determined as follows. Assuming $b \gg r_0$ the above equations can be solved for b .

$$b = \frac{r_0 E_0}{V_{dc}} \left[\sqrt{R^2 + b^2} - b + b \ln \left(\frac{2 b R / r_0}{\sqrt{R^2 + b^2} + b} \right) \right] \quad (\text{A.18})$$

This equation is solved iteratively and once b is known a and c can be easily calculated from (A.15) and (A.17). Equation (A.16) then gives the space charge distribution density throughout the concentric cylinder geometry.

3) The maximum space charge on the dc conductor surface for the actual line is assumed equal to the constant space charge density on the inner conductor in the concentric cylinders geometry. The space charge distribution on the surface of the dc conductor in the actual geometry is assumed to vary according to the relation:

$$\rho(\theta) = 0.5 \rho_{\max} [1 + \cos(\theta - \theta_{\text{peak}})] \quad (\text{A.19})$$

The maximum charge density occurs at an angle of $\theta = \theta_{\text{peak}}$, which is the point on the dc conductor surface of the actual geometry at which the maximum electric field occurs. This relation assumes a sinusoidal variation in the space charge on the surface of coronating conductors. Equation (A.19) ensures that the maximum space charge occurs at the point on the dc conductor surface where the maximum space charge free field occurs.

4) The space charge at any point along an electric field line is determined from:

$$\rho(\theta, L) = \frac{\epsilon_0 a [1 + \cos(\theta - \theta_{\text{peak}})]}{\sqrt{L^2 + b^2}} \quad (\text{A.20})$$

where L is the distance from the dc conductor node (measured along the electric field line) and θ is the angle on the dc conductor of the dc conductor node where the field line originates. In this manner the approximate space charge is calculated at each node of the FE mesh and then converted to a triangle quantity by taking the arithmetic average of the space charge values at the three nodes of an element.

A.3 Empirical I-V Relationship for Hybrid AC/DC Lines

Previous researchers have derived some simple, semi-empirical expressions for the current-voltage (I-V) characteristic of a unipolar dc conductor in corona over a ground plane. One of the most detailed of these is given by Popkov [5]:

$$0.41 P \frac{V - V_0}{V_0} \ln\left(\frac{2H}{r_0}\right) = \sqrt{1+Y} - 1 + \ln\left(\frac{2}{1+\sqrt{1+Y}}\right) \quad (\text{A.21})$$

$$Y = \frac{PI}{2\pi\epsilon_0 k} \left(\frac{H}{E_0 r_0}\right)^2 \quad (\text{A.22})$$

where V_o and E_o are the onset potential and electric fields on the dc conductor. r_o is the radius of the conductor and H is the height of the conductor above ground. P is a parameter which accounts for the non-uniform current distribution on the ground plane. I and V give the I-V characteristics of the line. This equation is based on an equivalent concentric cylinders geometry.

This equation is modified to give results for the actual geometries in question by replacing H with the parameter H_{eq} , which is defined below:

$$H_{eq} = \frac{r_o}{2} \exp\left(\frac{V_o}{E_o r_o}\right) \quad (A.23)$$

H_{eq} is the height of a single conductor over ground with the same V_o and E_o as the actual geometry.

The fact that not all of the current leaving the dc conductors reaches a given ac conductor is accounted for by dividing the current by a factor c which represents the fraction of the emitted current which is injected into the ac conductor. E.g. the fraction emitted within the region of interest.

$$c = \frac{1}{2\pi} \int_{\theta_{min}}^{\theta_{max}} \left\{ 1 + \cos\left[\theta - \left(\frac{\theta_{max} - \theta_{min}}{2}\right)\right] \right\} d\theta \quad (A.24)$$

where θ_{max} and θ_{min} are the angles of the artificial boundaries determined in Subsection 3.2.3.

The I_{inj} - V characteristics for the actual geometry are given by:

$$0.41 P \frac{V - V_o}{V_o} \ln\left(\frac{2H_{eq}}{r_o}\right) = \sqrt{1+Y} - 1 + \ln\left(\frac{2}{1+\sqrt{1+Y}}\right) \quad (A.25)$$

$$Y = \frac{P I_{inj}/c}{2\pi \epsilon_0 k} \left(\frac{H_{eq}}{E_0 r_0} \right)^2 \quad (A.26)$$

The results of these equations are compared with those of the iterative FE method in Section 4.5.

Appendix B

PROGRAM LISTING

B.1 Angle Determination Program

```
//APENNER JOB ',';AC-DC 2 CONDUCTOR'
// EXEC WATFIV
//FT05F001 DD *
$JOB
C
C THIS PROGRAM DETERMINES THE PATH OF A PARTICLE USING
C A RUNGE-KUTTA 4TH ORDER METHOD
C
      REAL*8  A,B,C,DET,VDC,VAC,PHI,H1,H2,W,R,TOT,TNMIN,TNMAX,TSTEP
      REAL*8  RH,X,Y,T,H,TN1,THETA,PI,K,THETAU,THETAL,X1,Y1,D
      INTEGER I,J
      COMMON  A,B,C,D,DET,VDC,VAC,PHI,H1,H2,W
C
C INPUT THETA IN DEGREES AND PHI IN RADIANS
C
      THETAU=90.0
      THETAL=0.0
      PI=3.141592654
      H1=0.8
      H2=0.65
      PHI=11.0*PI/8.0
      R=0.000815
      W=120.0*PI
      K=0.00015
      TSTEP=0.0000001
      A=DLOG(H2/R)
      B=-DLOG(H1/(H1-H2))
      C=-DLOG(H2/(H1-H2))
      D=DLOG(H1/R)
      DET=A*D-B*C
C
      VDC=30000.0
      DO 4 J=1,7
          VDC=VDC+5000.0
          VAC=-40000.0D0*DSQRT(2.0D0)
          DO 2 I=1,7
              VAC=VAC+10000.0D0*DSQRT(2.0D0)
              TOT=SQRT(EX(0.0D0,(H1-R),0.0D0)**2+EY(0.0D0,(H1-R),0.0D0)**2)
2          PRINT,VDC,VAC,TOT
4          CONTINUE
      VDC=38000.0
      VAC=0.0D0
C
C DETERMINE THETA
C
5      IF ((THETAU-THETAL).LT.(0.1)) STOP
      THETA=THETAL+(THETAU-THETAL)/2.0
```

```

      H=K*TSTEP
C
C MAXIMUM AND MINIMUM DISTANCES BETWEEN SUCCESSION POINTS
C
      TNMIN=0.0000001
      TNMAX=0.0000001
      X=R*DSIN(PI*THETA/180.0)
      Y=H1-R*DCOS(PI*THETA/180.0)
      T=0.0
C
      DO 10 I=1,10000
          RH=DSQRT((Y-H2)**2+X**2)
          IF (RH.LT.R) GO TO 50
          IF (Y.LE.0.0) GO TO 60
20      CALL RK4(X,Y,X1,Y1,T,H,TN1,K)
          IF (TN1.LT.TNMAX) GO TO 30
C DECREASE STEP SIZE
          H=H*0.8
          GO TO 20
30      IF (TN1.GT.TNMIN) GO TO 40
C INCREASE STEP SIZE
          H=H*1.2
          GO TO 20
C
C INCREMENT TIME
C
40      T=T+H/K
          X=X1
          Y=Y1
C
10      CONTINUE
          PRINT55
C
C HIT
C
50      TOT=T
          PRINT70,THETA,TOT
          THETA1=THETA
          GO TO 5
C
C MISS
C
60      PRINT80,THETA
          THETAU=THETA
          GO TO 5
70      FORMAT(' ','HIT, THETA= ',F10.7,'TOT= ',F10.7)
80      FORMAT(' ','MISS, THETA= ',F10.7)
55      FORMAT(' ','T-MAX EXCEEDED')
          END
C
C THIS SUBROUTINE PERFORMS A SINGLE STEP OF THE R-K METHOD
C
      SUBROUTINE RK4(XN,YN,XN1,YN1,T,H,TN1,K)
C

```

```

REAL*8  T,H,XN,YN,XN1,YN1,TN1,KX1,KX2,KX3,KX4,KX5,KX6
REAL*8  KY1,KY2,KY3,KY4,KY5,KY6,K,TT,XP,YP
C
KX1=EX(XN,YN,T)
KY1=EY(XN,YN,T)
C
XP=XN+H*KX1/2.0
YP=YN+H*KY1/2.0
TT=T+H/2.0/K
KX2=EX(XP,YP,TT)
KY2=EY(XP,YP,TT)
C
XP=XN+H*(KX1+KX2)/4.0
YP=YN+H*(KY1+KY2)/4.0
TT=T+H/2.0/K
KX3=EX(XP,YP,TT)
KY3=EY(XP,YP,TT)
C
XP=XN-H*KX2+2.0*H*KX3
YP=YN-H*KY2+2.0*H*KY3
TT=T+H/K
KX4=EX(XP,YP,TT)
KY4=EY(XP,YP,TT)
C
XP=XN+H*(7.0*KX1+10.0*KX2+KX4)/27.0
YP=YN+H*(7.0*KY1+10.0*KY2+KY4)/27.0
TT=T+H/1.5/K
KX5=EX(XP,YP,TT)
KY5=EY(XP,YP,TT)
C
XP=XN+H*(28.0*KX1-125.0*KX2+546.0*KX3+54.0*KX4-378.0*KX5)/625.0
YP=YN+H*(28.0*KY1-125.0*KY2+546.0*KY3+54.0*KY4-378.0*KY5)/625.0
TT=T+H/5.0/K
KX6=EX(XP,YP,TT)
KY6=EY(XP,YP,TT)
C
XN1=XN+H*(KX1+4.0*KX3+KX4)/6.0
YN1=YN+H*(KY1+4.0*KY3+KY4)/6.0
C CALCULATION OF ESTIMATE OF TRUNCATION ERROR
XP=(-42.0*KX1-224.0*KX3-21.0*KX4+162.0*KX5+125.0*KX6)
YP=-42.0*KY1-224.0*KY3-21.0*KY4+162.0*KY5+125.0*KY6
TN1=H*DSQRT(XP**2+YP**2)/336.0
RETURN
END
C
C THIS FUNCTION EVALUATES THE FIELD IN THE X DIRECTION AT
C A GIVEN TIME AND POSITION
C
FUNCTION EX(X,Y,T)
C
REAL*8  X,Y,T,A,B,C,DET,VDC,VAC,W,PHI,Q1,Q2,H1,H2,EX1,EX2
REAL*8  EX3,EX4,D1,D2,D3,D4,X2,D
COMMON  A,B,C,D,DET,VDC,VAC,PHI,H1,H2,W
C

```

```

C CALCULATE CHARGE ON CONDUCTORS
C
  Q1=(A*VDC+B*VAC*DSIN(W*T-PHI))/DET
  Q2=(C*VDC+D*VAC*DSIN(W*T-PHI))/DET
C
  X2=X**2
  D1=(H1-Y)**2+X2
  D2=(H2-Y)**2+X2
  D3=(H2+Y)**2+X2
  D4=(H1+Y)**2+X2
C
  EX1=Q1*X/D1
  EX2=Q2*X/D2
  EX3=-Q2*X/D3
  EX4=-Q1*X/D4
C
  EX=EX1+EX2+EX3+EX4
  RETURN
  END
C
C THIS FUNCTION EVALUATES THE ELECTRIC FIELD IN THE Y DIRECTION
C FOR A GIVEN TIME AND POSITION
C
  FUNCTION EY(X,Y,T)
C
  REAL*8  X,Y,T,A,B,C,DET,VDC,VAC,W,PHI,Q1,Q2,H1,H2,EY1,EY2
  REAL*8  EY3,EY4,D1,D2,D3,D4,X2,D
  COMMON  A,B,C,D,DET,VDC,VAC,PHI,H1,H2,W
C
C DETERMINE THE CHARGE ON THE CONDUCTORS
C
  Q1=(A*VDC+B*VAC*DSIN(W*T-PHI))/DET
  Q2=(C*VDC+D*VAC*DSIN(W*T-PHI))/DET
C
  X2=X**2
  D1=(H1-Y)**2+X2
  D2=(H2-Y)**2+X2
  D3=(H2+Y)**2+X2
  D4=(H1+Y)**2+X2
C
  EY1=-Q1*(H1-Y)/D1
  EY2=Q2*(Y-H2)/D2
  EY3=-Q2*(Y+H2)/D3
  EY4=-Q1*(Y+H1)/D4
C
  EY=EY1+EY2+EY3+EY4
  RETURN
  END
$ENTRY
/ *

```

B.2 Mesh Generation Program

```

//APENNER JOB ',,I=20','AC-DC FEPMAP'
// EXEC FORTXCLG,USERLIB='SYS4.DRIVER.DYLOAD'
//FORT.SYSIN DD *
C
C THIS PROGRAM DETERMINES A FINITE ELEMENT MESH FOR
C THE TWO CONDUCTOR PROBLEM
C
      REAL*8  TH,VDC,VAC,TSTEP,H1,H2,R,PHI,THS,THM,TD,PI,TNW(700,3)
      REAL*8  X(1000),Y(1000),D(1000),XN(50),YN(50),A,B,C,DET,W,TH2
      REAL*8  TNMIN,TNMAX,G,XA(150),YA(150),XS(400),YS(400),ID,P(700)
      REAL  XP(400),YP(400)
      INTEGER NL,NN(10),NP,I,J,K,IBUF(10000),L,M,T(700,3),NT
      COMMON  A,B,C,DET,VDC,VAC,PHI,H1,H2,W
C
C MAINLINE
C
      THM=55.2
      VDC=38000.0
      VAC=0.0*DSQRT(2.0D+0)
      ID=4.0D-6
      TSTEP=0.0000001
      PI=3.141592653
      H1=0.8
      H2=0.65
      R=0.000815
      PHI=PI
      L=0
      W=60.0*PI
      TNMIN=0.0000001
      TNMAX=0.000001
      G=1.5
      NL=THM/20.0+2
      THS=THM/(NL-1)
C
      DO 10 I=1,NL
          TH=THS*(I-1)
          TH=TH+THS*(NL-I)*(I-1)**2/(NL-1)**3
          CALL RKP(TH,TSTEP,R,NP,TD,X,Y,D,TNMIN,TNMAX)
C
C DEFINE POINTS ON BOTTOM CONDUCTOR
C
          IF (I.EQ.1) GO TO 25
          TH2=DATAN((H2-Y(NP))/X(NP))
          X(NP)=R*DCOS(TH2)
          Y(NP)=H2-R*DSIN(TH2)
          GO TO 26
25      X(NP)=0.0
          Y(NP)=H2+R
26      CONTINUE
          IF (I.EQ.NL) GO TO 40
          CALL PATH(NP,TD,NN(I),XN,YN,R,X,Y,D,G)

```

```

        GO TO 70
40      CALL APATH(NP,TD,NN(I),XN,YN,R,X,Y,D,G,XA,YA)
70      M=NN(I)
        DO 20 J=1,M
            K=L+J
            XS(K)=XN(J)
20      YS(K)=YN(J)
10      L=L+NN(I)
C
C PRINT NODES
C
        PRINT50
        DO 30 I=1,L
            XP(I)=1000.0*XS(I)
            YP(I)=1000.0*YS(I)
30      PRINT60,XP(I),YP(I),I
        CALL TRIANG(NL,NN,T,NT)
        CALL NEUM(NN,NL)
        CALL DIRI(VDC,VAC,NN,NL)
        CALL CDN(NN,NL,R,THS,XA,YA)
        CALL TDIST(T,NT,XS,YS,TNW)
C      CALL MESH(XP,YP,T,NT)
        CALL EMESH(XP,YP,T,NT,XA,YA,NN,NL)
        STOP
50      FORMAT(' ','NODES')
60      FORMAT(' ',F19.15,F20.15,I4)
        END
C
C THIS SUBROUTINE TAKES THE PATH AND RETURNS THE NODES
C
        SUBROUTINE PATH(NP,TD,NN,XN,YN,R,X,Y,D,G)
C
        REAL*8 X(1000),Y(1000),D(1000),TD,XN(50),YN(50),S,R,TEMP,G
        INTEGER I,K,NN,NP,NH,J
C
        S=TD/2.0
        TEMP=DLOG(1.0+S*(G-1.0)/(0.5*R))/DLOG(G)
        NN=TEMP
        NN=2*NN+1
        NH=NN/2+1
        XN(1)=X(1)
        YN(1)=Y(1)
        I=2
        TEMP=(0.5*R)
C
        DO 220 J=1,NP
            IF (D(J).LE.TEMP) GO TO 220
            XN(I)=X(J)
            YN(I)=Y(J)
            TEMP=D(J)+(0.5*R)*G**(I-1)
            I=I+1
            IF (I.GE.NH) GO TO 230
220     CONTINUE
230     CONTINUE

```

```

C
  DO 235 K=I,NP
    IF (D(K).LT.S) GO TO 235
    XN(NH)=X(K)
    YN(NH)=Y(K)
    GO TO 237
235  CONTINUE
237  CONTINUE
C
  XN(NN)=X(NP)
  YN(NN)=Y(NP)
  I=NN-1
  TEMP=TD-(0.5*R)
C
  DO 240 J=1,NP
    K=NP-J+1
    IF (D(K).GT.TEMP) GO TO 240
    XN(I)=X(K)
    YN(I)=Y(K)
    TEMP=D(K)-(0.5*R)*G**(NN-I)
    I=I-1
    IF (I.LE.NH) GO TO 250
240  CONTINUE
250  RETURN
  END
C
C THIS SUBROUTINE DEFINES THE TRIANGLES USED IN THE MESH
C
  SUBROUTINE TRIANG(NL,NN,T,NT)
C
  INTEGER T(700,3),NL,NN(10),NT,I,J,K,L,NL1,NN1,NND
C
  K=0
  NT=0
  NL1=NL-1
  DO 310 I=1,NL1
    NN1=2*NN(I)-NN(I+1)-1
C
    DO 320 J=1,NN1
C
      T(NT+1,1)=K+J
      T(NT+1,2)=K+NN(I)+J
      T(NT+1,3)=K+NN(I)+J+1
C
      T(NT+2,1)=K+J
      T(NT+2,2)=K+NN(I)+J+1
      T(NT+2,3)=K+J+1
320  NT=NT+2
C
  K=K+NN(I)
  IF (NN(I+1).EQ.NN(I)) GO TO 310
  NND=NN(I+1)-NN(I)
C
  DO 330 L=1,NND

```

```

      T(NT+1,1)=K-NND+L-1
      T(NT+1,2)=K+NN(I)-NND+2*L-2
      T(NT+1,3)=K+NN(I)-NND+2*L-1
      T(NT+2,1)=K-NND+L-1
      T(NT+2,2)=K+NN(I)-NND+2*L-1
      T(NT+2,3)=K-NND+L
      T(NT+3,1)=K+NN(I)-NND+2*L-1
      T(NT+3,2)=K+NN(I)-NND+2*L
      T(NT+3,3)=K-NND+L
330     NT=NT+3
310     CONTINUE
C
      NT=0
      PRINT370
      DO 340 I=1,NL1
      NT=NT+(NN(I)-1)*2
340     NT=NT+NN(I+1)-NN(I)
C
      DO 350 I=1,NT
350     PRINT360,T(I,1),T(I,2),T(I,3),I
C
      RETURN
C
360     FORMAT(' ',I3,3I4)
370     FORMAT(' ', 'TRIANGLES')
      END
C
C THIS SUBROUTINE WILL PRINT OUT THE TRIANGULAR MESH
C (MORE OR LESS)
C
      SUBROUTINE MESH(XP,YP,T,NT)
C
      REAL XP(400),YP(400),XL(6),YL(6)
      INTEGER NT,T(700,3),IBUF(10000),I,J
C
      CALL PLOTS(IBUF,10000)
      CALL PLOT(1.5,0.5,-3)
      CALL AXIS(0.0,0.0,'X',-1,6.0,0.0,0.0,25.0)
      CALL AXIS(0.0,0.0,'Y',+1,10.0,90.0,550.0,25.0)
C
      XL(5)=0.0
      YL(5)=550.0
      XL(6)=25.0
      YL(6)=25.0
      DO 410 I=1,NT
      DO 420 J=1,3
      XL(J)=XP(T(I,J))
420     YL(J)=YP(T(I,J))
      XL(4)=XP(T(I,1))
      YL(4)=YP(T(I,1))
410     CALL LINE(XL,YL,4,1,+0,0)
      CALL PLOT(0.0,0.0,9999)
      RETURN
      END

```

```

C
C
C THIS SUBROUTINE WILL PRINT OUT THE TRIANGULAR MESH NEAR
C THE AC CONDUCTOR (MORE OR LESS)
C
SUBROUTINE EMESH(XP,YP,T,NT,XA,YA,NN,NL)
C
REAL*8 XA(150),YA(150)
REAL XP(400),YP(400),XL(6),YL(6)
INTEGER NT,T(700,3),IBUF(10000),I,J,NN(10),NL
C
CALL PLOTS(IBUF,10000)
CALL PLOT(1.5,0.5,-3)
CALL AXIS(0.0,0.0,'X',-1,6.0,0.0,0.0,5.0)
CALL AXIS(0.0,0.0,'Y',+1,10.0,90.0,575.0,5.0)
C
XL(5)=0.0
YL(5)=575.0
XL(6)=5.0
YL(6)=5.0
DO 410 I=1,NT
DO 420 J=1,3
XL(J)=XP(T(I,J))
420 YL(J)=YP(T(I,J))
XL(4)=XP(T(I,1))
YL(4)=YP(T(I,1))
410 CALL LINE(XL,YL,4,1,+1,4)
J=2*NN(NL)-2
DO 430 I=1,J
XP(I)=XA(I)
430 YP(I)=YA(I)
XP(J+1)=0.0
YP(J+1)=575.0
XP(J+2)=5.0
YP(J+2)=5.0
CALL LINE(XP,YP,J,1,-1,4)
CALL PLOT(0.0,0.0,9999)
RETURN
END
C
C THIS PROGRAM DETERMINES THE PATH OF A PARTICLE USING
C A RUNGE-KUTTA 4TH ORDER METHOD
C
SUBROUTINE RKP(TH,TSTEP,R,NP,TD,X,Y,D,TNMIN,TNMAX)
C
REAL*8 A,B,C,DET,VDC,VAC,PHI,H1,H2,W,R,TOT,TNMIN,TNMAX,TSTEP
REAL*8 RH,X(1000),Y(1000),T,H,TN1,TH,PI,K,D(1000),TD,DS
INTEGER I,J,ND
COMMON A,B,C,DET,VDC,VAC,PHI,H1,H2,W
C
C
PI=3.141592654
K=0.00015
A=DLOG(2.0*H2/R)

```

```

      B=-DLOG((H1+H2)/(H1-H2))
      C=DLOG(2.0*H1/R)
      DET=A*C-B**2
      H=K*TSTEP
C
C MAXIMUM AND MINIMUM DISTANCES BETWEEN SUCCESSION POINTS
C
      X(1)=R*DSIN(PI*TH/180.0)
      Y(1)=H1-R*DCOS(PI*TH/180.0)
      T=0.0
      D(1)=0.0
C
      DO 110 I=1,1000
          RH=DSQRT((Y(I)-H2)**2+X(I)**2)
          IF (RH.LT.R) GO TO 150
          IF (Y(I).LE.0.0) GO TO 160
120      CALL  RK4(X(I),Y(I),X(I+1),Y(I+1),T,H,TN1,K)
          IF (TN1.LT.TNMAX) GO TO 130
C DECREASE STEP SIZE
          H=H*0.5
          GO TO 120
130      DS=DSQRT((X(I+1)-X(I))**2+(Y(I+1)-Y(I))**2)
          IF (DS.LT.R) GO TO 170
          H=H*0.5
          GO TO 120
C
C INCREASE STEP SIZE
C
170      IF (TN1.GT.TNMIN) GO TO 140
          H=H*2.0
C
C INCREMENT TIME
C
140      T=T+H/K
          D(I+1)=D(I)+DS
C
110      CONTINUE
C
C HIT
C
150      TOT=T
          NP=I
          TD=D(NP)
          RETURN
C
C MISS
C
160      PRINT180,THETA
          STOP
180      FORMAT(' ','MISS, THETA= ',F11.7)
          END
C
C THIS SUBROUTINE PERFORMS A SINGLE STEP OF THE R-K METHOD
C

```

```

SUBROUTINE RK4(XN,YN,XN1,YN1,T,H,TN1,K)
C
REAL*8 T,H,XN,YN,XN1,YN1,TN1,KX1,KX2,KX3,KX4,KX5,KX6
REAL*8 KY1,KY2,KY3,KY4,KY5,KY6,K,TT,XP,YP
C
KX1=EX(XN,YN,T)
KY1=EY(XN,YN,T)
C
XP=XN+H*KX1/2.0
YP=YN+H*KY1/2.0
TT=T+H/2.0/K
KX2=EX(XP,YP,TT)
KY2=EY(XP,YP,TT)
C
XP=XN+H*(KX1+KX2)/4.0
YP=YN+H*(KY1+KY2)/4.0
TT=T+H/2.0/K
KX3=EX(XP,YP,TT)
KY3=EY(XP,YP,TT)
C
XP=XN-H*KX2+2.0*H*KX3
YP=YN-H*KY2+2.0*H*KY3
TT=T+H/K
KX4=EX(XP,YP,TT)
KY4=EY(XP,YP,TT)
C
XP=XN+H*(7.0*KX1+10.0*KX2+KX4)/27.0
YP=YN+H*(7.0*KY1+10.0*KY2+KY4)/27.0
TT=T+H/1.5/K
KX5=EX(XP,YP,TT)
KY5=EY(XP,YP,TT)
C
XP=XN+H*(28.0*KX1-125.0*KX2+546.0*KX3+54.0*KX4-378.0*KX5)/625.0
YP=YN+H*(28.0*KY1-125.0*KY2+546.0*KY3+54.0*KY4-378.0*KY5)/625.0
TT=T+H/5.0/K
KX6=EX(XP,YP,TT)
KY6=EY(XP,YP,TT)
C
XN1=XN+H*(KX1+4.0*KX3+KX4)/6.0
YN1=YN+H*(KY1+4.0*KY3+KY4)/6.0
C CALCULATION OF ESTIMATE OF TRUNCATION ERROR
XP=(-42.0*KX1-224.0*KX3-21.0*KX4+162.0*KX5+125.0*KX6)
YP=-42.0*KY1-224.0*KY3-21.0*KY4+162.0*KY5+125.0*KY6
TN1=H*DSQRT(XP**2+YP**2)/336.0
RETURN
END
C
C THIS FUNCTION EVALUATES THE FIELD IN THE X DIRECTION AT
C A GIVEN TIME AND POSITION
C
FUNCTION EX(X,Y,T)
C
REAL*8 X,Y,T,A,B,C,DET,VDC,VAC,W,PHI,Q1,Q2,H1,H2,EX1,EX2
REAL*8 EX3,EX4,D1,D2,D3,D4,X2

```

```

COMMON A,B,C,DET,VDC,VAC,PHI,H1,H2,W
C
C CALCULATE CHARGE ON CONDUCTORS
C
Q1=(A*VDC+B*VAC*DSIN(W*T-PHI))/DET
Q2=(B*VDC+C*VAC*DSIN(W*T-PHI))/DET
C
X2=X**2
D1=(H1-Y)**2+X2
D2=(H2-Y)**2+X2
D3=(H2+Y)**2+X2
D4=(H1+Y)**2+X2
C
EX1=Q1*X/D1
EX2=Q2*X/D2
EX3=-Q2*X/D3
EX4=-Q1*X/D4
C
EX=EX1+EX2+EX3+EX4
RETURN
END
C
C THIS FUNCTION EVALUATES THE ELECTRIC FIELD IN THE Y DIRECTION
C FOR A GIVEN TIME AND POSITION
C
FUNCTION EY(X,Y,T)
C
REAL*8 X,Y,T,A,B,C,DET,VDC,VAC,W,PHI,Q1,Q2,H1,H2,EY1,EY2
REAL*8 EY3,EY4,D1,D2,D3,D4,X2
COMMON A,B,C,DET,VDC,VAC,PHI,H1,H2,W
C
C DETERMINE THE CHARGE ON THE CONDUCTORS
C
Q1=(A*VDC+B*VAC*DSIN(W*T-PHI))/DET
Q2=(B*VDC+C*VAC*DSIN(W*T-PHI))/DET
C
X2=X**2
D1=(H1-Y)**2+X2
D2=(H2-Y)**2+X2
D3=(H2+Y)**2+X2
D4=(H1+Y)**2+X2
C
EY1=-Q1*(H1-Y)/D1
EY2=Q2*(Y-H2)/D2
EY3=-Q2*(Y+H2)/D3
EY4=-Q1*(Y+H1)/D4
C
EY=EY1+EY2+EY3+EY4
RETURN
END
C
C THIS SUBPROGRAM DEFINES THE NEUMAN BOUNDARY CONDITIONS
C
SUBROUTINE NEUM(NN,NL)

```

```

C
  REAL*8 H,SIG
  INTEGER NN(10),NL,NN1,I,J,N1,N2
C
  H=0.0
  SIG=0.0
  PRINT510
  NN1=NN(1)-1
  DO 520 I=1,NN1
    N2=I+1
520  PRINT550,I,N2,H,SIG
    J=0
    DO 530 I=1,NL
530  J=J+NN(I)
    J=J-NN(NL)
    NN1=NN(NL)-1
    DO 540 I=1,NN1
      N1=J+I
      N2=J+I+1
540  PRINT550,N1,N2,H,SIG
    RETURN
510  FORMAT(' ','NEUMAN')
550  FORMAT(' ',I3,I4,2F10.5)
  END
C
C THIS SUBPROGRAM DEFINES THE DIRICHLET BOUNDARY
C CONDITIONS
C
  SUBROUTINE DIRI(VDC,VAC,NN,NL)
C
  REAL*8 VDC,VAC,V
  INTEGER NN(10),NL,NL1,I,J,N1,N2
C
  PRINT630
  NL1=NL-1
  J=0
  DO 620 I=1,NL1
    N1=J+1
    N2=J+NN(I)+1
    PRINT610,N1,N2,VDC
    J=J+NN(I)
    N2=J+NN(I+1)
620  PRINT610,J,N2,VAC
  RETURN
610  FORMAT(' ',I3,I4,' ',F10.3)
630  FORMAT(' ','DIRICHLET')
  END
C
C THIS SUBROUTINE DETERMINES THE ALTERED NODES FOR THE
C FINITE ELEMENT PROGRAM
C
  SUBROUTINE CDN(NN,NL,R,THS,XA,YA)
C
  REAL*8 R,XP,YP,A,B,C,DET,VDC,VAC,THS,H1,H2,W,PHI,TH1,PI,TH

```

```

REAL*8  XA(150),YA(150)
INTEGER NN(10),NL,NL1,I,K,NS,N,L
COMMON  A,B,C,DET,VDC,VAC,PHI,H1,H2,W

C
NL1=NL-1
K=0
PI=3.141592653
NS=2*(2*NL1+NN(NL)-1)
PRINT520,NS
DO 510 I=1,NL1
  K=K+1
  TH=THS*(I-1+(NL-I)*(I-1)**2/NL1**3)
  TH1=THS*(I+(NL-I+1)*I**2/NL1**3)
  TH=(TH+(TH1-TH)*.333D0)*PI/180.0D0
  NS=4
  XP=R*DSIN(TH)
  YP=(H1-R*DCOS(TH))
  PRINT530,K,NS,XP,YP
  TH=THS*(I-1+(NL-I)*(I-1)**2/NL1**3)
  TH1=THS*(I+(NL-I+1)*I**2/NL1**3)
  TH=(TH+(TH1-TH)*.6667D0)*PI/180.0D0
  NS=5
  XP=R*DSIN(TH)
  YP=H1-R*DCOS(TH)
  PRINT530,K,NS,XP,YP
  K=K+NN(I)+NN(I+1)-3
  TH=PI*(I-0.333)/NL1
  NS=6
  XP=R*DSIN(TH)
  YP=(H2+R*DCOS(TH))
  PRINT530,K,NS,XP,YP
  TH=PI*(I-0.667D0)/NL1
  NS=7
  XP=R*DSIN(TH)
  YP=H2+R*DCOS(TH)
510  PRINT530,K,NS,XP,YP
C
C PRINT ALTERED NODES FOR LAST LINE OF MESH
C
  L=-NN(NL-1)-NN(NL)+2
  DO 550 I=1,NL1
550  L=L+NN(I)+NN(I+1)-2
      N=2*NN(NL-1)-NN(NL)-1
      DO 540 I=1,N
        K=L+I*2-1
        NS=6
        PRINT530,K,NS,XA(2*I-1),YA(2*I-1)
      NS=7
540  PRINT530,K,NS,XA(2*I),YA(2*I)
      L=2*N
      N=NN(NL)-NN(NL1)
      K=K+1
      DO 560 I=1,N
        IF (N.EQ.0) GO TO 570

```

```

      K=K+1
      NS=6
      PRINT530,K,NS,XA(L+4*I-3),YA(L+4*I-3)
      NS=7
      PRINT530,K,NS,XA(L+4*I-2),YA(L+4*I-2)
      K=K+2
      NS=4
      PRINT530,K,NS,XA(L+4*I-1),YA(L+4*I-1)
      NS=5
560  PRINT530,K,NS,XA(L+4*I),YA(L+4*I)
570  RETURN
520  FORMAT(' ','ALTERED NODES ',I4)
530  FORMAT(' ',I3,I4,' ',2F20.15)
      END

C
C
C THIS SUBROUTINE TAKES THE PATH AND RETURNS THE NODES
C ALONG WITH ALTERED NODES FOR THE ARTIFICIAL BOUNDARY
C
      SUBROUTINE APATH(NP,TD,NN,XN,YN,R,X,Y,D,G,XA,YA)
C
      REAL*8  X(1000),Y(1000),D(1000),TD,XN(50),YN(50),S,R,TEMP,G
      REAL*8  XA(150),YA(150)
      INTEGER I,K,NN,NP,NH,J
C
      S=TD/2.0
      TEMP=DLOG(1.0+S*(G-1.0)/R)/DLOG(G)
      NN=TEMP
      NN=2*NN+1
      NH=(NN*3)/2+1
      XA(1)=X(1)
      YA(1)=Y(1)
      I=2
      TEMP=R/3.0D0
C
      DO 220 J=1,NP
          IF (D(J).LE.TEMP) GO TO 220
          XA(I)=X(J)
          YA(I)=Y(J)
          TEMP=D(J)+R/3.0D0*G**((I-1)/3)
          I=I+1
          IF (I.GE.NH) GO TO 230
220  CONTINUE
230  CONTINUE
C
      DO 235 K=I,NP
          IF (D(K).LT.S) GO TO 235
          XA(NH)=X(K)
          YA(NH)=Y(K)
          GO TO 237
235  CONTINUE
237  CONTINUE
C
      XA(3*NN-2)=X(NP)

```

```

YA(3*NN-2)=Y(NP)
I=3*(NN-1)
TEMP=TD-R/3.0D0
C
DO 240 J=1,NP
  K=NP-J+1
  IF (D(K).GT.TEMP) GO TO 240
  XA(I)=X(K)
  YA(I)=Y(K)
  TEMP=D(K)-R/3.0D0*G**((3*NN-2-I)/3)
  I=I-1
  IF (I.LE.NH) GO TO 250
240 CONTINUE
250 CONTINUE
  NH=NN-1
  DO 260 J=1,NH
    XN(J)=XA(3*J-2)
    YN(J)=YA(3*J-2)
    XA(2*J-1)=XA(3*J-1)
    YA(2*J-1)=YA(3*J-1)
    XA(2*J)=XA(3*J)
    YA(2*J)=YA(3*J)
260 XN(NN)=XA(3*NN-2)
    YN(NN)=YA(3*NN-2)
  RETURN
  END
C
C THIS SUBROUTINE DETERMINES THE WEIGHT OF EACH OF THE NODES
C IN FINDING THE AVERAGE CHARACTERISTICS OF THE TRIANGLES
C
  SUBROUTINE TDIST(T,NT,XN,YN,TNW)
C
  REAL*8 XN(400),YN(400),TNW(700,3),D12,D23,D31,DD
  INTEGER T(700,3),NT,J
C
  DO 810 J=1,NT
    D12=DSQRT((XN(T(J,1))-XN(T(J,2)))**2+(YN(T(J,1))-YN(T(J,2)))**2)
    D23=DSQRT((XN(T(J,2))-XN(T(J,3)))**2+(YN(T(J,2))-YN(T(J,3)))**2)
    D31=DSQRT((XN(T(J,3))-XN(T(J,1)))**2+(YN(T(J,3))-YN(T(J,1)))**2)
    DD=D12+D23+D31
    TNW(J,1)=1.0D0-(D12+D31)/DD
    TNW(J,2)=1.0D0-(D12+D23)/DD
810 TNW(J,3)=1.0D0-(D23+D31)/DD
  RETURN
  END
/ *
//GO.FT22F001 DD SYSOUT=A
//GO.FT23F001 DD DSN=SYS4.EPIC.PARMS,DISP=SHR
//GO.FT24F001 DD DSN=&&FT01F001,SPACE=(6136,300),
// DCB=(BLKSIZE=6136,DSORG=DA,OPTCD=C,RECFM=F),
// DISP=(,PASS),UNIT=SYSDA
//GO.PLOTLIB DD DSN=SYS4.DRIVER.XEROX,DISP=SHR
// EXEC XPLOT

```

B.3 Initial Space Charge Distribution Approximations

B.3.1 Deutsch Initial Approximation Program

```

//APENNER JOB ','; 'C-ROE'
// EXEC FORTXCLG,OPT=2,SIZE=512K,
// USERLIB='FEDOR.NAG.LOADLIB'
//FORT.SYSIN DD *
C
C THIS PROGRAM DETERMINES AN ESTIMATE OF THE INITIAL CHARGE
C DISTRIBUTION FOR THE TWO CONDUCTOR PROBLEM BASED ON
C DEUTSCH'S ASSUMPTION
C
REAL*8    S(15000),X(1000),Y(1000),DIR(1000),P(400),B(1000),IS(10)
REAL*8    A1(160),A2(160),A3(160),SUB(5),R,ID,THM,XN(400),YN(400)
REAL*8    VN(400),F(400),AA,BB,CC,DET,VDC,VAC,PH,H1,H2,W,E(400)
REAL*8    TXP,TXM,TYP,TYM,XXP,XXM,XYP,XYM,YXM,YXP,YYP,YYM,XX,YY
REAL*8    EM,EXPM,EXMM,EYPM,EYMM,EE,EXPE,EXME,EYPE,EYME,TX,TY,TD
REAL*8    XALT(100),YALT(100),DEN,DETR,PI
INTEGER   IL1(15000),IL2(15000),IS1(1000),IS2(1000),IS3(1000),N3
INTEGER   S4(1000),INODE(6000),I,NNT,NN(10),NL,T(700,3),NT,N1,N2
INTEGER   I2,NL1,NALT
C
COMMON   AA,BB,CC,DET,VDC,VAC,PH,H1,H2,W
C
VDC=35000.0
VAC=0.0
H1=0.8
H2=0.65
PI=3.14159265
W=120.0*PI
THM=55.2
ID=4.0D-6
R=0.000815
NNT=103
NL=4
NN(1)=24
NN(2)=24
NN(3)=26
NN(4)=29
NN(5)=0
NT=147
NALT=12
DEN=0.0
DETR=0.0
C
AA=DLOG(2.0*H2/R)
BB=-DLOG((H1+H2)/(H1-H2))
CC=DLOG(2.0*H1/R)
DET=AA*CC-BB**2
C
CALL   MAIND(S,IL1,IL2,X,Y,DIR,B,IS1,IS2,IS3,IS4,A1,A2,A3,
&INODE,15000,1000,160,6000)

```

```

C
DO 10 I=1,NNT
10 READ(11,70) XN(I),YN(I)
DO 15 I=1,NT
15 READ(12,75) T(I,1),T(I,2),T(I,3)
DO 30 I=1,NNT
  VN(I)=POT(XN(I),YN(I),0.0D0)
  TXP=XN(I)+1.0D-6
  TXM=XN(I)-1.0D-6
  TYP=YN(I)+1.0D-6
  TYM=YN(I)-1.0D-6
  XX=PHI(XN(I),YN(I),1,X,Y,B,INODE,SUB)
  YY=PHI(XN(I),YN(I),2,X,Y,B,INODE,SUB)
  XXP=PHI(TXP,YN(I),1,X,Y,B,INODE,SUB)
  YXP=PHI(TXP,YN(I),2,X,Y,B,INODE,SUB)
  XXM=PHI(TXM,YN(I),1,X,Y,B,INODE,SUB)
  YXM=PHI(TXM,YN(I),2,X,Y,B,INODE,SUB)
  XYP=PHI(XN(I),TYP,1,X,Y,B,INODE,SUB)
  YYP=PHI(XN(I),TYP,2,X,Y,B,INODE,SUB)
  XYM=PHI(XN(I),TYM,1,X,Y,B,INODE,SUB)
  YYM=PHI(XN(I),TYM,2,X,Y,B,INODE,SUB)
  EM=DSQRT(XX**2+YY**2)
  EXPM=DSQRT(XXP**2+YXP**2)
  EXMM=DSQRT(XXM**2+YXM**2)
  EYPM=DSQRT(XYP**2+YYP**2)
  EYMM=DSQRT(XYM**2+YYM**2)
  XX=EX(XN(I),YN(I),0.0D0)
  YY=EY(XN(I),YN(I),0.0D0)
  XXP=EX(TXP,YN(I),0.0D0)
  YXP=EY(TXP,YN(I),0.0D0)
  XXM=EX(TXM,YN(I),0.0D0)
  YXM=EY(TXM,YN(I),0.0D0)
  XYP=EX(XN(I),TYP,0.0D0)
  YYP=EY(XN(I),TYP,0.0D0)
  XYM=EX(XN(I),TYM,0.0D0)
  YYM=EY(XN(I),TYM,0.0D0)
  EE=DSQRT(XX**2+YY**2)
  EXPE=DSQRT(XXP**2+YXP**2)
  EXME=DSQRT(XXM**2+YXM**2)
  EYPE=DSQRT(XYP**2+YYP**2)
  EYME=DSQRT(XYM**2+YYM**2)
  DEN=2.0*((EM-EE)/(EM+EE))
  DETR=DETR+DEN**2
  PRINT80,I,XN(I),YN(I),EM,EE,DEN
  PRINT80,I,XP,YN(I),EXPM,EXPE
  PRINT80,I,TXM,YN(I),EXMM,EXME
  PRINT80,I,XN(I),TYP,EYPM,EYPE
30 PRINT80,I,XN(I),TYM,EYMM,EYME
  DETR=DSQRT(DETR/NNT)
  PRINT95,DETR
  DETR=0.0
C
DO 20 I=1,NT
  N1=1

```

```

N2=2
N3=3
DO 25 I2=1,3
    TX=(XN(T(I,N2))+XN(T(I,N3)))/2.0D0
    TY=(YN(T(I,N2))+YN(T(I,N3)))/2.0D0
    TD=DSQRT(TX**2+TY**2)
    TX=XN(T(I,N1))+(TX-XN(T(I,N1)))*1.0D-6/TD
    TY=YN(T(I,N1))+(TY-YN(T(I,N1)))*1.0D-6/TD
    XX=PHI(TX,TY,1,X,Y,B,INODE,SUB)
    YY=PHI(TX,TY,2,X,Y,B,INODE,SUB)
    EE=DSQRT(XX**2+YY**2)
    PRINT90,T(I,N1),I,TX,TY,EE
    N2=N3
    N3=N1
25  N1=N1+1
20  CONTINUE
C
DEN=0.0
I2=1
DO 40 I=1,NL
    TX=XN(I2)
    TY=YN(I2)
    XX=PHI(TX,TY,1,X,Y,B,INODE,SUB)
    YY=PHI(TX,TY,2,X,Y,B,INODE,SUB)
    EM=DSQRT(XX**2+YY**2)
    XX=EX(TX,TY,0.0D0)
    YY=EY(TX,TY,0.0D0)
    EE=DSQRT(XX**2+YY**2)
    I2=I2+NN(I)
    DETR=2.0*((EE-EM)/(EE+EM))
    DEN=DEN+DETR**2
40  PRINT80,I,TX,TY,EM,EE,DETR
    DEN=DSQRT(DEN/NL)
    PRINT95,DEN
    DETR=0.0
    DEN=0.0
C
C COMPARE E IN INTERIOR OF TRIANGLES
C
DO 60 I=1,NT
    TX=(XN(T(I,1))+XN(T(I,2))+XN(T(I,3)))/3.0D0
    TY=(YN(T(I,1))+YN(T(I,2))+YN(T(I,3)))/3.0D0
    XX=PHI(TX,TY,1,X,Y,B,INODE,SUB)
    YY=PHI(TX,TY,2,X,Y,B,INODE,SUB)
    EM=DSQRT(XX**2+YY**2)
    XX=EX(TX,TY,0.0D0)
    YY=EY(TX,TY,0.0D0)
    EE=DSQRT(XX**2+YY**2)
    DEN=2.0*((EE-EM)/(EE+EM))
    DETR=DETR+DEN**2
60  PRINT80,I,TX,TY,EM,EE,DEN
    DETR=DSQRT(DETR/NT)
    PRINT95,DETR
C

```

```

CALL FINT(VN,NN,NL,F,XN,YN,E)
CALL DELTAI(IS,F,E,THM,R,NN,NL,NNT,VDC,VAC,VN)
CALL CROE(XN,YN,NN,NL,THM,R,ID,P,F,NNT,E,IS)
STOP
70  FORMAT(2G20.10)
75  FORMAT(3I4)
80  FORMAT(' ',I3,' ',F15.10,' ',F15.10,' ',F20.5,' ',F20.5,
&' ',E12.5)
85  FORMAT(' ',I3,' ',F20.15,' ',F20.15,' ',F20.5)
90  FORMAT(' ',I3,' ',I3,' ',F20.15,' ',F20.15,' ',F20.5)
95  FORMAT(' ',E10.5)
END

C
C THIS FUNCTION EVALUATES THE FIELD IN THE X DIRECTION AT
C A GIVEN TIME AND POSITION
C
FUNCTION EX(X,Y,T)
C
REAL*8 X,Y,T,AA,BB,CC,DET,VDC,VAC,W,PHI,Q1,Q2,H1,H2,EX1,EX2
REAL*8 EX3,EX4,D1,D2,D3,D4,X2
COMMON AA,BB,CC,DET,VDC,VAC,PHI,H1,H2,W

C
C CALCULATE CHARGE ON CONDUCTORS
C
Q1=(AA*VDC+BB*VAC*DSIN(W*T-PHI))/DET
Q2=(BB*VDC+CC*VAC*DSIN(W*T-PHI))/DET
C
X2=X**2
D1=(H1-Y)**2+X2
D2=(H2-Y)**2+X2
D3=(H2+Y)**2+X2
D4=(H1+Y)**2+X2
C
EX1=Q1*X/D1
EX2=Q2*X/D2
EX3=-Q2*X/D3
EX4=-Q1*X/D4
C
EX=EX1+EX2+EX3+EX4
RETURN
END

C
C THIS FUNCTION EVALUATES THE ELECTRIC FIELD IN THE Y DIRECTION
C FOR A GIVEN TIME AND POSITION
C
FUNCTION EY(X,Y,T)
C
REAL*8 X,Y,T,AA,BB,CC,DET,VDC,VAC,W,PHI,Q1,Q2,H1,H2,EY1,EY2
REAL*8 EY3,EY4,D1,D2,D3,D4,X2
COMMON AA,BB,CC,DET,VDC,VAC,PHI,H1,H2,W

C
C DETERMINE THE CHARGE ON THE CONDUCTORS
C
Q1=(AA*VDC+BB*VAC*DSIN(W*T-PHI))/DET

```

```

      Q2=(BB*VDC+CC*VAC*DSIN(W*T-PHI))/DET
C
      X2=X**2
      D1=(H1-Y)**2+X2
      D2=(H2-Y)**2+X2
      D3=(H2+Y)**2+X2
      D4=(H1+Y)**2+X2
C
      EY1=-Q1*(H1-Y)/D1
      EY2=Q2*(Y-H2)/D2
      EY3=-Q2*(Y+H2)/D3
      EY4=-Q1*(Y+H1)/D4
C
      EY=EY1+EY2+EY3+EY4
      RETURN
      END
C
C THIS SUBROUTINE INTEGRATES THE INVERSE OF THE ELECTROSTATIC
C ELECTRIC FIELD WRT THE VOLTAGE
C
      SUBROUTINE FINT(VN,NN,NL,F,XN,YN,E)
      REAL*8  VN(400),F(400),XN(400),YN(400),XE,YE,E(400)
      INTEGER NN(10),I,N,J,NL,L
C
      L=0
      DO 110 I=1,NL
          N=NN(I)-1
          L=L+1
          F(L)=0.0
          XE=EX(XN(L),YN(L),0.0D0)
          YE=EY(XN(L),YN(L),0.0D0)
          E(L)=DSQRT(XE**2+YE**2)
          DO 120 J=1,N
              L=L+1
              XE=EX(XN(L),YN(L),0.0D0)
              YE=EY(XN(L),YN(L),0.0D0)
              E(L)=DSQRT(XE**2+YE**2)
              F(L)=F(L-1)+(VN(L-1)-VN(L))*(1.0/E(L)**2+1.0/E(L-1)**2)/2.0
120      CONTINUE
110      CONTINUE
          RETURN
          END
C
C THIS SUBROUTINE PROVIDES THE COEFFICIENTS FOR
C LAPLACE'S EQUATION
C
      SUBROUTINE ABC(ITR,XG,YG,A1,B1,C1,D1,E1,P1)
C
      REAL*8  XG,YG,A1,B1,C1,D1,E1,P1,PI,E0
      INTEGER ITR
C
      PI=3.141592654
      E0=1.0D-9/36.0/PI
      A1=E0

```

```

      B1=0.0
      C1=E0
      D1=0.0
      E1=0.0
      P1=0.0
      RETURN
      END
C
C THIS SUBROUTINE ESTIMATES ROE FROM THE GIVEN QUANTITIES
C
      SUBROUTINE CROE(XN,YN,NN,NL,THM,R,ID,P,F,NNT,E,IS)
C
      REAL*8  XN(400),YN(400),THM,ID,P(400),R,F(400),K,PI,D,EA
      REAL*8  E(400),E0,EON,IS(10),EE,EP(400),A
      INTEGER NN(10),NL,I,J,NNT,L,N
C
      EON=5.8D+6
      PI=3.141592654
      E0=1.0D-9/36.0/PI
      K=0.00015
      L=1
      XN(NNT+1)=XN(NNT-NN(NL)-NN(NL-1)+1)
      YN(NNT+1)=YN(NNT-NN(NL)-NN(NL-1)+1)
C
      DO 210 I=1,NL
C
      IS(I)=ID/THM
      EA=E(L)*PI*R/180.0D0
      A=(EON/E(L))**2
      N=NN(I)
      DO 220 J=1,N
      EP(L)=E(L)*DSQRT(A+(2.0*IS(I)*F(L))/(E0*K*EA))
      P(L)=IS(I)*E(L)/(EP(L)*EA*K)
220    L=L+1
210    CONTINUE
C
      PRINT280
      DO 230 I=1,NNT
230    PRINT260,EP(I)
C
      PRINT290
      DO 240 I=1,NNT
240    PRINT270,P(I)
      RETURN
260    FORMAT(' ',F20.5)
270    FORMAT(' ',F19.15)
280    FORMAT(' ','ELECTRIC FIELD WITH SPACE CHARGE')
290    FORMAT(' ','GUESS AT INITIAL CHARGE DISTRIBUTION')
      END
C
C THIS SUBROUTINE DETERMINES THE CURRENT IN A TUBE
C
      SUBROUTINE DELTAI(IS,F,E,THM,R,NN,NL,NNT,VDC,VAC,VN)
C
      REAL*8  IS(10),F(400),VDC,VAC,E(400),THM,R,PI,E0,K

```

```

REAL*8 EON,VEI,A,EA,VN(400)
INTEGER NN(10),NL,NNT,I,J,NN1,L
C
PI=3.14159265
E0=1.0D-9/36.0D0/PI
K=0.00015
EON=5.8D+6
L=0
DO 310 I=1,NL
  NN1=NN(I)-1
  L=L+1
  A=(EON/E(L))**2
  EA=E(L)*PI*R/180.0D0
  IS(I)=4.0D-6/THM
  L=L+NN1
340  L=L-NN1
  VEI=0.0
  DO 320 J=1,NN1
    VEI=VEI+0.5D0*(DSQRT(A+2.0D0*IS(I)*F(L)/E0/K/EA)+
&      DSQRT(A+2.0D0*IS(I)*F(L+1)/E0/K/EA))*(VN(L)-VN(L+1))
320  L=L+1
  PRINT390,I,IS(I),VEI
  IF (DABS(VEI-VDC).LT.1.0D1) GO TO 350
  IF (VEI.GT.VDC) GO TO 330
  IS(I)=IS(I)*(1.0D0-(VEI-VDC)/VDC)
330  IF (VEI.LT.VDC) GO TO 340
  IS(I)=IS(I)*(1.0D0-(VEI-VDC)/VDC)
  GO TO 340
350  CONTINUE
310  CONTINUE
  RETURN
390  FORMAT(' ',I4,' ',F20.15,' ',F20.5)
  END
C
C THIS FUNCTION EVALUATES THE ELECTRIC FIELD IN THE Y DIRECTION
C FOR A GIVEN TIME AND POSITION
C
  FUNCTION POT(X,Y,T)
C
REAL*8 X,Y,T,A,B,C,DET,VDC,VAC,W,PHI,Q1,Q2,H1,H2,EY1,EY2
REAL*8 EY3,EY4,D1,D2,D3,D4,X2,V1,V2,V3,V4
COMMON A,B,C,DET,VDC,VAC,PHI,H1,H2,W
C
C DETERMINE THE CHARGE ON THE CONDUCTORS
C
  Q1=(A*VDC+B*VAC*DSIN(W*T-PHI))/DET
  Q2=(B*VDC+C*VAC*DSIN(W*T-PHI))/DET
C
  X2=X**2
  D1=DSQRT((H1-Y)**2+X2)
  D2=DSQRT((H2-Y)**2+X2)
  D3=DSQRT((H2+Y)**2+X2)
  D4=DSQRT((H1+Y)**2+X2)
C

```

```
V1=+Q1*DLOG(H1/D1)
V2=+Q2*DLOG(H2/D2)
V3=-Q2*DLOG(H2/D3)
V4=-Q1*DLOG(H1/D4)
```

C

```
POT=V1+V2+V3+V4
RETURN
END
```

```
//GO.SYSIN DD DSN=APENNER.FEPD1I(MF1I35),DISP=SHR
//GO.FT11F001 DD DSN=APENNER.FEPD1I(NDS1I),DISP=SHR
//GO.FT12F001 DD DSN=APENNER.FEPD1I(TRI1I),DISP=SHR
```

B.3.2 Concentric Cylinders Initial Approximation Program

```

//APENNER JOB ',,CCROE
// EXEC WATFIV
//FT05F001 DD *
$JOB
C
C THIS PROGRAM DETERMINES THE TOTAL CURRENT EMMITED FROM A
C CONDUCTOR USING THE "EQUIVALENT CONCENTRIC
C CYLINDERS GEOMETRY
C
REAL*8    VDC,A,B,RO,R,EON,C,VON,ITOT,THETA,THM,THS
REAL*8    PI/3.141593D0/,EO/8.854D-12/,KM/0.00015D0/
REAL*8    ROE(400),DIST(400)
INTEGER   I,J,NL,NN(10),L,N,NNT
C
EON=5.8D+6
VON=34200.0*5.8/6.105
RO=0.000815
R=RO*DEXP(VON/(EON*RO))
PRINT,R
THM=55.2
THETA=0.0
NNT=150
NL=6
NN(1)=24
NN(2)=24
NN(3)=24
NN(4)=24
NN(5)=26
NN(6)=28
VDC=60000.0
A=100000.0
READ70,(DIST(I),I=1,NNT)
L=0
THS=THM/(NL-1)
DO 10 I=1,20
    B=RO*EON/A
    A=(VDC+RO*EON*(1.0-DLOG(2.0*B/RO)))/(DSQRT(R**2+B**2)-
&      B*DLOG((DSQRT(R**2+B**2)+B)/R))
10 PRINT,I,VDC,A,B
C
DO 30 I=1,NL
    THETA=THETA+THS*(NL-I)*(I-1)**2/(NL-1)**3
    N=NN(I)
    DO 40 J=1,N
        L=L+1
40 ROE(L)=EO*A*(1.0+DCOS(PI*THETA/180.0D0))/DSQRT(DIST(L)**2+B**2)
30 CONTINUE
ITOT=2.0*PI*EO*KM*A**2
PRINT80,ITOT
ITOT=ROE(1)*0.14841D0
ITOT=ITOT+ROE(25)*0.30142D0

```

```
ITOT=ITOT+ROE(49)*0.30372D0
ITOT=ITOT+ROE(73)*0.29222D0
ITOT=ITOT+ROE(97)*0.26691D0
ITOT=ITOT+ROE(123)*0.12540D0
PRINT80,ITOT
PRINT80,(ROE(I),I=1,NNT)
70  FORMAT(' ',F20.15)
80  FORMAT(' ',F19.15)
STOP
END
$ENTRY
```

B.4 Iterative Finite Element Program

```

//APENNER JOB ',,T=20M,I=100','ETMF3',CLASS=1
// EXEC FORTXCLG,OPT=2,SIZE=1024K,LIST=NOLIST,
// USERLIB='FEDOR.NAG.LOADLIB'
//FORT.SYSIN DD *
C
C THIS PROGRAM PERFORMS THE ITERATIVE PROCEDURE TO SOLVE
C THE DIFFERENTIAL EQUATIONS
C
REAL*8 S(30000),X(2000),Y(2000),DIR(2000),B(2000),A1(160)
REAL*8 A2(160),A3(160),SUB(5),P(700),AC(700),ROT(700),PEX(400)
REAL*8 PEY(400),IEX(400),IEY(400),XN(400),YN(400),DIFF,EON
REAL*8 PV(400),IV(400),TNW(700,3),RON(400),DN(100),DPON(100)
REAL*8 DION(100),DV(100),XT(700),YT(700),DP(100),XCN(10),YCN(10)
REAL*8 EPCN(10),EICN(10),CD(9),THETA(10),R,EE,EEX,EEY,DTRI(700)
REAL*8 ECD
C
INTEGER IL1(30000),IL2(30000),IS1(2000),IS2(2000),IS3(2000)
INTEGER IS4(2000),INODE(6000),M,N,L,I,NT,J,T(700,3),NI
INTEGER NL,NNT,NN(6),K,NL1,LT
C
COMMON /PAC/ P,AC
C
M=30000
N=2000
L=160
I=6000
NT=238
NNT=150
NL=6
NN(1)=24
NN(2)=24
NN(3)=24
NN(4)=24
NN(5)=26
NN(6)=28
C
C ONSET ELECTRIC FIELD IN VOLTS/METER
EON=6.105D+6
DIFF=1.0D+10
C
CALL INP(NT,NNT,T,RON,XN,YN)
CALL TDIST(T,NT,XN,YN,TNW)
DO 30 NI=1,NT
    XT(NI)=(XN(T(NI,1))+XN(T(NI,2))+XN(T(NI,3)))/3.0D0
    YT(NI)=(YN(T(NI,1))+YN(T(NI,2))+YN(T(NI,3)))/3.0D0
    ROT(NI)=RON(T(NI,1))*TNW(NI,1)+RON(T(NI,2))*TNW(NI,2)+RON(
&T(NI,3))*TNW(NI,3)
30 WRITE(13,90) XT(NI),YT(NI)
C
K=1
NL1=NL-1

```

```

DO 40 NI=1,NL
  XCN(NI)=XN(K)
  YCN(NI)=YN(K)
  THETA(NI)=DATAN(XCN(NI)/(0.8D0-YCN(NI)))
  K=K+NN(NI)
40 WRITE(13,90) XCN(NI),YCN(NI)
C
R=0.000815
DO 50 NI=1,NL1
50 CD(NI)=R*(THETA(NI+1)-THETA(NI))
C
J=1
DO 60 NI=1,NL1
  EEX=EX(XCN(NI),YCN(NI),0.0D0)
  EEY=EY(XCN(NI),YCN(NI),0.0D0)
  EE=DSQRT(EEX**2+EEY**2)
  ECD=EE*CD(NI)
  LT=NN(NI)+NN(NI+1)-2
  DO 70 K=1,LT
    EEX=EX(XT(J),YT(J),0.0D0)
    EEY=EY(XT(J),YT(J),0.0D0)
    EE=DSQRT(EEX**2+EEY**2)
    DTRI(J)=ECD/EE
70 J=J+1
60 CONTINUE
C
DO 10 NI=1,30
  IF (DIFF.LE.1.0D+2) GO TO 20
  CALL ITOP(NT,ROT,RON,TNW,T)
  CALL MAIND(S,IL1,IL2,X,Y,DIR,B,IS1,IS2,IS3,IS4,A1,A2,
&A3,INODE,M,N,L,I)
  REWIND 5
  CALL PEOUT(X,Y,B,INODE,SUB,PEX,PEY,XN,YN,NNT,NI,PV,NT,XT,YT,
&XCN,YCN,EPCN,NL)
  CALL PTOI(NT,ROT,RON,TNW,T)
  CALL MAIND(S,IL1,IL2,X,Y,DIR,B,IS1,IS2,IS3,IS4,A1,A2,
&A3,INODE,M,N,L,I)
  REWIND 5
  CALL IEOUT(X,Y,B,INODE,SUB,IEX,IEY,XN,YN,NNT,NI,IV,NT,XT,YT,
&XCN,YCN,EICN,NL)
10 CALL NEWRO(T,NT,NNT,ROT,PEX,PEY,IEX,IEY,DIFF,EON,NL,NN,NI,PV,
&IV,TNW,RON,DN,DPON,DION,DV,EPCN,EICN,DP,CD,DTRI)
20 CONTINUE
  STOP
90 FORMAT(' ',2G20.10)
  END
C
C THIS SUBROUTINE READS IN THE INITIAL GUESS FOR ROE
C
SUBROUTINE INP(NT,NNT,T,RON,XN,YN)
C
REAL*8 P(700),AC(700),RON(400),XN(400),YN(400)
INTEGER NT,NNT,T(700,3),J
COMMON /PAC/ P,AC

```

```

C
  DO 110 J=1,NNT
    READ(10,160) RON(J)
110  WRITE(13,160) RON(J)
    DO 120 J=1,NNT
      READ(11,170) XN(J),YN(J)
120  WRITE(13,170) XN(J),YN(J)
      DO 130 J=1,NT
        READ(12,180) T(J,1),T(J,2),T(J,3)
130  WRITE(13,180) T(J,1),T(J,2),T(J,3)
      RETURN
160  FORMAT(G20.15)
170  FORMAT(2G20.10)
180  FORMAT(3I4)
    END

C
C THIS SUBROUTINE GIVES THE COEFFICIENTS OF THE DIFFERENTIAL
C EQUATIONS
C
C   SUBROUTINE ABC(ITR,XG,YG,A1,B1,C1,D1,E1,P1)
C
C   REAL*8 XG,YG,A1,B1,C1,D1,E1,P1,P(700),AC(700)
C   INTEGER ITR
C   COMMON /PAC/ P,AC
C
C   A1=AC(ITR)
C   B1=0.0
C   C1=AC(ITR)
C   D1=0.0
C   E1=0.0
C   P1=P(ITR)
C   RETURN
C   END

C
C THIS SUBROUTINE CALCULATES THE ELECTRIC FIELD FROM THE
C SOLUTION OF POISSON'S EQUATION
C
C   SUBROUTINE PEOUT(X,Y,B,INODE,SUB,PEX,PEY,XN,YN,NNT,NI,PV,NT
C   &,XT,YT,XCN,YCN,EPCN,NL)
C
C   REAL*8 X(1000),Y(1000),B(1000),SUB(5),PEX(400),PEY(400)
C   REAL*8 XN(400),YN(400),PV(400),XT(700),YT(700),XCN(10),YCN(10)
C   REAL*8 EPCN(10)
C   INTEGER NNT,INODE(6000),ITYPE,J,NI,NT,NL,NL1
C
C   WRITE(13,250) NI
C   DO 210 J=1,NT
C     PEX(J)=PHI(XT(J),YT(J),1,X,Y,B,INODE,SUB)
C     PEY(J)=PHI(XT(J),YT(J),2,X,Y,B,INODE,SUB)
C     PV(J)=PHI(XT(J),YT(J),0,X,Y,B,INODE,SUB)
C   WRITE(13,260) PEX(J),PEY(J),PV(J)
C
C210 CONTINUE
C
C   NL1=NL-1

```

```

      DO 220 J=1,NL1
        PEX(400)=PHI(XCN(J),YCN(J),1,X,Y,B,INODE,SUB)
        PEY(400)=PHI(XCN(J),YCN(J),2,X,Y,B,INODE,SUB)
C      WRITE(13,260) PEX(400),PEY(400)
220    EPCN(J)=DSQRT(PEX(400)**2+PEY(400)**2)
      RETURN
250    FORMAT(' POISSON ELECTRIC FIELD ITERATION # ',I3)
260    FORMAT(' ',D19.10,' ',D19.10,' ',F19.10)
      END
C
C THIS SUBROUTINE CHANGES THE COEFFICENTS OF THE DIFFERENTIAL
C EQUATION SO THE INHOMOGENEOUS EQUATION IS SOLVED RATHER THAN
C POISSON'S EQUATION
C
      SUBROUTINE PTOI(NT,ROT,RON,TNW,T)
      REAL*8 ROT(700),P(700),AC(700),RON(400),TNW(700,3)
      INTEGER NT,J,T(700,3)
      COMMON /PAC/ P,AC
      DO 310 J=1,NT
        P(J)=0.0
C      ROT(J)=RON(T(J,1))*TNW(J,1)+RON(T(J,2))*TNW(J,2)
C      ROT(J)=ROT(J)+RON(T(J,3))*TNW(J,3)
310    AC(J)=ROT(J)
      RETURN
      END
C
C THIS SUBROUTINE OUTPUTS THE ELECTRIC FIELD FROM THE SOLUTION
C OF THE INHOMOGENEOUS LAPLACE EQUATION
C
      SUBROUTINE IEOUT(X,Y,B,INODE,SUB,IEX,IEY,XN,YN,NNT,NI,IV,NT
&,XT,YT,XCN,YCN,EICN,NL)
C
      REAL*8 X(1000),Y(1000),B(1000),SUB(5),IEX(400),IEY(400)
      REAL*8 XN(400),YN(400),IV(400),XT(700),YT(700),XCN(10),YCN(10)
      REAL*8 EICN(10)
      INTEGER NNT,INODE(6000),ITYPE,J,NI,NT,NL,NL1
C
      WRITE(13,450) NI
      DO 410 J=1,NT
        IEX(J)=PHI(XT(J),YT(J),1,X,Y,B,INODE,SUB)
        IEY(J)=PHI(XT(J),YT(J),2,X,Y,B,INODE,SUB)
        IV(J)=PHI(XT(J),YT(J),0,X,Y,B,INODE,SUB)
C      WRITE(13,460) IEX(J),IEY(J),IV(J)
410    CONTINUE
C
      NL1=NL-1
      DO 420 J=1,NL1
        IEX(400)=PHI(XCN(J),YCN(J),1,X,Y,B,INODE,SUB)
        IEY(400)=PHI(XCN(J),YCN(J),2,X,Y,B,INODE,SUB)
C      WRITE(13,460) IEX(400),IEY(400)
420    EICN(J)=DSQRT(IEX(400)**2+IEY(400)**2)
      RETURN
450    FORMAT(' INHOM. LAPLACE ELECTRIC FIELD ITERATION # ',I3)
460    FORMAT(' ',D19.10,' ',D19.10,' ',F19.10)

```

```

      END
C
C THIS SUBROUTINE CHANGES THE COEFFICIENTS OF THE DIFF.
C EQUATION SO THAT POISSON'S EQUATION IS SOLVED
C
      SUBROUTINE ITOP(NT,ROT,RON,TNW,T)
      REAL*8  ROT(700),P(700),AC(700),PI,E0,RON(400),TNW(700,3)
      INTEGER NT,J,T(700,3)
      COMMON /PAC/ P,AC
      PI=3.141592654
      E0=1.0D-9/36.0D0/PI
      DO 510 J=1,NT
C       ROT(J)=RON(T(J,1))*TNW(J,1)+RON(T(J,2))*TNW(J,2)
C       ROT(J)=ROT(J)+RON(T(J,3))*TNW(J,3)
      P(J)=+ROT(J)/E0
510    AC(J)=1.0D0
      RETURN
      END
C
C THIS SUBROUTINE UPDATES THE GUESS AT THE CHARGE DISTRIBUTION
C
      SUBROUTINE NEWRO(T,NT,NNT,ROT,PEX,PEY,IEX,IEY,DIFF,EON,NL,NN,
&NI,PV,IV,TNW,RON,DN,DPON,DION,DV,EPCN,EICN,DP,CD,DTRI)
C
      REAL*8  ROT(700),PEX(400),PEY(400),IEX(400),IEY(400),DIFF,RON(400)
      REAL*8  EON,PE(400),IE(400),COR(400),PV(400),IV(400),TNW(700,3)
      REAL*8  DN(100),DPON(100),DION(100),DV(100),EPCN(10),EICN(10)
      REAL*8  CCOR(10),OED(700),OEPCND(10),OEICND(10),A(700),B(10)
      REAL*8  C(10),CD(10),IC,KM,DTRI(700),ITRI(700),IAVE(10),DP(100)
      INTEGER T(700,3),NT,NNT,NN(6),NL,J1,J2,J3,J,NN1,JC,NL1
C
      KM=0.00015
      DIFF=0.0
      DV(NI)=0.0
      DO 610 J1=1,NT
      DV(NI)=DV(NI)+((IV(J1)-PV(J1))/(IV(J1)+1.0D-9))**2
      PE(J1)=DSQRT(PEX(J1)**2+PEY(J1)**2)
610    IE(J1)=DSQRT(IEX(J1)**2+IEY(J1)**2)
      DO 615 J1=1,NT
      ITRI(J1)=ROT(J1)*KM*DTRI(J1)*(PE(J1)+IE(J1))/2.0D0
615    DIFF=DIFF+(IE(J1)-PE(J1))**2
C
      DP(NI)=0.0
      DPON(NI)=0.0
      DION(NI)=0.0
      J2=1
      NL1=NL-1
      DO 635 J=1,NL1
      DPON(NI)=DPON(NI)+(EON-EPCN(J))**2
      DION(NI)=DION(NI)+(EON-EICN(J))**2
      IAVE(J)=0.0
      NN1=NN(J)+NN(J+1)-2
      DO 637 J1=1,NN1
      IAVE(J)=IAVE(J)+ITRI(J2)

```

```

637      J2=J2+1
          IAVE(J)=IAVE(J)/NN1
635      WRITE(13,680) EPCN(J),EICN(J),IAVE(J)
C
          IF (NI.GT.1) GO TO 612
C
          DO 613 J=1,NL1
            B(J)=-1.0D0
613      C(J)=-0.5D0
          DO 614 J=1,NT
614      A(J)=-2.0D0
C
612      CONTINUE
C
C IF A,B&C ARE CONSTANT SKIP NEXT 8 LINES
C
C      DO 616 J=1,NL1
C      IF (DABS(EON-EPCN(J)).LT.OEPCND(J)) B(J)=B(J)*1.2D0
C      IF (DABS(EON-EPCN(J)).GT.OEPCND(J)) B(J)=B(J)*(-0.5D0)
C      IF (DABS(EON-EICN(J)).LT.OEICND(J)) C(J)=C(J)*1.2D0
C616  IF (DABS(EON-EICN(J)).GT.OEICND(J)) C(J)=C(J)*(-0.5D0)
C      DO 617 J=1,NT
C      IF (DABS(PE(J)-IE(J)).LT.OED(J)) A(J)=A(J)*1.2D0
C617  IF (DABS(PE(J)-IE(J)).GT.OED(J)) A(J)=A(J)*(-0.5D0)
C
          DO 621 J=1,NL1
            OEPCND(J)=DABS(EON-EPCN(J))
621      OEICND(J)=DABS(EON-EICN(J))
          DO 622 J=1,NT
622      OED(J)=DABS(PE(J)-IE(J))
C
          J=0
          DO 620 J1=1,NL1
            CCOR(J1)=(1.0D0+B(J1)*(EON-EPCN(J1))/EON)*
&              (1.0D0+C(J1)*(EON-EICN(J1))/EON)
            NN1=NN(J1)+NN(J1+1)-2
            DO 630 J2=1,NN1
              J=J+1
              COR(J)=(1.0D0+A(J)*(PE(J)-IE(J))/(PE(J)+IE(J)))*
&              (CCOR(J1)**(FLOAT(NN1-J2)/FLOAT(NN1)))
630      CONTINUE
620      CONTINUE
C
          DO 640 J=1,NT
            DP(NI)=DP(NI)+(1.0D0-COR(J))**2
            ROT(J)=ROT(J)*COR(J)
C      WRITE(13,670) J,ROT(J),PV(J),IV(J),PE(J),IE(J),COR(J),ITRI(J)
640      CONTINUE
          DIFF=DSQRT(DIFF/NT)
          DV(NI)=DSQRT(DV(NI)/NT)
          DPON(NI)=DSQRT(DPON(NI)/NL1)
          DION(NI)=DSQRT(DION(NI)/NL1)
          DP(NI)=DSQRT(DP(NI)/NT)
          DN(NI)=DIFF

```

```

C
    IC=0.0
    J3=1
    DO 650 J=1,NL1
    IC=IC+CD(J)*KM*EON*ROT(J3)*2.0D0
650  J3=J3+NN(J)+NN(J+1)-2
C
    WRITE(13,660) NI,DIFF,IC
    RETURN
660  FORMAT(' ITERATION # ',I3,' DIFF= ',D12.5,' ICOR= ',E12.5)
670  FORMAT(' ',I3,' ',E12.5,' ',F8.1,' ',F8.1,' ',
&         F10.1,' ',F10.1,' ',F7.5,' ',E12.5)
680  FORMAT(' ',F10.1,' ',F10.1,' ',E12.5)
    END

C
C THIS SUBROUTINE DETERMINES THE WEIGHT OF EACH OF THE NODES
C IN FINDING THE AVERAGE CHARACTERISTICS OF THE TRIANGLES
C
    SUBROUTINE TDIST(T,NT,XN,YN,TNW)
C
    REAL*8  XN(400),YN(400),TNW(700,3),D12,D23,D31,DD
    INTEGER T(700,3),NT,J
C
    DO 810 J=1,NT
        D12=DSQRT(((XN(T(J,1))-XN(T(J,2))))**2+(YN(T(J,1))-
&YN(T(J,2))))**2)
        D23=DSQRT(((XN(T(J,2))-XN(T(J,3))))**2+(YN(T(J,2))-
&YN(T(J,3))))**2)
        D31=DSQRT(((XN(T(J,3))-XN(T(J,1))))**2+(YN(T(J,3))-
&YN(T(J,1))))**2)
        DD=D12+D23+D31
        TNW(J,1)=0.5D0*(D12+D31)/DD
        TNW(J,2)=0.5D0*(D12+D23)/DD
810    TNW(J,3)=0.5D0*(D23+D31)/DD
    RETURN
    END

C
C THIS FUNCTION EVALUATES THE FIELD IN THE X DIRECTION AT
C A GIVEN TIME AND POSITION
C
    FUNCTION EX(X,Y,T)
C
    REAL*8  X,Y,T,AA,BB,CC,DET,VDC,VAC,W,PHI,Q1,Q2,H1,H2,EX1,EX2
    REAL*8  EX3,EX4,D1,D2,D3,D4,X2,R
    VDC=80000.0
    VAC=0.0
    PHI=0.0
    H1=0.80
    H2=0.65
    W=3.14*120.0
    R=0.000815
    AA=DLOG(2.0*H2/R)
    BB=DLOG((H1+H2)/(H1-H2))
    CC=DLOG(2.0*H1/R)

```

```

      DET=AA*CC-BB**2
C
C CALCULATE CHARGE ON CONDUCTORS
C
      Q1=(AA*VDC+BB*VAC*DSIN(W*T-PHI))/DET
      Q2=(BB*VDC+CC*VAC*DSIN(W*T-PHI))/DET
C
      X2=X**2
      D1=(H1-Y)**2+X2
      D2=(H2-Y)**2+X2
      D3=(H2+Y)**2+X2
      D4=(H1+Y)**2+X2
C
      EX1=Q1*X/D1
      EX2=Q2*X/D2
      EX3=-Q2*X/D3
      EX4=-Q1*X/D4
C
      EX=EX1+EX2+EX3+EX4
      RETURN
      END
C
C THIS FUNCTION EVALUATES THE ELECTRIC FIELD IN THE Y DIRECTION
C FOR A GIVEN TIME AND POSITION
C
      FUNCTION EY(X,Y,T)
C
      REAL*8  X,Y,T,AA,BB,CC,DET,VDC,VAC,W,PHI,Q1,Q2,H1,H2,EY1,EY2
      REAL*8  EY3,EY4,D1,D2,D3,D4,X2,R
C
      VDC=80000.0
      VAC=0.0
      PHI=0.0
      H1=0.80
      H2=0.65
      W=120.0*3.14
      R=0.000815
      AA=DLOG(2.0*H2/R)
      BB=-DLOG((H1+H2)/(H1-H2))
      CC=DLOG(2.0*H1/R)
      DET=AA*CC-BB**2
C
C DETERMINE THE CHARGE ON THE CONDUCTORS
C
      Q1=(AA*VDC+BB*VAC*DSIN(W*T-PHI))/DET
      Q2=(BB*VDC+CC*VAC*DSIN(W*T-PHI))/DET
C
      X2=X**2
      D1=(H1-Y)**2+X2
      D2=(H2-Y)**2+X2
      D3=(H2+Y)**2+X2
      D4=(H1+Y)**2+X2
C
      EY1=-Q1*(H1-Y)/D1

```

```
EY2=Q2*(Y-H2)/D2
EY3=-Q2*(Y+H2)/D3
EY4=-Q1*(Y+H1)/D4
C
EY=EY1+EY2+EY3+EY4
RETURN
END
//GO.FT06F001 DD DUMMY
//GO.SYSIN DD DSN=APENNER.FEPD1M(MF1M50),DISP=SHR
//GO.FT10F001 DD DSN=APENNER.R1MCC(R1MCC50),DISP=SHR
//GO.FT11F001 DD DSN=APENNER.FEPD1M(NDS1M),DISP=SHR
//GO.FT12F001 DD DSN=APENNER.FEPD1M(TR11M),DISP=SHR
//GO.FT13F001 DD DSN=APENNER.EOUT,DISP=OLD
```